STUDIA

UNIVERSITATIS BABEŞ-BOLYAI

PHYSICA

38(2)

1993

CLUJ-NAPOCA

Anul XXXVIII · 1993

STUDIA
UNIVERSITATIS BABEŞ-BOLYAI

PHYSICA

2

Redacţia 3400 CLUJ-NAPOCA str M Kogălniceanu nr 1 ▸ Telefon 116101

SUMAR - CONTENTS - SOMMAIRE

Theoretical Physics

Plasma Physics

Optics, Spectrometry and Nuclear Physics

STUDIA UNIV BABEŞ-BOLYAI, PHYSICA, XXXVIII, 2, 1993

A STUDY OF A SIMPLE NONLINEAR MECHANICAL SYSTEM

S. CODREANU*, Tb. COLOŞI**, M. DANCA**

Received 30 05 1994

ABSTRACT. - The aim of a paper is an analitical and numerical investigation of a nonlinear mechanical system. This system is a parametrically forced mechanical oscillator, with cubic nonlinearity We demonstrate that the system exhibits a very complicated dynamics, including equilibrium points, limit cycles and complicated chaotic attractors For the numerical simulation we have used an original method

Introduction. The irregular and unpredictable time evolution of many nonlinear systems has been called chaos or deterministic chaos It occurs in many and different domains of the science like physics, chemistry, astronomy, biology, economy etc [1], [2] For example it can be observed in mechanical oscillators such as forced pendula or vibrating object [3], [4], but also in rotating or heated fluids [5], [6], in nonlinear circuits [7], in laser cavities [8], in nonlinear optical devices [9], [10], in Josephson junction [11]-[13], in plasmas [14], in some chemical reactions [15]-[17], in biological and ecological models [18], [19] or in stimulated heart cells [20] and in Electroencephalogram data [21]

The central characteristic of the systems which exhibit a chaotical dynamics is that the systems do not repeat their past behavior although they follow deterministic equations For chaotic systems the slightly different initial conditions lead to an error in prediction that grows exponentially in time This characteristic, which occurs only when the governing equations are nonlinear, is known as sensitivity to initial conditions The first who recognized

* *"Babeş-Bolyai" University, Faculty of Physics, 3400 Cluj-Napoca, Romania*

** *Technical University, 3400 Cluj-Napoca, Romania*

this phenomenon was Henri Poincare (1913) Although a chaotic system can resemble a stochastic one, (i e a system subject to a random external force), the sourse of the irregularity is quite different For the chaos the irregularity is part of the intrinsic dynamics of the system, not unpredictable outside influences If the dynamical system is described by a set of first order differential equations the necessary conditions for chaotic motion are that the system has at least three independent dynamical variables and the equation of motion contain a nonlinear term

The equations can often be expressed in the form

$$\frac{dx_i}{dt} = F_i(x_1, x_2, \ldots, x_n)$$

where $i = 1, 2, \ldots, n$ ($n \geq 3$) and with F for example of the form

$$F = ax_1 + bx_2 + cx_1x_2 + \ldots + fx_n$$

where a,b,c,f are constants For some choise of the constants, such systems are often chaotic

From historical point of view the development of the study of chaotic systems is a recent one, despite the fact that chaotic systems are deterministic and are described by many of the well known equations This is due to the fact that, with the exception of some first order equations, nonlinear differential equations are either difficult or impossible to solve analitically So, the solution of nonlinear differential equations generally requires numerical methods The first who detected chaos in a nonlinear dynamical system by a numerical study was E Lorenz [22]

One of the simplest physical system with a rich and complex behavior, which has been intensively analyzed, is the damped driven pendulum [23], [24] This is a based nonlinear model system for different more complicated physical problems (nonlinear oscillators) like

the forced motions of a particle in a two-well potential (such an electron in a plasma) [25], [26], the magnetic pendulum [27], or the radio-frequency driven Josephson junctions [11], [28]

In the same class of nonlinear dynamical systems is also the motion of a shallow arch subjected to horizontal and vertical pulsating loads proposed by Szemplinska-Stupnicka [29] and recently explored by Lamarque end Malasoma [30] The aim of our paper is an analitical study of the stady states of this system and then a numerical integration of differential equation which models the system by using an original method proposed by one of the authors [31]

The model and its fixed points. The equation of motion for a particular shallow arch subjected to horizontal and vertical pulsating loads is·

$$\ddot{x} + a\dot{x} - 0{,}5(1 - 2f\cos\omega t - x^2)x = f\cos\omega t \tag{1}$$

where a is the damping coefficient, f and ω are the amplitude and the circular frequency of parametric excitation

To analize the behavior of the system we consider the following system of autonomous equations, which is equivalent to the differential equation (1).

$$\begin{aligned} \dot{x} &= y \\ \dot{y} &= -ay + 0{,}5(1 - 2f\cos z)x - 0{,}5x^3 + f\cos z \\ \dot{z} &= \omega \end{aligned} \tag{2}$$

We can see that this set of equations (or this flow) describes a dissipative system for any $a > 0$ A system is dissipative if an arbitrary volume V, enclosed by some surface S in

the pbase space of the variables of the system, contracts The surface S evolves by having each point on it follow an orbit generated by (2) If the system (2) has the general form

$$\dot{\vec{x}} = F(\vec{x}), \quad \vec{x} = (x_1 = x, x_2 = y, x_3 = z) \tag{3}$$

The statement of divergence theorem is

$$\frac{dV}{dt} = \int_V \left(\sum_{i=1}^{d} \frac{\partial F_i}{\partial x_i} \right) d_x^d$$

and the dissipative system is defined by $\frac{dV}{dt} < 0$

In the case of the flow defined by (2)

$$\frac{dV}{dt} = -aV \quad \text{or} \quad V(t) = V(0)e^{-at} \tag{4}$$

i e the volume element contracts exponentially in time for $a > 0$

If the parametric excitation is swiched off ($f = 0$), the system (2) becomes

$$\begin{aligned} \dot{x} &= y \\ \dot{y} &= -ay + 0{,}5x - 0{,}5x^3 \end{aligned} \tag{5}$$

and from $F(\vec{x}) = 0$, we find the following fixed points of the system (5)

$$\vec{x}_1(0,0), \ \vec{x}_2(-1,0), \ \vec{x}_3(1,0) \tag{6}$$

If $f \neq 0$, from (2) one finds the fixed points (the steady states)

$$\vec{x}_1(1,0,0), \ \vec{x}_2\left(-\frac{1}{2} + \frac{1}{2}\sqrt{1-8f}, 0, 0\right), \ \vec{x}_3\left(-\frac{1}{2} - \frac{1}{2}\sqrt{1-8f}, 0, 0\right) \tag{7}$$

with the obvious condition of reality of them $f \leq \frac{1}{8}$

The stability of the steady states. First we investigate the stability of the fixed points (6) For $\vec{x}_1(0,0)$, the matrix of stability is

$$\begin{vmatrix} 0 & 1 \\ 0{,}5 & -a \end{vmatrix}$$

and the characteristic equation

$$\begin{vmatrix} -\lambda & 1 \\ -0,5 & -a-\lambda \end{vmatrix} = 0 \tag{8}$$

The eigenvalues of (8) are

$$\lambda_{1,2} = \frac{1}{2}\left(-a \pm \sqrt{a^2+2}\right) \tag{9}$$

and we have $\lambda_1 > 0$ and $\lambda_2 < 0$ for any $a > 0$ Thus the origin ($x = 0$) is a saddle fixed point

For the fixed points $\vec{x}_2(-1,0)$ and $\vec{x}_3(1,0)$, the characteristic equation is

$$\begin{vmatrix} -\lambda & 1 \\ -1 & -a-\lambda \end{vmatrix} = 0$$

with the eigenvalues

$$\lambda_{1,2} = \frac{1}{2}\left(-a \pm \sqrt{a^2-4}\right) \tag{10}$$

In this case $\lambda_1 < 0$ and $\lambda_2 < 0$ for any $a \geq 2$ If $\lambda_{1,2}$ has the form $\lambda_{1,2} = \lambda' \pm i\lambda''$ we observe that $\lambda' < 0$ for any $a > 0$ Thus $x = -1$ and $x = 1$ are stable fixed points, or stable equilibrium

The stability of the fixed points (7) is investigated by the same method One finds for $x = 1$, the characteristic equation

$$\begin{vmatrix} -\lambda & 1 & 0 \\ -1-f & -a-\lambda & 0 \\ 0 & 0 & -\lambda \end{vmatrix} = 0$$

with the eigenvalues

$$\lambda_1 = 0,\ \lambda_{2,3} = \frac{1}{2}\left(-a \pm \sqrt{a^2-4(1+f)}\right)$$

If $-1 \leq f \leq \frac{1}{8}$, λ_2 is real and negative, also if $f < \frac{a^2}{4} - 1$, λ_3 is real and negative If $\frac{a^2}{4} - 1 < f \leq \frac{1}{8}$, $\lambda_{2,3} = \lambda \pm i\Lambda$ with $\lambda < 0$ for $a > 0$ Thus $x = 1$ remains a stable fixed point in the presence of the parametric excitation ($f \neq 0$)

For the fixed points $x = \frac{1}{2}\left(-1 + \sqrt{1-8f}\right)$ and $x = \frac{1}{2}\left(-1 - \sqrt{1-8f}\right)$, the eigenvalues of the characteristic equations are

$$\lambda_1 = 0$$

$$\lambda_{2,3} = \frac{1}{2}\left[-a \pm \left(a^2 + 8f - 1 \pm 3\sqrt{1-8f}\right)^{1/2}\right]$$

with $\lambda_2 > 0$ and $\lambda_3 < 0$, respectively $\lambda_2 < 0$ and $\lambda_3 > 0$ We conclude that for $0 < f < \frac{1}{8}$ these fixed points are unstables

But the system has, beside the steady states, also the other important behaviors like limit cycles with different periods, which form a cascade of period doubling cumulating in chaos, as the amplitude of parametric excitation is used as a control paramater We observed this benhavior by numerical investigation of (2) for different values of f, ω and a being constants

The numerical study. We have performed a numerical investigation of equation (1), or of equivalent set of equations (2), by using a new method of integration based on local linearization iterative (L L I) This method realises, with remarcable performances, the numerical approximation of the solutions through the segments of straight, considered in the neighbourhood of a pivot moment With this method the relative errors cumulated was smaller than 0,1%, for sufficient large characteristic time intervals Also, in the same domain of errors, the computing time is smaller than those spent with usual fourth order Runge-Kutta method

By fixing the parameters at the following values $a = 1{,}5$, $\omega = 8$, except the amplitude of parametric excitation f, which was used as a control parameter, we have constructed the projections of the trajectories in the phase space for a wide range of the control parameter Thus, for $f = 0$, when the parametric excitation is awiched off, we found the stable

equilibrium $x = -1$ and $x = 1$ Because the trajectory goes to one or another fixed point, for different initial conditions, we drew the basins of attraction of these coexisting stable solutions Figure 1 ahows the basins of attraction in the phase space region defined by -20 $\leq x \leq 20$, and -20 $\leq y \leq 20$ The basin of equilibrium point $x = -1$ is colored in white, while that of $x = 1$ is in black In Figure 2 we present two projections in XOY and XOZ planes of the trajectory in this case

With parametric excitation ($f \neq 0$), the focus $x=1$ remain a solution of equation (1) This point is numerically found to be a stable equilibrium state until the amplitude f is $f \approx 29{,}28$, when a limit cycle is created The projections in XOY plane of the trajectories with $f=5$ and $f=20$ are shown in Figures 3 and 4 Figure 5 shows two projections in XOY and YOZ planes of the trajectory when $f = 29{,}28$ When $f = 29{,}29713$ we can see, from Figure 6, that a cycle limit is created In Figure 7 a and b we present the cycle limit for $f = 32$ in two projections on XOY and ZOX planes This period-1 limit cycle is also stable until amplitude f is $f = 45{,}5$ when a period-2 motion is created (see Figure 8) At $f = 47{,}5$ we can see, from Figure 9, that a period-4 motion is generated As f increases further, a period doubling cascade followed by chaos is clearly visible We presents this in Figures 10-12 for $f = 47{,}7$, $f = 48$ and $f = 55$ At $f = 65$ a new period-1 limit cycle is created (see Figure 13), and the same scenario of period doubling cascade followed by chaos is visible We have carried out extensive numerical simulation and we found the same behavior for

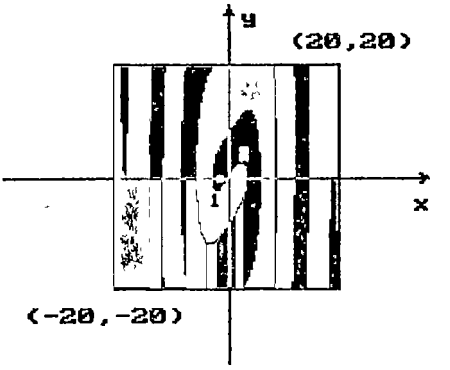

Fig 1

different values of f Figures 14-16 show some particular trajectories

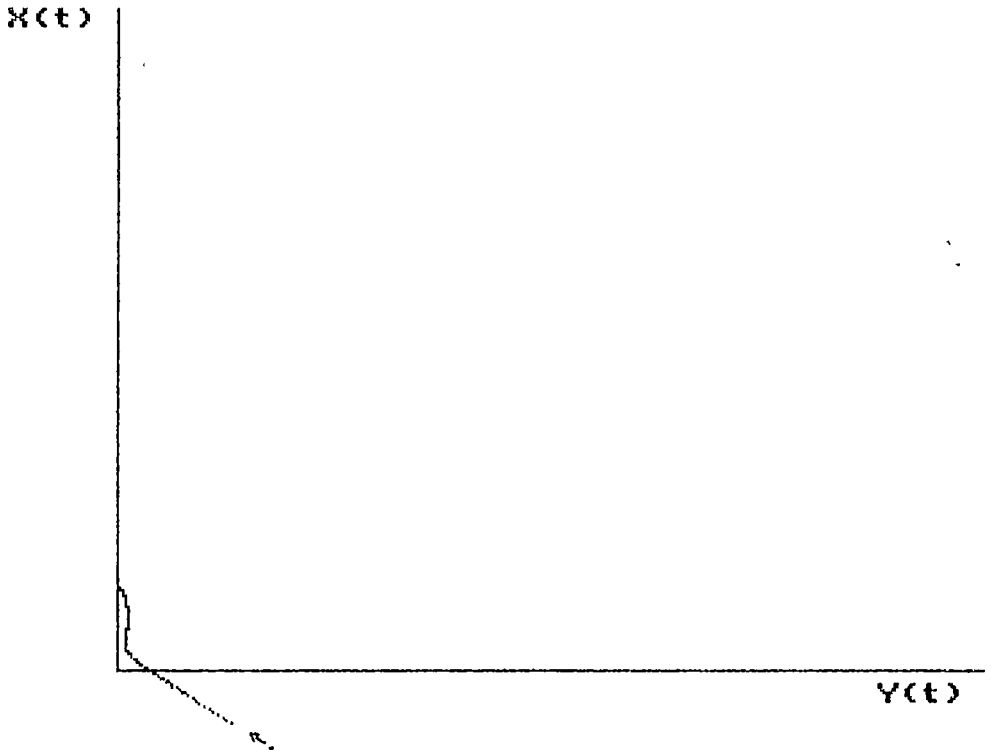

Fig 2

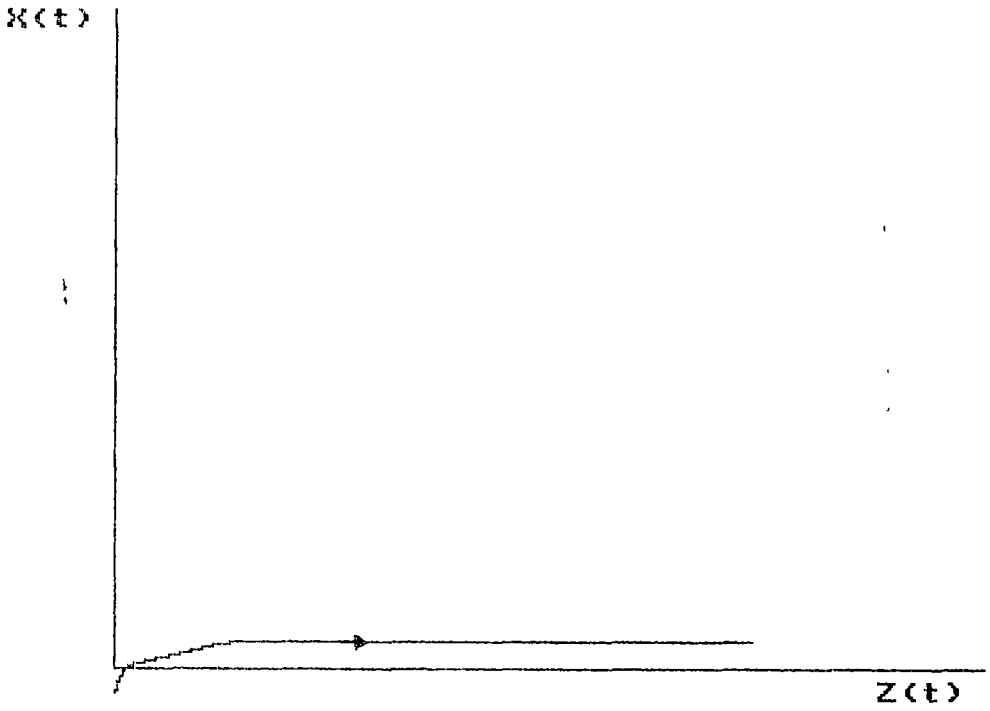


```
Damp. coef. = 1.5000000000E+00
Amplitude = 0.0000000000E+00
Circ. freq. = 8.0000000000E+00

X init=-1.0000000000E+00
Y init= 2.0000000000E+00
Z init= 0.0000000000E+00
V Scale= 1.0000000000E+01
H Scale= 5.0000000000E-01
```

Fig 3

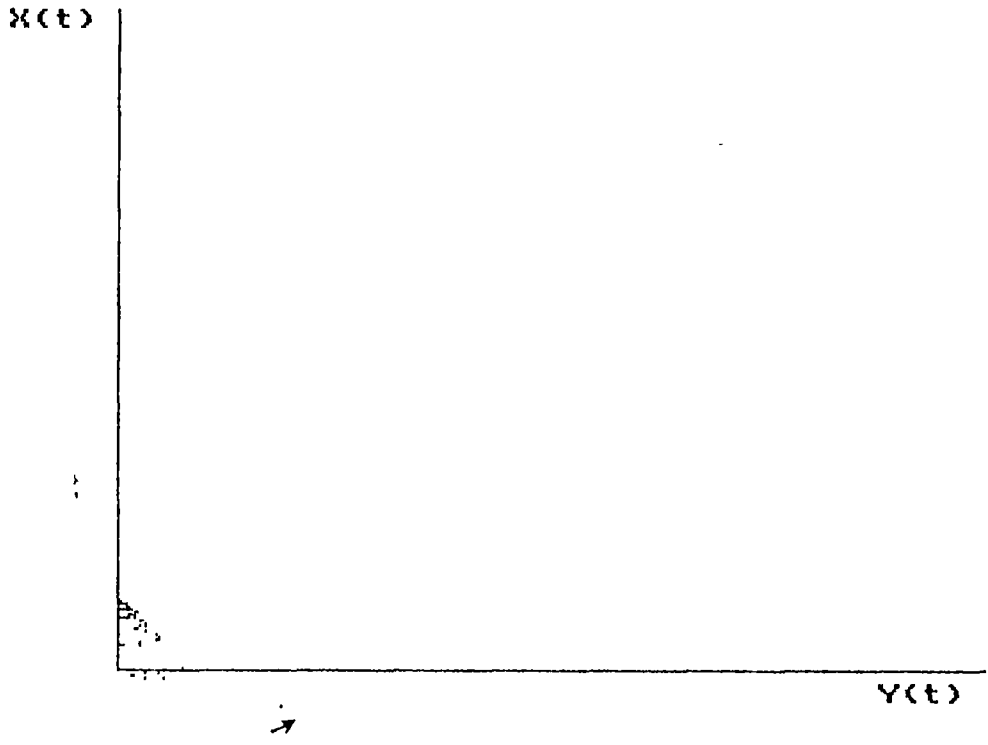

Damp. coef. = 1.5000000000E+00
Amplitude = 5.0000000000E+00
Circ. freq. = 8.0000000000E+00

X init=-1.0000000000E+00
Y init= 2.0000000000E+00
Z init= 0.0000000000E+00
V Scale= 2.5000000000E+01
H Scale= 2.5000000000E+01

Fig 4

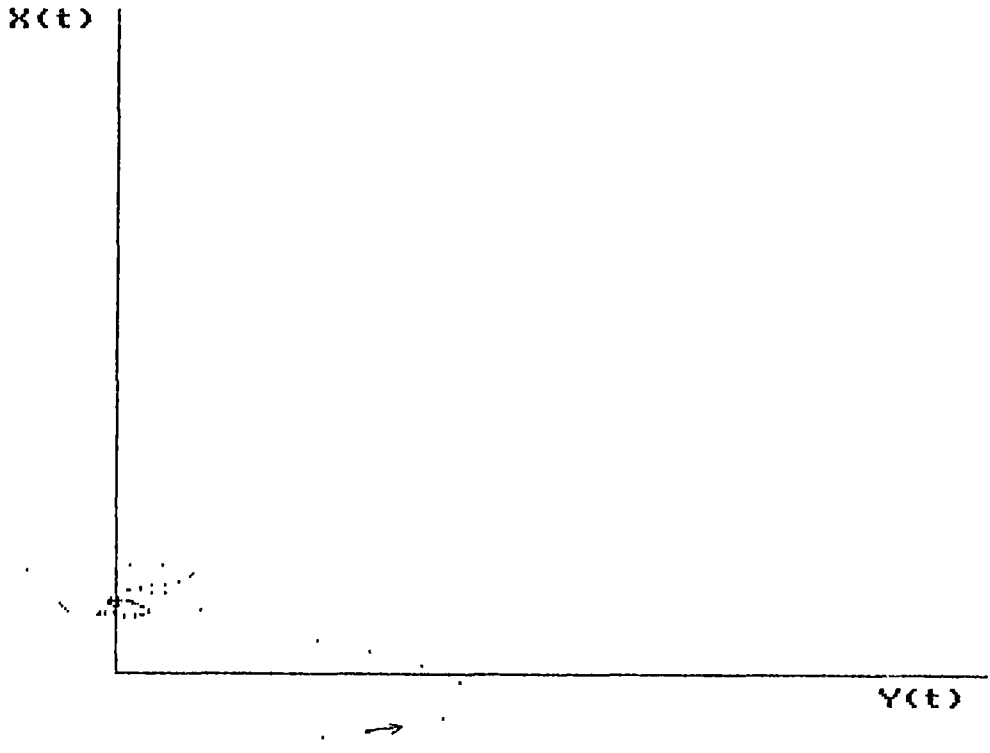


```
Damp. coef. = 1.5000000000E+00
Amplitude = 2.0000000000E+01
Circ. freq. = 8.0000000000E+00

X init=-1.0000000000E+00
Y init= 2.0000000000E+00
Z init= 0.0000000000E+00
V Scale= 2.5000000000E+01
H Scale= 2.5000000000E+01
```

Fig.5

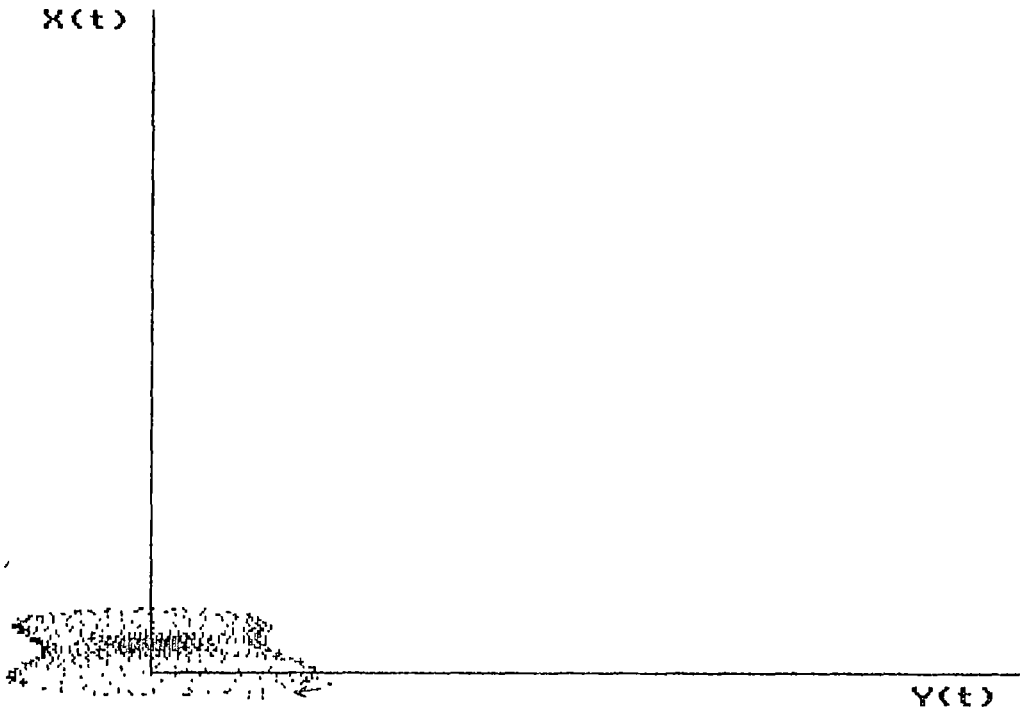


```
Damp. coef. = 1.5000000000E+00
Amplitude = 2.9280000000E+01
Circ. freq. = 8.0000000000E+00

X init=-1.0000000000E+00
Y init= 2.0000000000E+00
Z init= 0.0000000000E+00
V Scale= 1.0000000000E+01
H Scale= 1.0000000000E+01
```

Fig 6

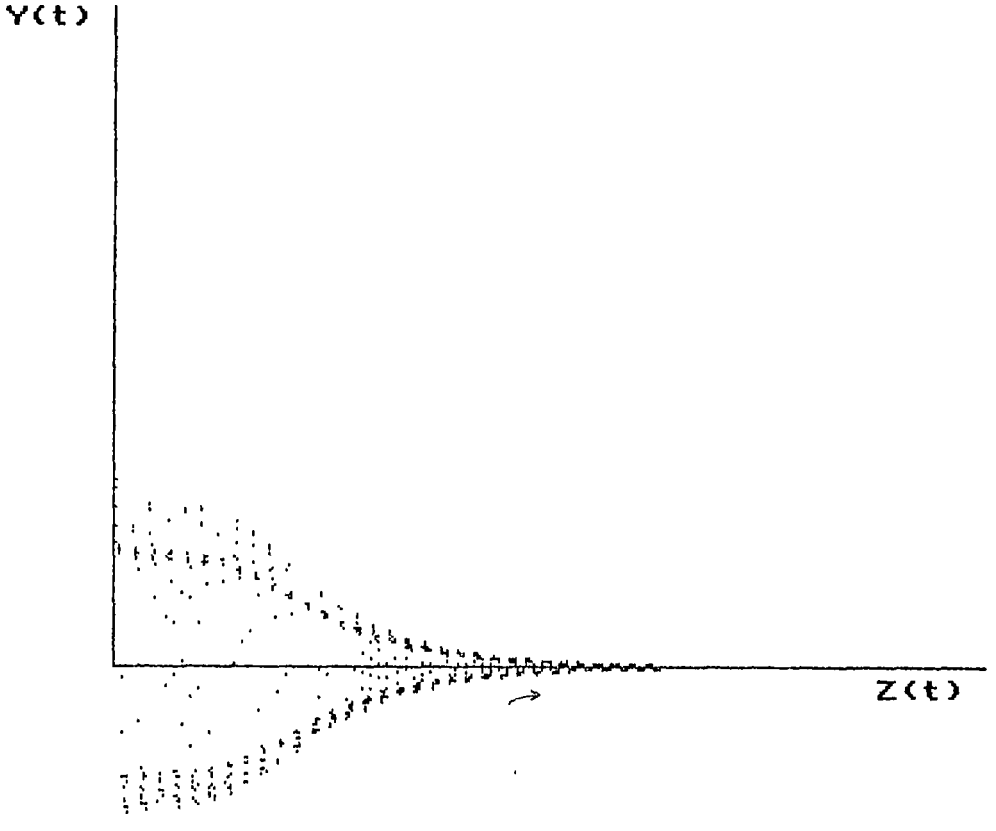


```
Damp. coef. = 1.5000000000E+00
Amplitude = 2.9280000000E+01
Circ. freq. = 8.0000000000E+00

X init=-1.0000000000E+00
Y init= 2.0000000000E+00
Z init= 0.0000000000E+00
U Scale= 1.0000000000E+01
H Scale= 5.0000000000E-01
```

Fig 7

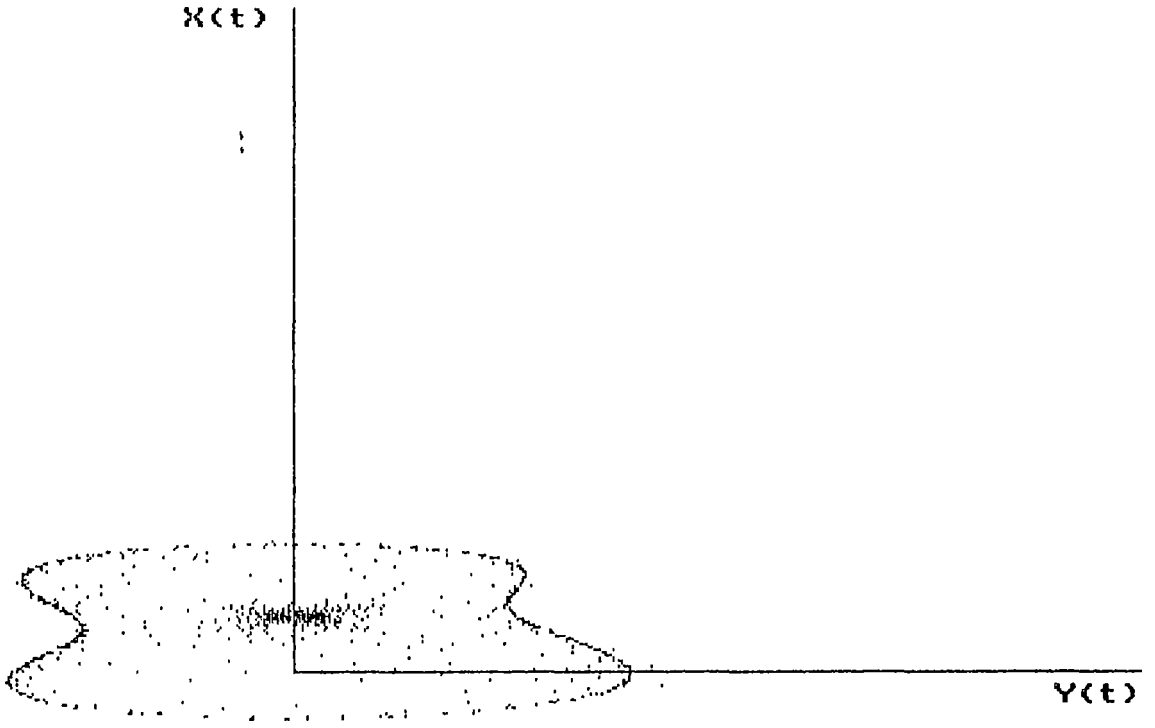


```
Damp. coef. = 1.5000000000E+00
Amplitude = 2.9287130000E+01
Circ. freq. = 8.0000000000E+00

X init=-1.0000000000E+00
Y init= 2.0000000000E+00
Z init= 0.0000000000E+00
V Scale= 2.0000000000E+01
H Scale= 2.0000000000E+01
```

Fig.8

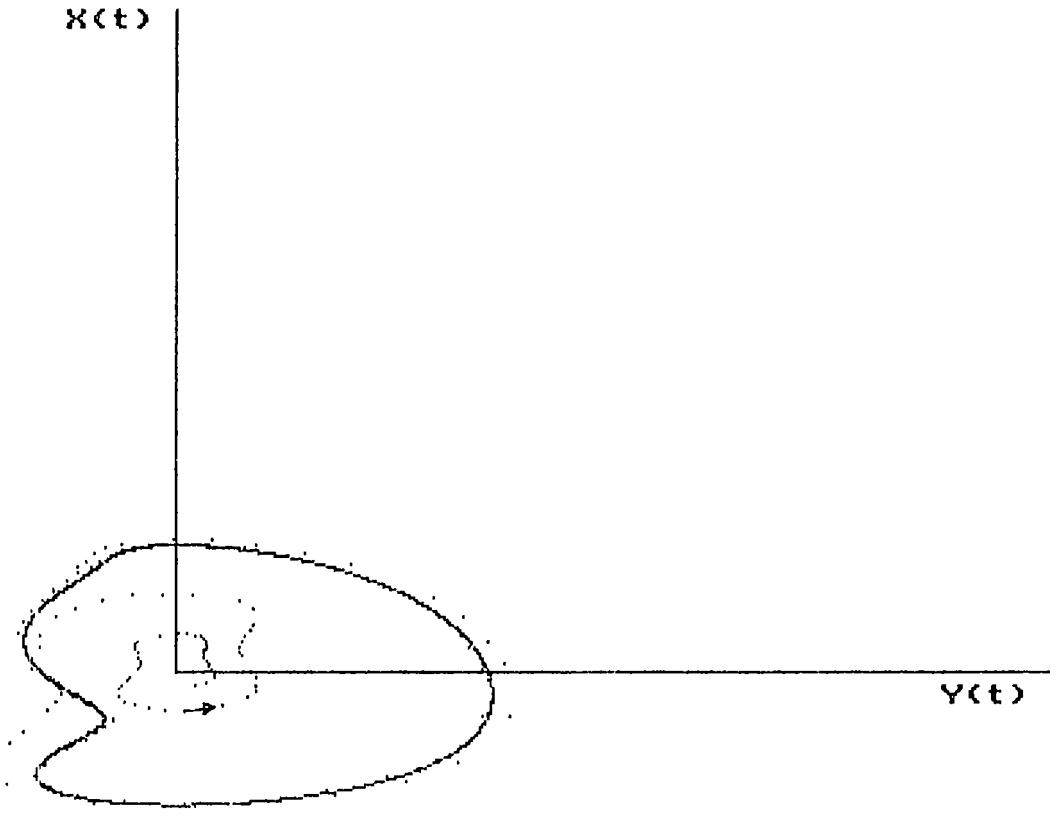


```
Damp. coef. = 1.5000000000E+00
Amplitude = 3.2000000000E+01
Circ. freq. = 8.0000000000E+00

X init=-1.0000000000E+00
Y init= 2.0000000000E+00
Z init= 0.0000000000E+00
V $cale= 5.0000000000E+00
H $cale= 2.0000000000E+00
```

Fig 9

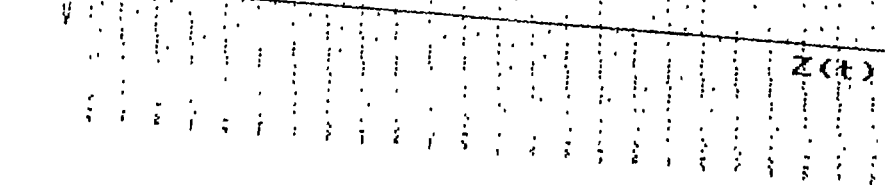


```
Damp. coef.  = 1.5000000000E+00
Amplitude    = 3.2000000000E+01
Circ. freq.  = 8.0000000000E+00

X init=-1.0000000000E+00
Y init= 2.0000000000E+00
Z init= 0.0000000000E+00
V Scale= 5.0000000000E+00
H Scale= 1.0000000000E+00
```

Fig.10

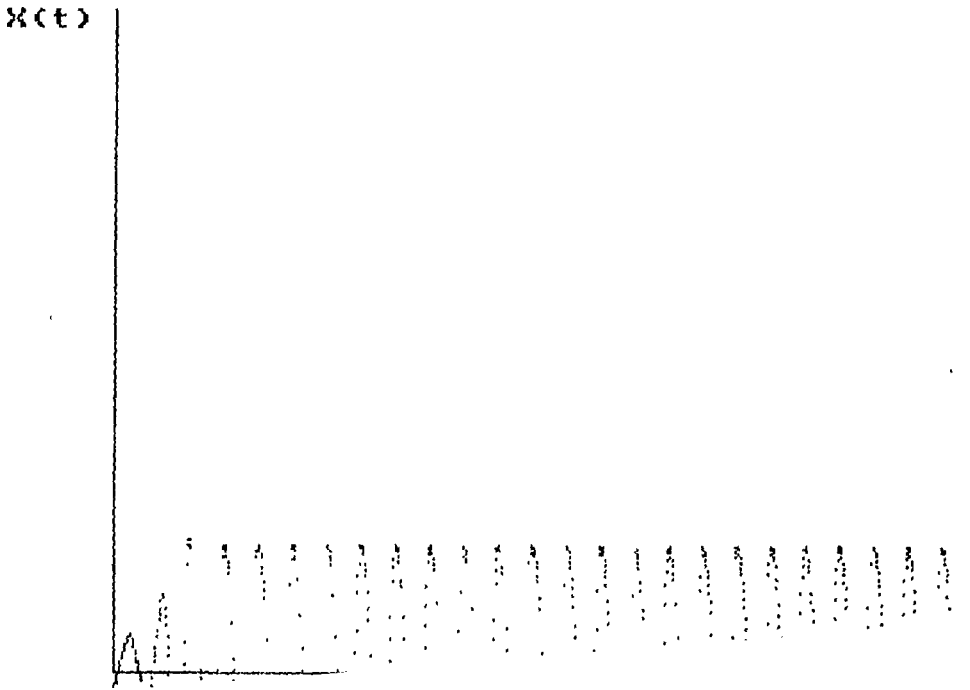
X(t)

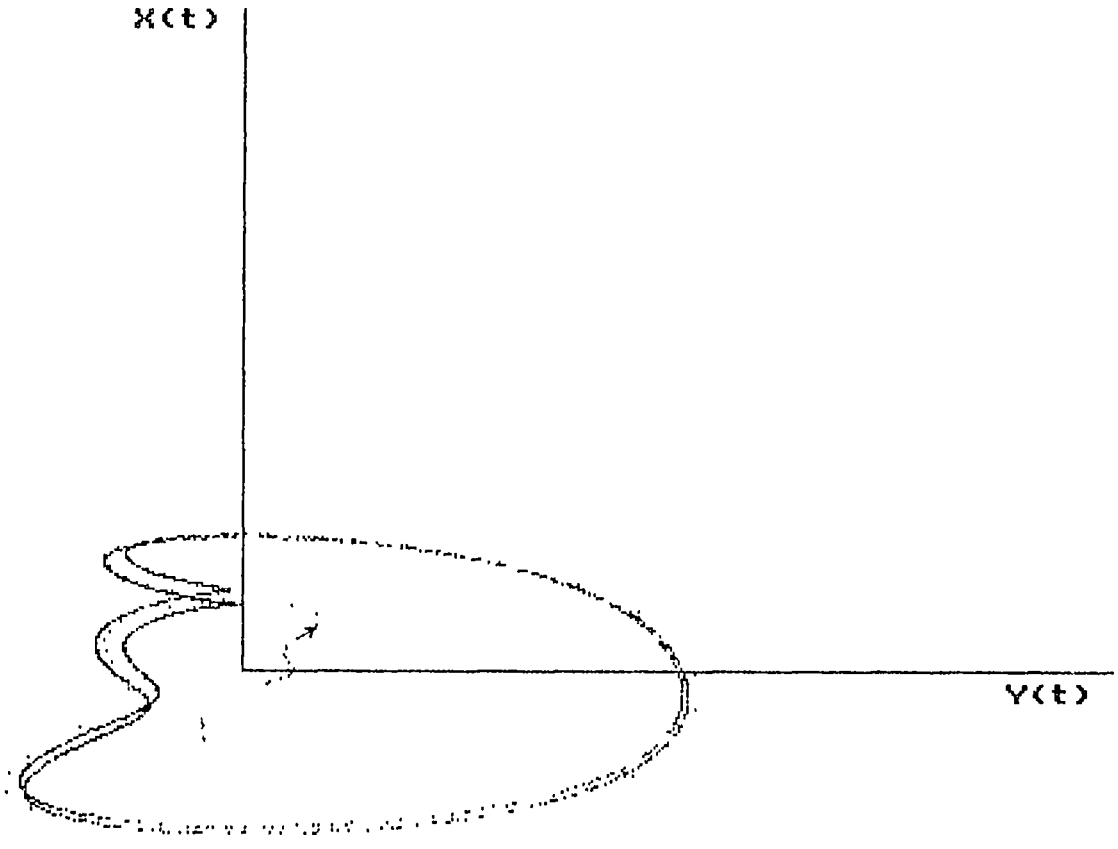


```
Damp. coef. = 1.5000000000E+00
Amplitude = 4.5500000000E+01
Circ. freq. = 8.0000000000E+00

X init=-1.0000000000E+00
Y init= 2.0000000000E+00
Z init= 0.0000000000E+00
V Scale= 5.0000000000E+00
H Scale= 2.0000000000E+00
```

Fig 11

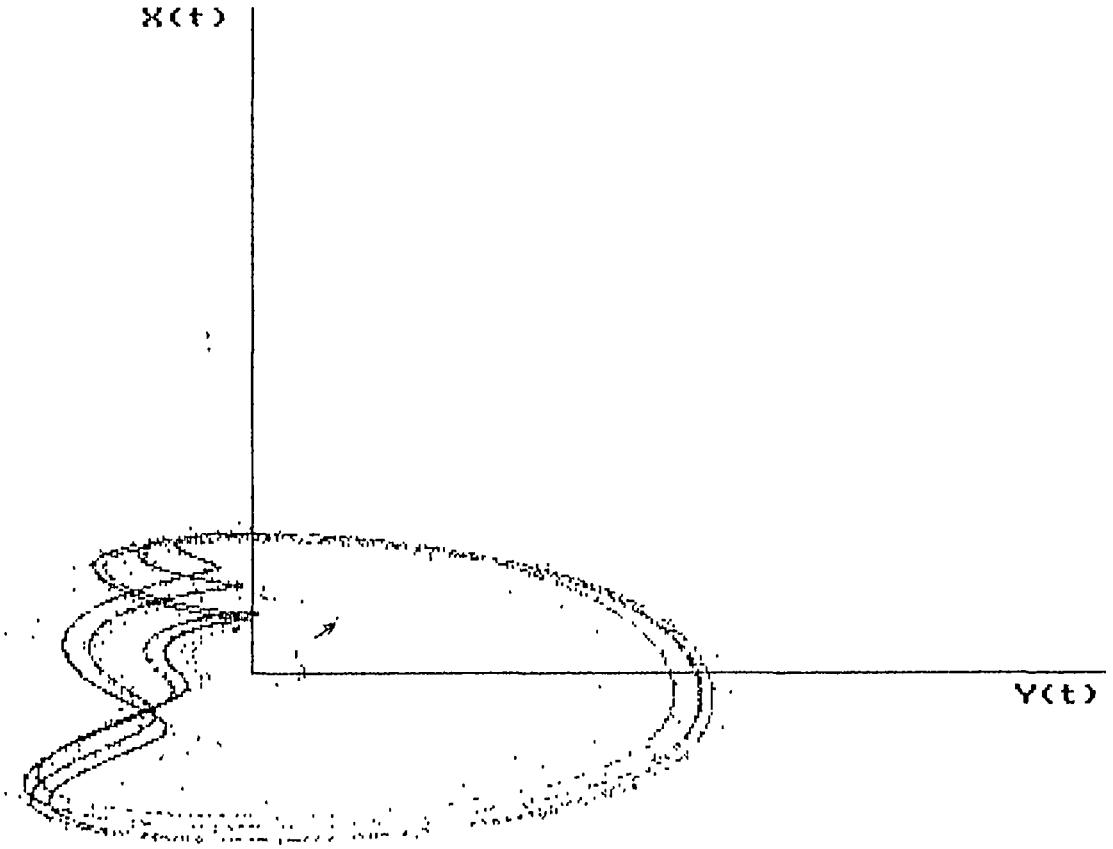

Damp. coef. = 1.5000000000E+00
Amplitude = 4.7500000000E+01
Circ. freq. = 8.0000000000E+00

X init=-1.0000000000E+00
Y init= 2.0000000000E+00
Z init= 0.0000000000E+00
U Scale= 5.0000000000E+00
H Scale= 2.0000000000E+00

Fig 12

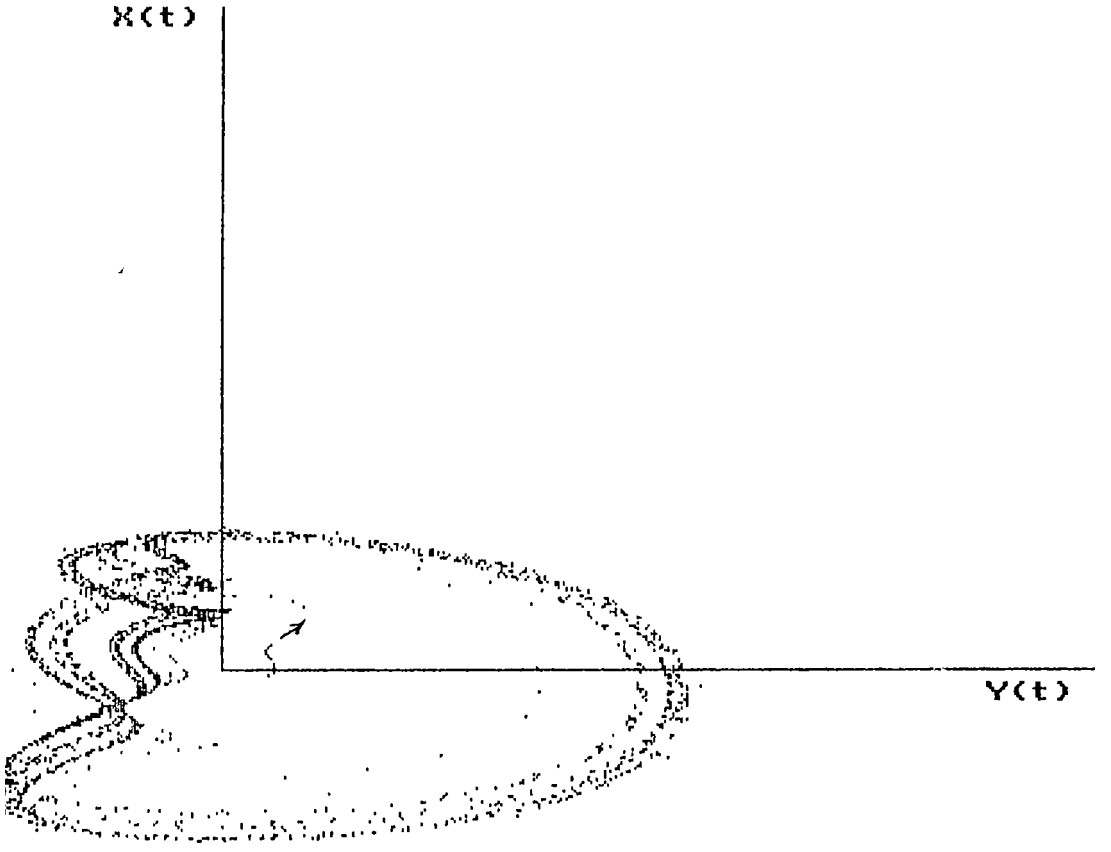


```
Damp. coef. = 1.5000000000E+00
Amplitude = 4.7700000000E+01
Circ. freq. = 8.0000000000E+00

X init=-1.0000000000E+00
Y init= 2.0000000000E+00
Z init= 0.0000000000E+00
V Scale= 5.0000000000E+00
H Scale= 2.0000000000E+00
```

Fig 13

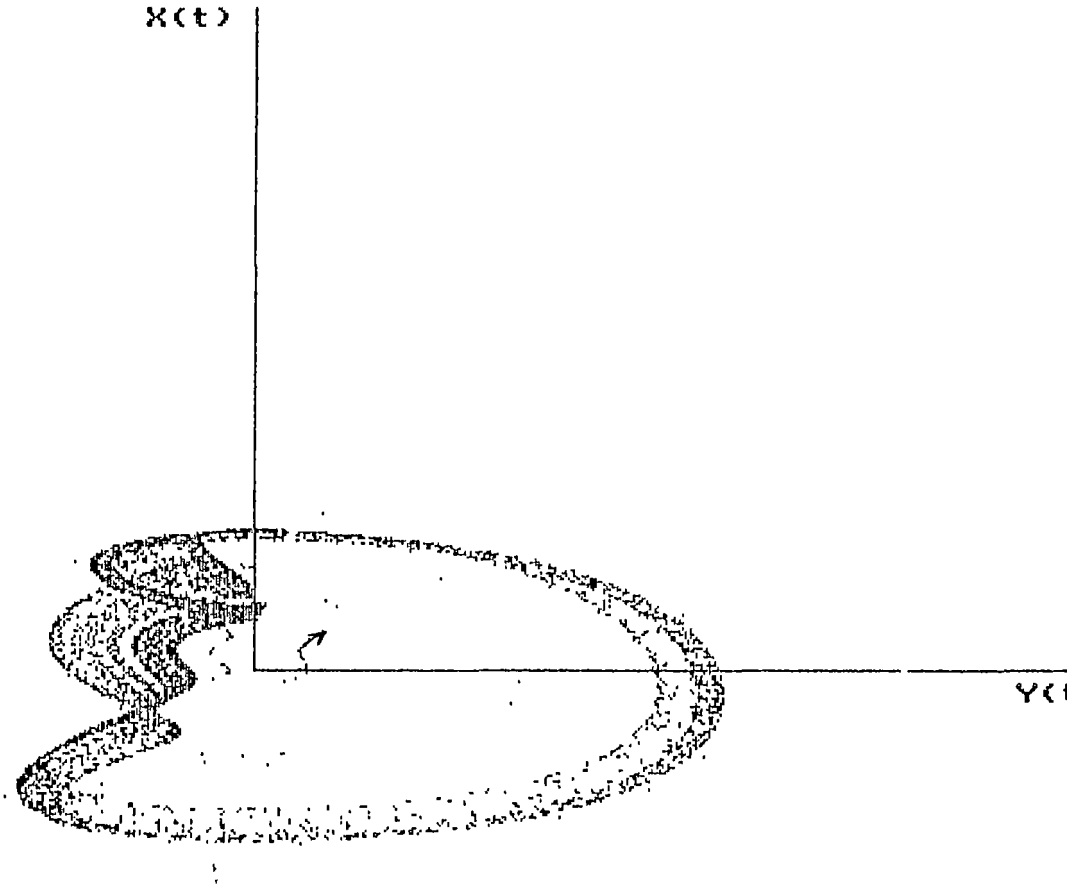
X(t)
Y(t
Damp. coef. = 1.5000000000E+00
Amplitude = 4.8000000000E+01
Circ. freq. = 8.0000000000E+00
X init=-1.0000000000E+00
Y init= 2.0000000000E+00
Z init= 0.0000000000E+00
V Scale= 5.0000000000E+00
H Scale= 2.0000000000E+00

Fig.14

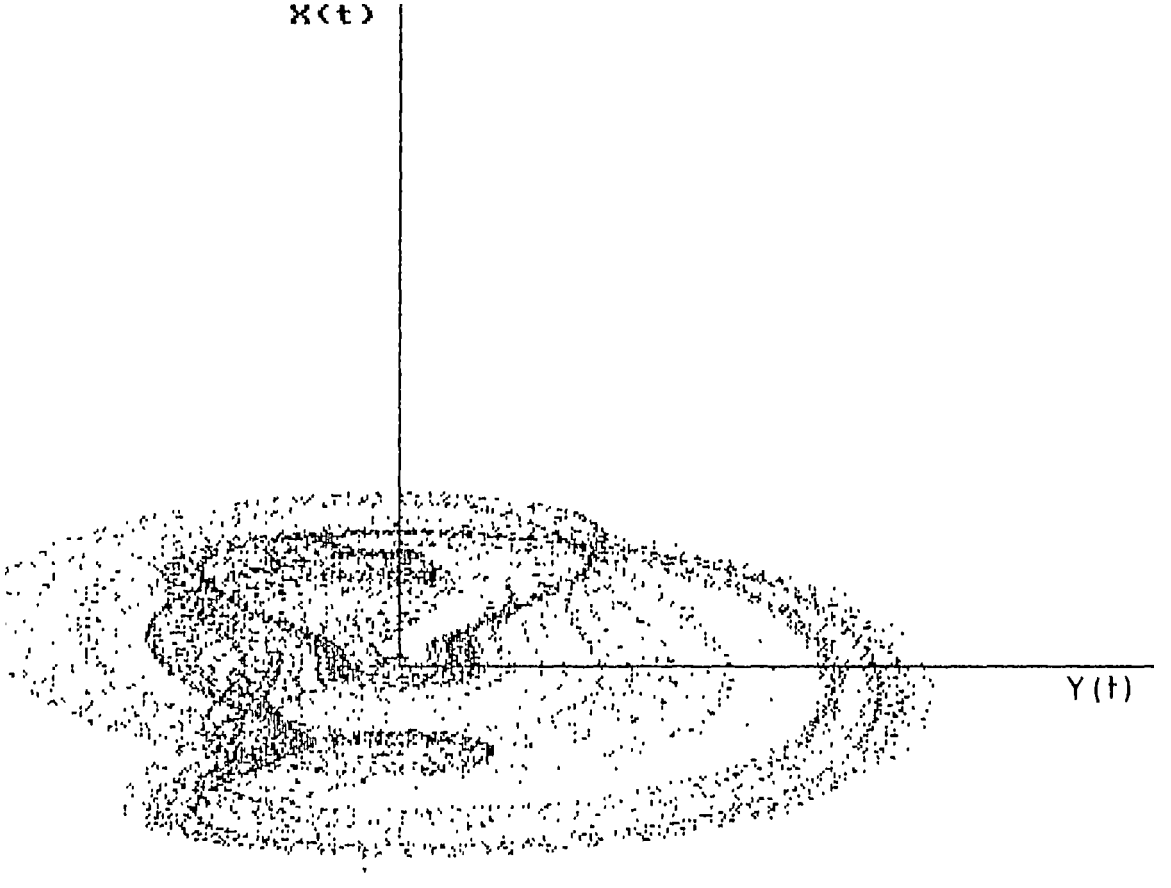

Damp. coef. = 1.5000000000E+00
Amplitude = 5.5000000000E+01
Circ. freq. = 8.0000000000E+00

X init=-1.0000000000E+00
Y init= 2.0000000000E+00
Z init= 0.0000000000E+00
V Scale= 5.0000000000E+00
H Scale= 2.0000000000E+00

Fig. 15

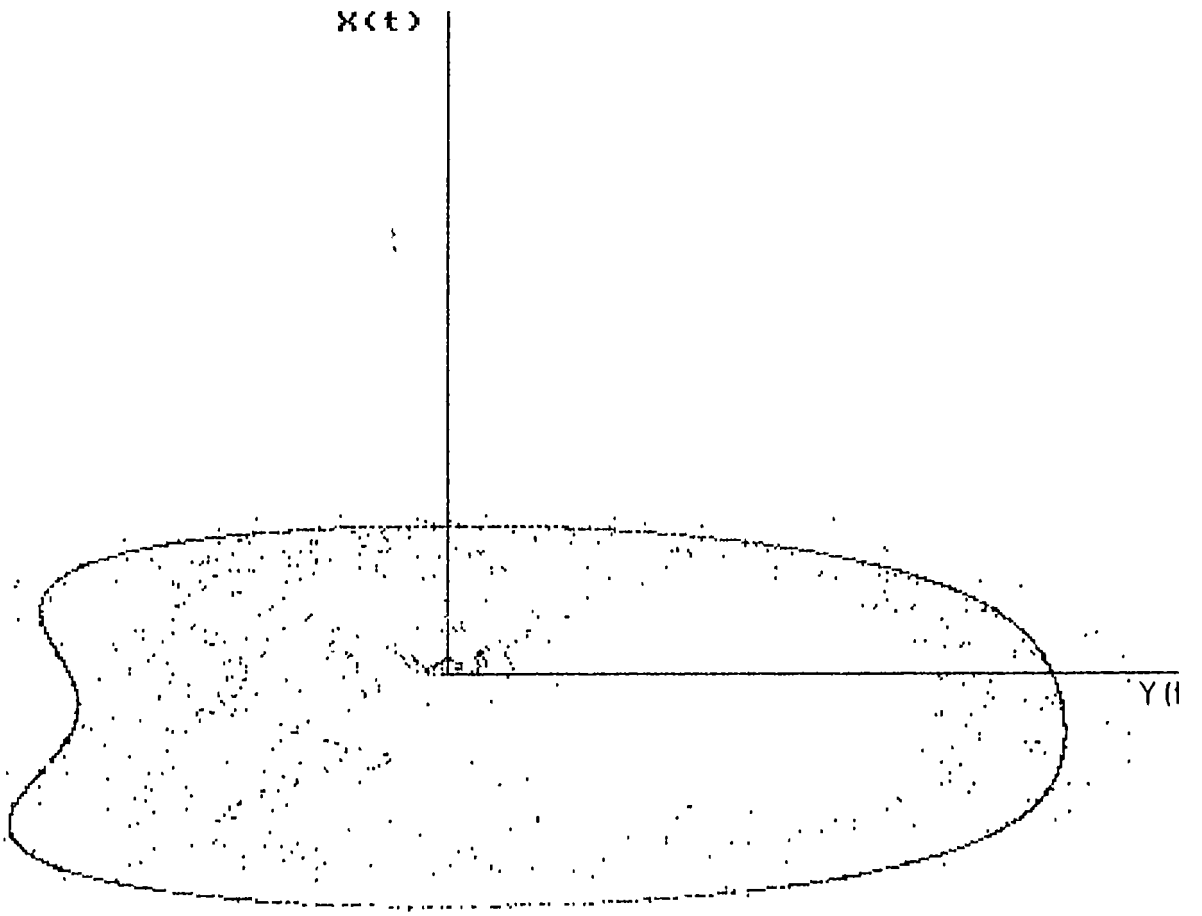

Damp. coef. = 1.5000000000E+00
Amplitude = 6.5000000000E+01
Circ. freq. = 8.0000000000E+00

X init=-1.0000000000E+00
Y init= 2.0000000000E+00
Z init= 0.0000000000E+00
V Scale= 5.0000000000E+00
H Scale= 2.0000000000E+00

Fig.16

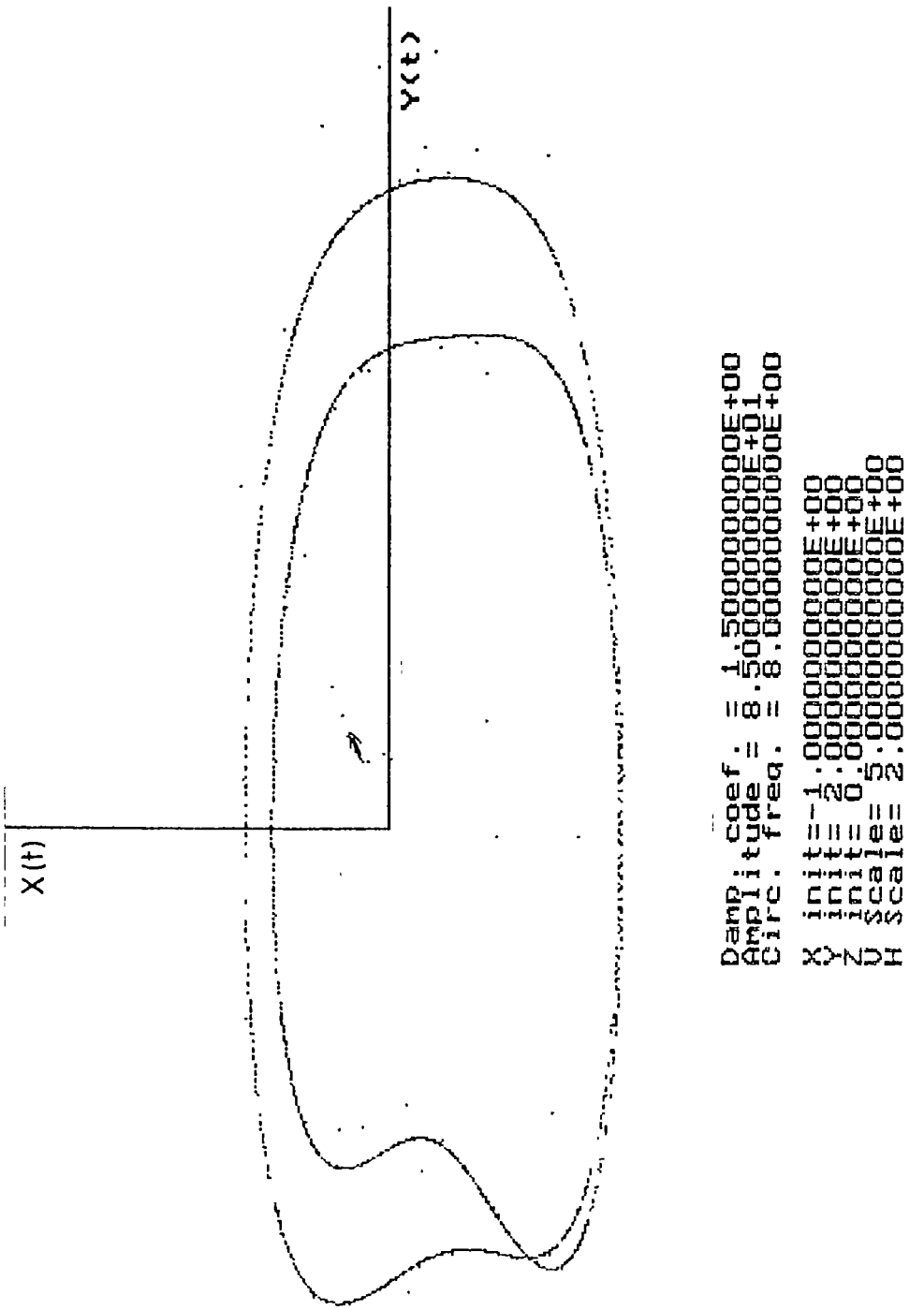
Y(t)
X(t)
Damp. coef. = 1.500000000000E+00
Amplitude = 8.500000000000E+01
Circ. freq. = 8.000000000000E+00
X init=-1.000000000000E+00
Y init= 2.000000000000E+00
Z init= 0.000000000000E+00
Y scale= 5.000000000000E+00
H scale= 2.000000000000E+00

Fig 17

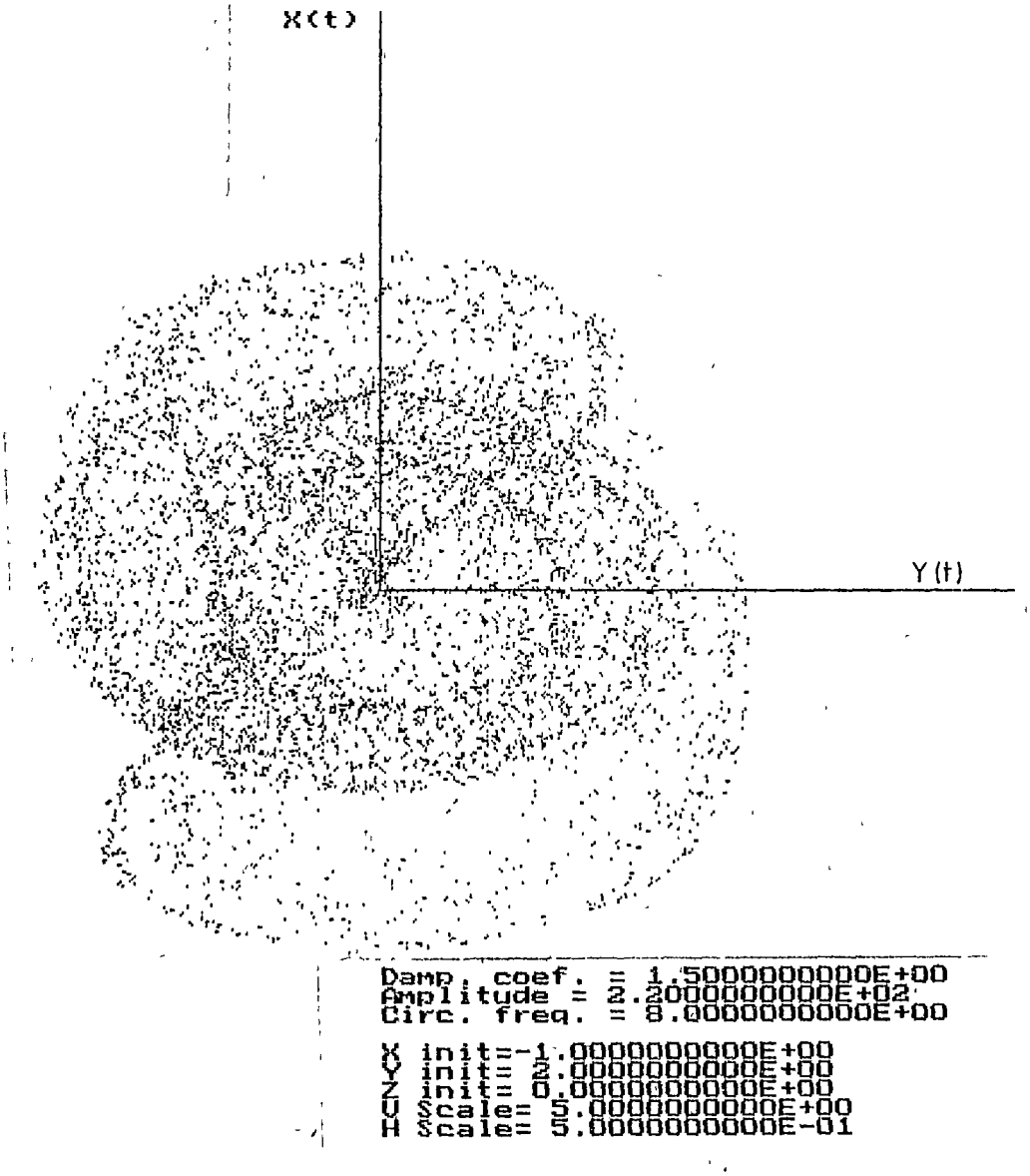
X(t)
Y(t)
Damp. coef. = 1.5000000000E+00
Amplitude = 2.2000000000E+02
Circ. freq. = 8.0000000000E+00
X init=-1.0000000000E+00
Y init= 2.0000000000E+00
Z init= 0.0000000000E+00
V Scale= 5.0000000000E+00
H Scale= 5.0000000000E-01

Fig. 18

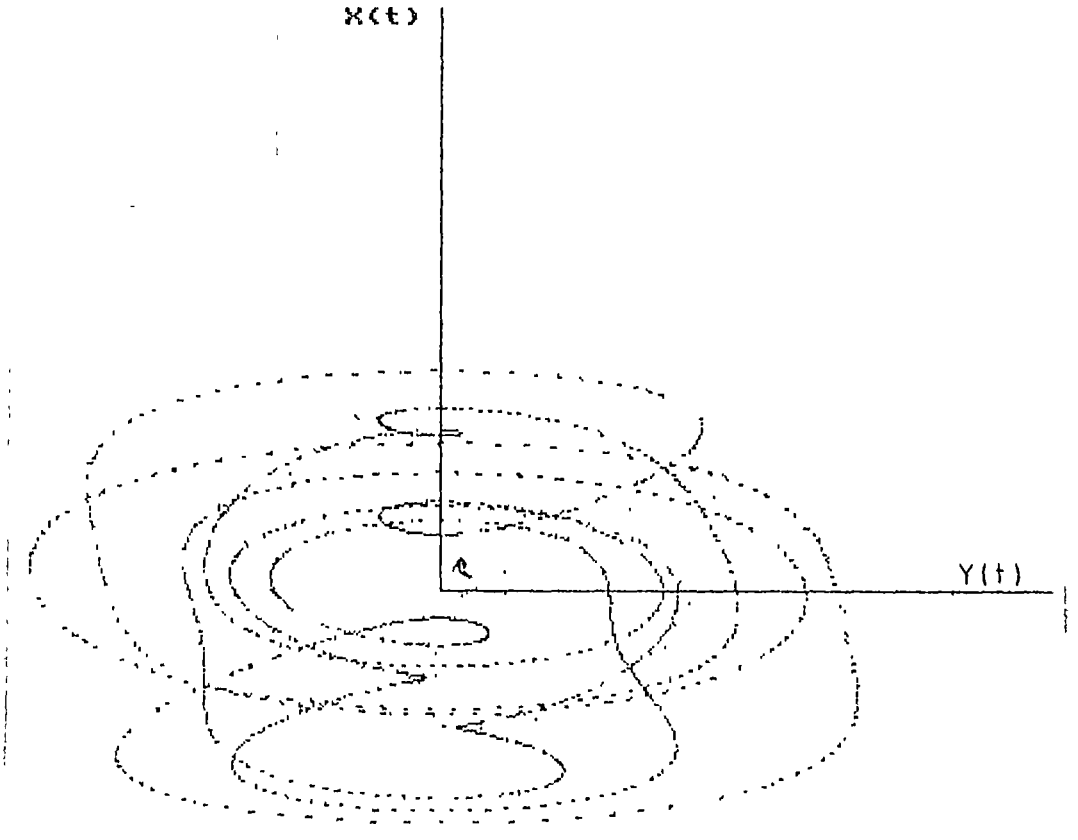


```
Damp. coef. = 1.5000000000E+00
Amplitude = 2.9000000000E+02
Circ. freq. = 8.0000000000E+00

X init=-1.0000000000E+00
Y init= 2.0000000000E+00
Z init= 0.0000000000E+00
V $cale= 3.0000000000E+00
H $cale= 5.0000000000E-01
```

Fig.19

Conclusions. This work investigated the nonlinear dynamics of a mechanical system with cubic nonlinearity and parametric excitation, by using the L L I. technique We have constructed different trajectories in the phase space as the amplitude of parametric excitation was used as a control parameter and shown that the system exhibits different chaotic behaviors The route to chaos is shown to be via period-doubling bifurcations

REFERENCES

1. H C. Schuster - Deterministic chaos, Physik-Verlag, 1984
2. Hao Bai-Lin - Chaos II, World Scientific, 1990
3. D D'Humières, M R Beasly, B A Hunberman, A Libchaber-Phys Rev 26A, 3483, 1982
4. F Moon- vol "Perspectives in Nonlinear Dynamics" World Sci , 230, 1985.
5. H I Swinney, J P Gollub-Hydrodynamic Instabilities and the Transition to Turbulence, Springer [illegible] 1981
6. A Libchaber-Proc Roy Soc London, A413, 633, 1987
7. B V Buskirk, C Jeffries-Phys Rev A31, 3332, 1985
8. C O Weiss, J Brock-Phys Rev Lett , 57, 2804, 1986
9. P A Hopf, D L Kaplan, H M Gibbs, R L Shoemaker-Phys Rev A25, 2172, 1982
10. R G Harrison, D J Biswas-Nature, 321, 394, 1986
11. M Cirillo, N F Pedersen-Phys , 90A, 150, 1982
12. E C Gwinn, R M Westervell-Phys Rev Lett Vol 54, Nr 15, 1613, 1985
13. G Cicogna-Phys Lett 131A, 98, 1988
14. C A Held, C D Jeffries-vol "Dimensions and Entropies in Chaotic Systems" editor G Mayer-Kress Springer-Verlag Berlin, p 158, 1986
15. O E. Rossler-Z Naturforsch 319, 1168, 1976
16. J C Roux, A. Rossi, S Bachelart, C Vidal-Phys Lett 77A, 391, 1980
17. M R Bassett, J L. Hudson-Physica 35D, 289, 1989.
18. L F Olsen, H Degh-Quarterly Rev. Biophys 18, 165, 1985
19. W M Schaffer-Ecology 66, 93, 1985
20. A L Goldberger, B.J West-Ann N Y Acad Sci , 504, 195, 1987
21. S P Layne, G Mayer-Kress, J Holzfuss-vol "Dimensions and Entropies [illegible] Verlag Berlin, p. 246, 1986
22. E N Lorenz-J Atmos Sci 20, 130, 1963
23. G I Baker, J P Gollub-Chaotic Dynamica, Cam
24. P Holmes-Phy l trans Roy Soc A292, 419, 1979
25. F C Moon-Phys Rev Lett, vol 53, Nr 14, 1439, 1984
26. F C Moon-Phys Rev Lett, vol 53, Nr 10, 967 1984
27. F C Moon-Chaotic Vibrations (transl in mss) Ed Mir [illegible]

28 M Iansiti, Qing Hu, R M Westervelt-Phys Rev Lett, vol 55, Nr 7, 1985
29 W Szemplinska-Stupnicka, R H Plant, J.C Hsieh-A.S M E J Apll Mech, 56, 947, 1989.
30 C H Lamarque, J M Malasoma-Eur. J Mech. A/Solids, 11, Nr 6, 781, 1992
31 T Coloşi-Regelungstechnik und Prozessdatenverbeitung München, Nr 4, S138, 1978




STUDIA UNIV BABEŞ-BOLYAI, PHYSICA, XXXVIII, 2, 1993

MASSIVE VECTOR, TENSOR AND SPIN-3/2 PARTICLES GRAVITATIONALLY SCATTERED ON SCHWARZSCHILD BACKROUND

D. ŢAŢOMIR, D. RADU, O. MIHALACHE*

Received 15 10 1993

ABSTRACT. - Using the *S*-matrix formalism and Feynman's diagram-technique, the gravitational scattering of the minimally coupled vector, tensor and spin-3/2 (Rarita-Schwinger) particles on Schwarzschild background is studied for any value of the scattering angle

We mention that accordingly to our knowledge the previous works in this branch dealed only with the small angle cases As it has been shown, in the small angle approximation and ultrarelativistic case, the differential cross-sections coincide with those corresponding to the photons, neutrinos, massless Rarita-Schwinger particles, gravitinos and gravitons, i e , the gravitational particle scattering is spin independent, in agreement with many autors' results, obtained by other means

As particularly interesting result, we point out that the differential cross-section for scattering of the vector particles in the backward direction and ultrarelativistic case is finite and the helicity is not conserved, while, for tensor and spin-3/2 particles in the same case the differential cross-section is clearly unlimited

In this paper, using the *S*-matrix formalism and Gupta's linear approximation [1]

$$\sqrt{-g}\, g^{\mu\nu} = \eta^{\mu\nu} - k y^{\mu\nu} \tag{1}$$

where $g^{\mu\nu}$, $\eta^{\mu\nu}$ and $y^{\mu\nu}$ are the metric tensor, the Minkowski tensor - diag (+1, -1, -1, -1) -and the tensor of the weak gravitational field, respectively, $g = \det g_{\mu\nu}$ and $k = \sqrt{16\pi G}$ (in natural units, G being the Newton constant), the scattering of the massive 1, 2 and 3/2 spin particles in the external gravitational field described by Schwarzschild metric is studied Also we discuss the differential backward-cross-section as an important particular case

In order to obtain the first-order interaction Lagrangians between the gravitational and

* *"Al I. Cuza" University, Department of Physics, 6600 Iassy, Romania*

the massive vector, tensor and Rarita-Schwinger fields we use the principle of minimal coupling [2] According to this principle, for vector and tensor fields, we must add to the expression of the gravitational field Lagrangian the complex massive vector and tensor field Lagrangians written in the curved space [3, 4]

$$\mathfrak{L}_{vect} = \sqrt{-g}\left(-\frac{1}{2}g^{\mu\alpha}g^{\nu\beta}G^{*}_{\mu\nu}G_{\alpha\beta} + m^2 g^{\nu\alpha}B^{*}_{\nu}B_{\alpha}\right) \tag{2}$$

$$\mathfrak{L}_{tens} = \sqrt{-g}\, g^{\mu\rho}g^{\nu\beta}\left(g^{\lambda\alpha}H^{*}_{\mu\nu\lambda}H_{\alpha\beta\rho} + m^2\phi^{*}_{\mu\nu}\phi_{\rho\beta}\right) \tag{3}$$

It is easy to see that for the vector field we considered the Proca formalism Here $G_{\mu\nu} = B_{\nu,\mu} - B_{\mu,\nu}$ ($B_{\mu,\nu}$ being the covariant derivative of the vector field function) is the tensor of the massive vector field Concerning the tensor field we must emphasize that we followed a Schwinger's idea [5] using the third rank tensor

$$H_{\mu\nu\lambda} = \phi_{\nu\lambda,\mu} + \phi_{\mu\lambda,\nu} - \phi_{\mu\nu,\lambda} \quad , \quad \left(H_{\mu\nu\lambda} = H_{\nu\mu\lambda}\right), \tag{4}$$

where $\phi_{\mu\nu,\lambda}$ is the covariant derivative of the tensor field function We note in passing that a remarcable analogy between the massive tensor and linearized (weak) gravitational fields is revealed by this Lagrangian's choice In the case of the Rarita-Schwinger field, besides principle of minimal coupling, we also used the "vierbein" formalism [6], so that, the Lagrangian of this system can be written as follows

$$\mathfrak{L}_{R-S} = \sqrt{-g}\, g^{\mu\nu}\left[\frac{i}{2}\left(\bar{\psi}_{\mu}\nabla_{\lambda}\gamma^{\lambda}\psi_{\nu} - \bar{\psi}_{\mu}\gamma^{\lambda}\nabla_{\lambda}\psi_{\nu}\right) + m\bar{\psi}_{\mu}\psi_{\nu}\right] = \mathfrak{L}_1 + \mathfrak{L}_2, \tag{5}$$

where

$$\mathfrak{L}_1 = \sqrt{-g}\, g^{\mu\nu}\left[\frac{i}{2}\left(\bar{\psi}_{\mu,\lambda}\gamma^{\lambda}\psi_{\nu} - \bar{\psi}_{\mu}\gamma^{\lambda}\psi_{\nu,\lambda}\right) + m\bar{\psi}_{\mu}\psi_{\nu}\right] \tag{6}$$

$$\mathfrak{L}_2 = \frac{i}{8}\sqrt{-g}\, g^{\mu\nu}\bar{\psi}_\mu\left(\gamma_{\rho\lambda}\gamma^\rho\gamma^\lambda + \gamma^\lambda\gamma_{\rho\lambda}\gamma^\rho\right)\psi_\nu, \tag{7}$$

$\psi_{\mu\lambda}$ being the usual derivative of the Rarita-Schwinger field function

The above expression for $\mathfrak{L}_1$ and $\mathfrak{L}_2$ have been obtained inserting the expression of the covariant of the spin-vectors:

$$\nabla_\mu\psi_\nu = \psi_{\nu,\mu} - \Gamma_\mu\psi_\nu\ , \quad \bar{\psi}_\nu\nabla_\mu = \bar{\psi}_{\nu,\mu} + \bar{\psi}_\nu\Gamma_\mu, \tag{8}$$

where Γ_μ are the Fock-Ivanenko spin coefficients of the affine connection [7] As it is known they have the following expression:

$$\Gamma_\mu = \frac{1}{4}\gamma_{\lambda;\mu}\gamma^\lambda, \tag{9}$$

where γ^μ are the generalized Dirac matrices [8,9]:

$$\gamma^\mu = L^\mu(\alpha)\gamma(\alpha)\ , \quad \gamma_\mu = L_\mu(\alpha)\gamma(\alpha), \tag{10}$$

$\gamma(\alpha)$ being the usual Dirac matrices The expression for $\gamma_{\lambda;\mu}$ is

$$\gamma_{\lambda,\mu} = \gamma_{\lambda,\mu} - \gamma_\rho\Gamma^\rho_{\lambda\mu} \tag{11}$$

In relations (10) $L^\mu(\alpha)$ and $L_\mu(\alpha)$ are the "vierbein" coefficients satisfying the following constraints.

$$L^\mu(\alpha)L^\nu(\alpha) = g^{\mu\nu}\ , \quad L_\mu(\alpha)L_\nu(\alpha) = g_{\mu\nu} \tag{12}$$

Since all our considerations refer only to the first-order approximation we give below the "linearized" relations for the quantities which appear in calculations [4,7]

$$g^{\mu\nu} = \eta^{\mu\nu} - kh^{\mu\nu} \tag{13}$$

$$g_{\mu\nu} = \eta_{\mu\nu} + kh_{\mu\nu} \tag{14}$$

$$h^\beta_\lambda = y^\beta_\lambda - \frac{1}{2}\delta^\beta_\lambda y\ , \quad h^{\mu\nu} - \frac{1}{2}\eta^{\mu\nu}y\ , \quad y = y^\alpha_\alpha \tag{15}$$

$$\Gamma^{\rho}_{\lambda\mu} = \frac{1}{2}k\left(h^{\rho}_{\lambda,\mu} + h^{\rho}_{\mu,\lambda} - h^{\rho}_{\lambda\mu,}\right) \quad \text{(the Christoffel symbols)} \tag{16}$$

$$\gamma_{\lambda} = \gamma_{\lambda} + \frac{1}{2}k\gamma_{\beta}h^{\beta}_{\lambda}\ , \quad \gamma^{\lambda} = \gamma^{\lambda} - \frac{1}{2}k\gamma_{\beta}h^{\lambda\beta} \tag{17}$$

It is very simply to show that the $\mathfrak{L}_2$ term in (5) has no contribution in the first-order approximation Indeed we have

$$\mathfrak{L}^{(1)}_2(k) = \frac{i}{16}k\bar{\psi}_{\mu}\gamma^{\lambda}\gamma_{\alpha}\dot{\gamma}^{\rho}\psi^{\mu}\left(h^{\alpha}_{\rho\lambda} - h^{\alpha}_{\lambda,\rho}\right) = \frac{i}{16}k\bar{\psi}_{\mu}\gamma^{\lambda}\left(\gamma^{\alpha}\gamma^{\rho} - \gamma^{\rho}\gamma^{\alpha}\right)\psi^{\mu}h_{\alpha\rho,\lambda} = 0, \tag{18}$$

where the well known anticommutation rules have been used:

$$\left\{\gamma^{\lambda},\gamma^{\nu}\right\} = \gamma^{\lambda}\gamma^{\nu} + \gamma^{\nu}\gamma^{\lambda} = 2\delta^{\lambda\nu} \tag{19}$$

Taking into account the previous considerations the first-order interaction Lagrangian between the weak gravitational and the massive Rarita-Schwinger fields reads

$$\begin{aligned}\mathfrak{L}^{(1)}_{mf}(k) = &-\frac{i}{4}k\left(\bar{\psi}_{\lambda,\mu}\dot{\gamma}_{\nu}\psi^{\lambda} - \bar{\psi}_{\lambda}\gamma_{\nu}\psi^{\lambda}_{\mu}\right)h^{\mu\nu} - \\ &-\frac{i}{2}k\left(\bar{\psi}_{\mu\lambda}\gamma^{\lambda}\psi_{\nu} - \bar{\psi}_{\nu}\gamma^{\lambda}\psi_{\nu\lambda}\right)\gamma^{\mu\nu} - km\bar{\psi}_{\mu}\psi_{\nu}\gamma^{\mu\nu}\end{aligned} \tag{20}$$

Passing to the flat space

$$x^0 = t,\ x^j,\ (j = 1,2,3) \to x_j,\ (j=1,2,3),\ x_4 = it, \tag{21}$$

$$\dot{\gamma}^{\mu} \to i\gamma_{\mu},\ \gamma^0 \to \gamma_4,\ \eta^{\mu\nu} \to -\delta_{\mu\nu}, \tag{22}$$

the first-order interaction Lagrangians between the gravitational and massive vector, tensor and Rarita-Schwinger fields, respectively, are

$$\mathfrak{L}^{(1)}_{mf}(k) = -k\left(G^{*}_{\mu\nu}G_{\mu\alpha}u_{\nu\alpha} + m^2B^{*}_{\nu}B_{\alpha}\gamma_{\nu\alpha}\right) \tag{23}$$

$$\mathfrak{L}^{(1)}_{mf}(k) = k\left[H^{*}_{\mu\nu\alpha}\left(H_{\alpha\nu\lambda} + H_{\alpha\lambda\nu}\right) + k^{*}_{\nu\mu}H_{\nu\mu\lambda} - 2m^2\phi^{*}_{\mu\nu}\phi_{\mu\lambda}\right]\gamma_{\mu\lambda} -$$

$$-k\left(H_{\mu\nu\lambda}H_{\lambda\nu\mu} - \frac{1}{2}m^2\phi^{*}_{\mu\nu}\phi_{\mu\nu}\right)\nu + k\left[H^{*}_{\mu\nu\lambda}\phi_{\nu\mu}\left(h_{\lambda\rho,\rho} + h_{\nu\rho,\rho} - h_{\rho\rho,\lambda}\right) + \right. \tag{24}$$

$$+ \phi^{*}_{\rho\lambda}\left(h_{\mu\rho,\nu} + h_{\nu\rho,\mu} - h_{\mu\nu,\rho}\right) H_{\lambda\nu\mu}\Big]$$

$$\mathfrak{L}^{(1)}_{int}(k) = \frac{1}{4} k\left(\bar{\psi}_{\alpha,\nu}\gamma_{\mu}\psi_{\alpha} - \bar{\psi}_{\alpha}\gamma_{\mu}\psi_{\alpha,\nu}\right) y_{\mu\nu} - \frac{1}{4} km\bar{\psi}_{\alpha}\psi_{\alpha} y, \tag{25}$$

where

$$u_{\mu\nu} = y_{\mu\nu} - \frac{1}{4}\delta_{\mu\nu} y_{\alpha\alpha} \tag{26}$$

$$G_{\mu\nu} = B_{\nu,\mu} - B_{\mu,\nu} \; ; \; H_{\mu\nu\lambda} = \phi_{\nu\lambda,\mu} + \phi_{\mu\lambda,\nu} - \phi_{\mu\nu,\lambda} , \tag{27}$$

$B_{\mu,\nu}$ and $\phi_{\mu\nu\lambda}$ being the usual derivatives of the vector and tensor field functions, respectively. Also we have taken advantage of the Rarita-Schwinger field equation

$$\gamma_{\mu}\psi_{\alpha,\mu} = -m\psi_{\alpha} \tag{28}$$

and its adjoint

According to the standard quantum field theory the parts of the (23), (24) and (25) Lagrangians-casted into the normal form - which describe the interaction of the massive vector, tensor and 3/2-spin particles, respectively, with gravity are [4]

$$N\left[\mathfrak{L}^{(1)}_{vec-g}(x)\right] = -k\left[G^{*(-)}_{\mu\nu}(x)\, G^{(+)}_{\mu\alpha}(x)\, u^{ext}_{\nu\alpha}(x) + m^{2} B^{*(-)}_{\nu}(x)\, B^{(+)}_{\alpha}(x)\, y^{ext}_{\nu\alpha}(x)\right] \tag{29}$$

$$N\left[\mathfrak{L}^{(1)}_{tens-g}(x)\right] = k\{\phi^{*(-)}_{\alpha\nu,\mu}(x)\left[3\phi^{(+)}_{\lambda\nu,\alpha}(x) - \phi^{(+)}_{\lambda\alpha,\nu}(x) - \phi^{(+)}_{\nu\alpha,\lambda}(x)\right] + \phi^{*(-)}_{\alpha\mu,\nu}(x) \times$$

$$\times\left[\phi^{(+)}_{\lambda\nu,\alpha}(x) + \phi^{(+)}_{\lambda\alpha,\nu}(x) + \phi^{(+)}_{\alpha\nu,\lambda}(x)\right] + \phi^{(+)}_{\mu\nu,\alpha}(x)\left[\phi^{(+)}_{\alpha\lambda,\nu}(x) + \phi^{(+)}_{\alpha\nu,\lambda}(x) - 3\phi^{(+)}_{\lambda\nu,\alpha}(x)\right] -$$

$$- 2m^{2}\phi^{*(-)}_{\mu\nu}(x)\phi^{(+)}_{\lambda\nu}(x)\} y^{ext}_{\mu\lambda}(x) - k\{\left[\phi^{*(-)}_{\lambda\nu,\mu}(x) + \phi^{*(+)}_{\lambda\mu,\nu}(x) - \phi^{*(+)}_{\mu\nu,\lambda}(x)\right] \times \tag{30}$$

$$\times\left[\phi^{(+)}_{\mu\nu,\lambda}(x) + \phi^{(+)}_{\mu\lambda,\nu}(x) - \phi^{(+)}_{\lambda\nu,\mu}(x)\right] - \frac{1}{2} m^{2}\phi^{*(-)}_{\mu\nu}(x)\,\phi^{(+)}_{\mu\nu}(x)\} y^{ext}(x) +$$

$$+k\left\{\left[\phi^{*(-)}_{\lambda\nu,\mu}(x)+\phi^{*(+)}_{\lambda\mu,\nu}(x)\right]\phi^{(+)}_{\mu\delta}(x)\left[h^{ext}_{\lambda\alpha,\nu}(x)+h^{ext}_{\nu\alpha,\lambda}(x)-h^{ext}_{\lambda\nu,\alpha}(x)\right]+\right.$$

$$\left.+\phi^{*(-)}_{\alpha\lambda}(x)\left[\phi^{(+)}_{\mu\nu,\lambda}(x)+\phi^{(-)}_{\mu\lambda,\nu}(x)-\phi^{(+)}_{\lambda\nu,\mu}(x)\right]\left[h^{ext}_{\mu\alpha,\nu}(\lambda)+h^{ext}_{\nu\alpha,\mu}(x)-h^{ext}_{\mu\nu,\alpha}(x)\right]\right\}$$

$$N\left[\underset{R}{\varrho}{}^{(1)}_{S-g}(x)\right]=\frac{1}{4}k\left[\bar{\psi}^{(-)}_{\alpha,\nu}(x)\gamma_\mu\psi^{(+)}_{\alpha}(x)-\bar{\psi}^{(-)}_{\alpha}(x)\gamma_\mu\psi^{(+)}_{\alpha,\nu}(x)\right]y^{ext}_{\mu\nu}(x)-$$

$$-\frac{1}{4}km\bar{\psi}^{(-)}_{\alpha}\psi^{(+)}_{\alpha}(x)\,y^{ext}(x) \qquad (31)$$

The processes are described by the following Feynman's diagram type, where p and (r) and also p' and (s) are the four-momenta and polarization indices (r,s = 1 to $2s+1$, where s is the spin of the particle) of the initial and final particles, and q is the four momentum of the virtual graviton

Fig 1 The wavy line represents a graviton

The solid lines represent either vector,

tensor or spin-3/2 quanta

Using the S-matrix formalism we deduced the Feynman-type rules for diagrams in the external gravitational field (described by Schwarzschild metric) which allowed us to calculate the matrix element $<p'|S|p>$ in the mentioned approximation.

Thus we find that [4].

$$u^{ext}_{\mu\nu}(\vec{q})=\left[\delta_{\mu'}\delta_{\nu'}-\frac{1}{4}\delta_{\mu\nu}\right]y^{ext}(\vec{q}) \qquad (32)$$

$$v^{ext}_{\mu\nu}(\vec{q})=\delta_{\mu'}\delta_{\nu'}y^{ext}(\vec{q}) \qquad (33)$$

$$h^{ext}_{\mu\nu,\alpha}(\vec{q})=\left[\delta_{\mu'}\delta_{\nu'}-\frac{1}{2}\delta_{\mu\nu}\right]y^{ext}_{\alpha}(\vec{q}) \qquad (34)$$

$$y^{ext}_{,\alpha}(\vec{q})=i\delta_{\alpha j}q_j y^{ext}(\vec{q})\ ,\ (i=\sqrt{-1}) \qquad (35)$$

Taking into account the Fourier transform of the static external gravitational potential

$$y^{ext}(\vec{q}) = \frac{1}{(2\pi)^{3/2}}\int e^{-i\vec{q}\vec{x}}\frac{kM}{4\pi|\vec{x}|}d^3x = \frac{kM}{(2\pi)^{3/2}|\vec{q}|^2}, \tag{36}$$

(where M is the mass of the central body that creates the gravitational field and $|\vec{x}|$ is the distance to this centre), the matrix elements in the external field approximation, corresponding to the diagram in fig 1 are respectively

$$S^{(1)}_{p'p} = <p'|S|p> = \frac{-ik^2M}{2(2\pi)^2\sqrt{p_0'p_0}}\int\frac{\delta(q_0)}{|\vec{q}|^2}\{\left[e^{(s)}_{\nu}(\vec{p}')p'_{\mu} - 2^{(s)}_{\mu}(\vec{p}')p'_{\nu}\right]\left[e^{(r)}_{\alpha}(\vec{p})p_{\mu} - e^{(r)}_{\mu}(\vec{p}')p_{\alpha}\right]\times$$

$$\times\left(\delta_{\nu\alpha'}\delta_{\alpha\nu'} - \frac{1}{4}\delta_{\nu\alpha}\right) + m^2e^{(s)}_{\nu}(\vec{p}')e^{(r)}_{\alpha}(\vec{p})\delta_{\nu\nu'}\delta_{\alpha\alpha'}\}\delta(\vec{p}'-\vec{p}-\vec{q})\,d^3q = F(p',p)\delta(p_0'-p_0) \tag{37}$$

$$S^{(2)}_{p'p} = <p'|S|p> = \frac{-ik^2M}{2(2\pi)^2\sqrt{p_0'p_0}}\int\frac{\delta(q_0)}{|\vec{q}|^2}\{[e^{(s)}_{\alpha\nu}(\vec{p}')p'_{\mu}\left(3e^{(r)}_{\lambda\nu}(\vec{p})p_{\alpha} - e^{(r)}_{\lambda\alpha}(\vec{p})p_{\nu} - e^{(r)}_{\nu\alpha}(\vec{p})p_{\lambda}\right) +$$

$$+ e^{(s)}_{\alpha\mu}(\vec{p}')p'_{\nu}\left(e^{(r)}_{\lambda\nu}(\vec{p})p_{\alpha} + e^{(r)}_{\lambda\alpha}(\vec{p})p_{\nu} + e^{(r)}_{\alpha\nu}(\vec{p})p_{\lambda}\right) + e^{(s)}_{\mu\nu}(\vec{p}')p'_{\lambda}(e^{(r)}_{\alpha\lambda}(\vec{p})p_{\nu} + e^{(r)}_{\alpha\nu}(\vec{p})p_{\lambda} -$$

$$- 3e^{(r)}_{\lambda\nu}(\vec{p})p_{\alpha}) - 2m^2e^{(s)}_{\mu\nu}(\vec{p}')e^{(r)}_{\lambda\nu}(\vec{p})]\delta_{\mu\alpha'}\delta_{\lambda\alpha} - [\left(e^{(s)}_{\lambda\nu}(\vec{p}')p'_{\mu} + e^{(s)}_{\lambda\mu}(\vec{p}')p'_{\nu} - e^{(s)}_{\mu\nu}(\vec{p}')p'_{\lambda}\right)\times$$

$$\times\left(e^{(r)}_{\mu\nu}(\vec{p})p_{\lambda} + e^{(r)}_{\mu\lambda}(\vec{p})p_{\nu} - e^{(r)}_{\lambda\nu}(\vec{p})p_{\mu}\right) - \frac{1}{2}m^2e^{(s)}_{\mu\nu}(\vec{p}')e^{(r)}_{\mu\nu}(\vec{p})] + [(e^{(s)}_{\lambda\nu}(\vec{p}')p'_{\mu} + e^{(s)}_{\lambda\nu}(\vec{p}')p'_{\nu} -$$

$$- e^{(s)}_{\mu\nu}(\vec{p}')p'_{\lambda})e^{(r)}_{\mu\alpha}(\vec{p})\left(\left(\delta_{\lambda\alpha'}\delta_{\alpha\nu'} - \frac{1}{2}\delta_{\lambda\alpha}\right)\delta_{\nu j} + \left(\delta_{\nu\alpha'}\delta_{\alpha\nu'} - \frac{1}{2}\delta_{\nu\alpha}\right)\delta_{\lambda j} - \left(\delta_{\lambda\alpha'}\delta_{\alpha\nu'} - \frac{1}{2}\delta_{\lambda\nu}\right)\delta_{\alpha j}\right) -$$

$$- e^{(s)}_{\alpha\lambda}(\vec{p}')\left(e^{(r)}_{\mu\nu}(\vec{p})p_{\lambda} + e^{(r)}_{\mu\lambda}(\vec{p})p_{\nu} - e^{(r)}_{\lambda\nu}(\vec{p})p_{\mu}\right)\left(\left(\delta_{\mu\alpha'}\delta_{\alpha\nu'} - \frac{1}{2}\delta_{\mu\nu}\right)\delta_{\alpha j} + \left(\delta_{\nu\alpha'}\delta_{\alpha\nu'} - \frac{1}{2}\delta_{\nu\alpha}\right)\times\right.$$

$$\left.\times\ \delta_{\mu j} - \left(\delta_{\mu\alpha'}\delta_{\nu\nu'} - \frac{1}{2}\delta_{\mu\nu}\right)\delta_{\alpha j}\right)]q_j\}\delta(\vec{p}'-\vec{p}-\vec{q})\,d^3q = F(p',p)\delta(q_0) \tag{38}$$

$$S^{(3/2)}_{p'\rho'} = \langle p'|S|p\rangle = \frac{ik^2mM}{4(2\pi)^2\sqrt{p_0' p_0}}\int\frac{\delta(q_0)}{|\vec{q}|^2}\{[ip_\nu'\bar{u}^{(s)}_\alpha(\vec{p}')\gamma_\mu u^{(r)}_\alpha(\vec{p})\delta_{\mu'}\delta_{\nu'} +$$

$$+ i\bar{u}^{(s)}_\alpha(\vec{p}')\gamma_\mu p_\nu u^{(r)}_\alpha(\vec{p})\delta_{\mu'}\delta_{\nu'} + m\bar{u}^{(s)}_\alpha(\vec{p}')u^{(r)}_\alpha(\vec{p})]\delta(\vec{p}'-\vec{p}-\vec{q})\}d^3q = \tag{39}$$

$$= F(p',p)\delta(p_0'-p_0),$$

where $e^{(r)}_\mu(\vec{p})$, $e^{(r)}_{\mu\nu}(\vec{p})$, $u^{(r)}_\mu(\vec{p})$, $\left[\bar{u}^{(r)}_\mu(\vec{p}) = u^{(r)*}_\mu(\vec{p})\gamma_4\right]$ and p_0 on the one hand, and $e^{(s)}_\mu(\vec{p}')$, $e^{(s)}_{\mu\nu}(\vec{p}')$, $u^{(s)}_\mu(\vec{p}')$, $\left[\bar{u}^{(s)}_\mu(\vec{p}') = u^{(s)*}_\mu(\vec{p}')\gamma_4\right]$ and p_0' on the other hand are the vectors, tensors, spin-vectors and the energy of the initial and final particles, respectively, and $q_0 = p_0' - p_0 = 0$ states for the energy conservation law We have denoted by the common notations m,p and p_0 the characteristical quantities (the mass, 4-momentum and the energy) for the all three fields respectively

The differential cross-section is given by the well known expression

$$d\sigma = (2\pi)^2 \langle \sum_{fsp} |F(p',p)|^2 \rangle_{isp}\, p_0^2\, d\Omega, \tag{40}$$

where $d\Omega = 2\pi \sin\theta\, d\theta$, θ being the scattering angle In order to evaluate the differential cross-section we must find the expression for $\langle \sum_{fsp} |F(p',p)|^2 \rangle_{isp}$ For $|F(p',p)|^2$ we get from (37), (38) and (39) relations respectively

$$|F(p',p)|^2 = \left(\frac{k^2M}{8(2\pi)^2 p_0 \vec{p}^2 \sin^2\frac{\theta}{2}}\right)\left[Q_{vect}(p',p)\right]^2 \tag{41}$$

$$|F(p',p)|^2 = \left(\frac{k^2M}{8(2\pi)^2 p_0 \vec{p}^2 \sin^2\frac{\theta}{2}}\right)^2\left[Q_{tens}(p',p)\right]^2 \tag{42}$$

$$|F(p',p)|^2 = \left(\frac{k^2mM}{16(2\pi)^2 p_0 (p_0^2-m^2)\sin^2\frac{\theta}{2}}\right)^2 |\bar{u}^{(s)}(p')\ldots$$

where t is given by

$$t = 2(\gamma_4 p_0 - im$$

Then, the expression $<\sum_{f,sp}|F(p',p)|^2>_{i,sp}$ for vector, tensor and respectively Rarita-Schwinger fields are

$$<\sum_{f,sp}|F(p',p)|^2>_{i,sp}=\left(\frac{k^2M}{8(2\pi)^2p_0(p_0^2-m^2)\sin^2\frac{\theta}{2}}\right)^2\left(\frac{1}{3}\sum_{pol}Q^2_{vect}\right) \tag{45}$$

$$<\sum_{f,sp}|F(p',p)|^2>_{i,sp}=\left(\frac{k^2M}{8(2\pi)^2p_0(p_0^2-m^2)\sin^2\frac{\theta}{2}}\right)^2\left(\frac{1}{5}\sum_{pol}Q^2_{tens}\right) \tag{46}$$

$$\begin{aligned}<\sum_{f,sp}|F(p',p)|^2>_{i,sp}&=\left(\frac{k^2mM}{16(2\pi)^2p_0(p_0^2-m^2)\sin^2\frac{\theta}{2}}\right)^2\frac{1}{4}\sum_{r,s=1}^{4}|\bar{u}^{(s)}_{\alpha}(\vec{p}')tu^{(r)}_{\alpha}(\vec{p})|^2=\\&=\left(\frac{k^2mM}{16(2\pi)^2p_0(p_0^2-m^2)\sin^2\frac{\theta}{2}}\right)^2\left(\frac{1}{4}\sum_{pol}Q^2_{R-S}\right),\end{aligned} \tag{47}$$

where $\sum_{pol}Q^2_{vect}$, $\sum Q^2_{tens}$ and $\sum_{pol}Q^2_{R-S}$ are the polarization sums for the vector, tensor and Rarita-Schwinger fields and because they have a long enough expressions we prefer not to give then here

In order to evaluate the polarization sums we take into account that the polarization vectors, tensors and spin-vectors, respectively, satisfy the relations [5, 10]

$$\sum_{\lambda=1}^{3}e^{(\lambda)}_{\mu}(\vec{p})\,e^{(\lambda)}_{\nu}(\vec{p})=d_{\mu\nu},\ \mu,\nu=1\ \text{to}\ 4 \tag{48}$$

$$\Pi_{\mu\nu\lambda\rho}=\sum_{r=1}^{5}e^{(r)}_{\mu\nu}(\vec{p})e^{(r)}_{\lambda\rho}(\vec{p})=\frac{1}{2}(d_{\mu\lambda}d_{\nu\rho}+d_{\mu\rho}d_{\nu\lambda})-\frac{1}{3}d_{\mu\nu}d_{\lambda\rho} \tag{49}$$

$$\sum_{r=1}^{4}u^{(r)}_{\mu}(\vec{p})\bar{u}^{(r)}_{\nu}(\vec{p})=\frac{\gamma_\alpha p_\alpha+im}{2im}\left[\delta_{\mu\nu}-\frac{1}{3}\gamma_\mu\gamma_\nu+\frac{i}{3m}(\gamma_\mu p_\nu-\gamma_\mu p_\mu)+\frac{2}{3m^2}p_\mu p_\nu\right]. \tag{50}$$

where $d_{\mu\nu}$ is given by. $d_{\mu\nu} = \delta_{\mu\nu} + \frac{p_\mu p_\nu}{m^2}$

After a laborious calculus, for the differential cross-section of the massive vector, tensor and Rarita-Schwinger particles one obtains the following expressions, respectively

$$d\sigma = \left(\frac{k^2 M}{16\pi}\right)^2 \frac{d\Omega}{\sin^4\frac{\theta}{2}} \left[\left(\frac{1+v^2}{2v^2}\right)^2 - \frac{2}{3}\sin^2\frac{\theta}{2}\left(\frac{2}{v^2} - \sin^2\frac{\theta}{2}\right)\right] \tag{51}$$

$$d\sigma = \left(\frac{k^2 M}{16\pi}\right)^2 \frac{d\Omega}{\sin^4\frac{\theta}{2}} \{\left(\frac{1+v^2}{2v^2}\right)^2 - \frac{4}{v^2}\sin^2\frac{\theta}{2} + \frac{2}{45(1-v^2)^4}\sin^4\frac{\theta}{2}[9(31 -$$

$$- 108v^2 + 146v^4 - 92v^6 + 23v^8) + 48v^2(7 - 18v^2 + 19v^4 - 8v^6)\sin^2\frac{\theta}{2} - \tag{52}$$

$$- 24v^4(5 - 6v^2 - 11v^4)\sin^4\frac{\theta}{2} - 192v^6(1 + v^2)\sin^6\frac{\theta}{2} + 128v^8\sin^8\frac{\theta}{2}]\}$$

$$d\sigma = \left(\frac{k^2 M}{16\pi}\right)^2 \frac{d\Omega}{\sin^4\frac{\theta}{2}} \{\left(\frac{1+v^2}{2v^2}\right)^2 - \frac{1}{36v^4(1-v^2)^2}[v^2(15 - 41v^2 + 5v^4 + 21v^6)\sin^2\frac{\theta}{2} + \tag{53}$$

$$+ 4v^4(3 - 6v^2 - 5v^4)\sin^4\frac{\theta}{2} + 8v^6(3 + v^2)\sin^6\frac{\theta}{2}]\},$$

where we denoted by v the $\frac{|\vec{p}|}{p_0}$ ratio

We shall notice that in the small angle approximation the polarization sums become

$$\sum_{pol} Q^2_{vect} = 3\vec{p}^4\left(\frac{1+v^2}{2v^2}\right)^2 \tag{54}$$

$$\sum_{pol} Q^2_{tens} = 5\vec{p}^4\left(\frac{1+v^2}{2v^2}\right)^2 \tag{55}$$

$$\sum_{pol} Q^2_{R-S} = 4p_0^2 \frac{(1+v^2)^2}{1-v^2} \tag{56}$$

Taking into account the previous relations, the differential cross-sections in the small angle approximation become

$$d\sigma_{small\theta} = \left(\frac{k^2 M}{16\pi}\right)^2 \frac{d\Omega}{\sin^4\frac{\theta}{2}} \left(\frac{1+v^2}{2v^2}\right) = d\sigma_{Ruth}\,, \tag{57}$$

i e , they are the differential cross-sections of Rutherford type As we can see from (51), (52) and (53) the expression for $d\sigma_{Ruth}$ is contained by these relations as a first term Since this term (i e $d\sigma_{Ruth}$) is quite the differential cross-section for the massive scalar particles (for instance the scalar mesons) we can interpret the second term in the (51), (52) and (53) relations as being the spin contribution of the vector, tensor and Rarita-Schwinger particles, respectively

A particular interest is presented by the back-scattering limit case In this special limit case we have worked out respectively

$$d\sigma^*_{vect} = \left(\frac{k^2 M}{16\pi}\right)^2 \left[\left(\frac{1+v^2}{2v^2}\right)^2 - \frac{2}{3}\frac{2-v^2}{v^2}\right] d\Omega^* \tag{58}$$

$$d\sigma^*_{tens} = \left(\frac{k^2 M}{16\pi}\right)^2 \frac{d\Omega^*}{180v^4(1-v^2)^4} \times \tag{59}$$

$$\times\ (45 - 810v^2 + 5067v^4 - 9228v^6 + 5475v^8 - 522v^{10} + 229v^{12})$$

$$d\sigma^*_{R\ s} = \left(\frac{k^2 M}{16\pi}\right)^2 \frac{9 - 6v^2 + 5v^4}{36v^4(1-v^2)} d\Omega\,, \tag{60}$$

where $d\sigma^* = d\sigma_{l.s.}$ and $d\Omega^* = 2\pi d\theta$

In the ultrarelativistic case ($v \to 1$) we get from (58)

$$\frac{d\sigma^*_{vect}}{d\Omega^*} = \frac{1}{3}(GM)^2 \qquad (UR) \tag{61}$$

i e , in the back-scatterıng and ultrarelativistic case, the differential cross-section $\frac{d\sigma^*}{d\Omega^*}$ for the vector field only (!) is constant (and non-zero), which means that in this case the helicity of the particles is not conserved, in agreement with [11].

Finally it's worthwhile to point out that in the small angle approximation, the differential cross-sections for scattering in Schwarzschild field of massive scalar, vector, spinor, Rarita-Schwinger and tensor particles have the same form and in ultrarelativistic case they coincide with those corresponding to the neutrinos, photons, gravitons and gravitinos, i.e , the gravitational particle scattering in this limit case is spin-independent [12, 13], in agreement with many authors' results, obtained by other means [14]

REFERENCES

1. S. Gupta, Proc Phys Soc. A 65, 161, 608, 1952.
2. De Witt B., Phys. Rev , 160, 1113, 1967 162, 1195, 1967. 162, 1239, 1967.
3. D. Tatomir, An. sc Univ. "Al.I.Cuza" Iaşi (n s), section I b, phys , tom XXIV, p 91, 1978.
4. D. Tatomir, "Contributions in Quantum Study of the Particles Interaction in the Presence of Gravitation" - Ph. D. Thesis, "Al I Cuza" Univ , Iaşi, 1981 (to be published)
5. J. Schwinger, "Particles, Sources and Fields", Addison-Wesley Publishing Company, 1970 (printed in U.S.A)
6. V Fock and D Ivanenko. C r. Acad. Sci , 188, 1470, 1929.
7. N Mitskevich, "Fiz polia v O T.O ", Izd.-vo "Nauka", Moskva, 1969.
8. R. Lias, Tr. Inst. fiz astr., ANESSR, Nr. 5, 25, 1957
9. Iu. Vladimirov, Izv. V.U Zov , Fizika, Nr 2, 133, 1963.
10. D Lurie, "Particles and Fields", J.Willey & Sons, New-York, 1968
11. W De Logi and S Kovacs, Phys. Rev , D, v. 16, Nr 2, 237, 1977.
12. D. Tatomir: "Abstracts of Contributed Papers for the Discussion Groups" Jena Univ , 14-19 July, 1980
13. D. Tatomir, "10-th International Conference in G R.G ", Padova, 4-9 July, 1983, Contributed Papers, 140
14. K Lotze, Acta Phys. Pol., B 9, 665, 677, 1978

STUDIA UNIV. BABEŞ-BOLYAI, PHYSICA, XXXVIII, 2, 1993

FOURTH ORDER TORSION L-TENSOR FORMULAS FOR ANHARMONIC FORCE CONSTANT TRANSFORMATION

T.A. BEU*

Received 15 12 1993

ABSTRACT. - New fourth order analytical torsion L-tensors are reported, which complete previously published third order expressions The formulas up to the third order are used in molecular normal mode analysis calculations for the nonlinear transformation of the force constants from internal coordinates to normal coordinates Sample calculations are presented

1. Introduction. Although, due to the advances in computer techniques, most of the computational effort of molecular normal mode analysis applications has been transferred to numerical methods, for large problems it may be still preferable to use analytical formulas for the L-tensors involved in the transformation of the force constants from internal- to normal coordinates, instead of numerically deriving the internal coordinates with respect to the normal coordinates, according to the definition of the L-tensors

L-tensors formulas for all elementary internal valence coordinates are available The torsional coordinates, however, require an especially delicate mathematical treatment, and give rise to the most complicated expressions. Formulas for planar equilibrium configurations [1], and more recently, general formulas [2] have been reported Alternative torsion L-tensor formulas have been presented in [3] (hereafter referred to as Paper I), which, in contrast to the analytical results of [2], are more compact, implying scalar operations with trigonometric functions instead of cumbersome vector operations

* *"Babeş-Bolyai" University, Faculty of Physics, 3400 Cluj-Napoca, Romania*

It is the purpose of this paper to present new fourth order torsion L-tensors, which complete the set reported in Paper I Due to the complexity of the calculations, extensive use was made of the symbolic computation package *Mathematica* The expressions up to the third order are equivalent to those of Paper I Results for methanol and hydrazine, obtained by the numerical implementation of these expressions, are presented and compared with similar results from the literature

2. Equations. The Taylor expansion of the potential energy with respect in terms of curvilinear internal displacement coordinates may be written as [1]

$$V = \frac{1}{2}\sum_{i,j} F_{ij} R_i R_j + \frac{1}{6}\sum_{i,j,k} F_{ijk} R_i R_j R_k + \frac{1}{24}\sum_{i,j,k,l} F_{ijkl} R_i R_j R_k R_l + \quad , \tag{1}$$

where the force constants F_{ij}, F_{ijk} and F_{ijkl} are the 2nd, 3rd and 4th derivatives of the potential energy to the coordinates R_i, referred to the equilibrium configuration of the molecule In order to perform a normal mode analysis, the vibrational-rotational Hamiltonian is, however, conveniently expressed in terms of the normal coordinates Q_r

$$V = \frac{1}{2}\sum_{r} \lambda_r Q_r^2 + \frac{1}{6}\sum_{r,s,t} \phi^{rst} Q_r Q_s Q_t + \frac{1}{24}\sum_{r,s,t,u} \phi^{rstu} Q_r Q_s Q_t Q_u + \quad , \tag{2}$$

where $\lambda_r = 4\pi^2 c^2 \omega_r^2$

The internal coordinates R_i can be expressed in terms of normal coordinates Q_r a nonlinear transformation

$$R_i = \sum_r L_i^r Q_r + \sum_{r,s} L_i^{rs} Q_r Q_s + \sum_{r,s,t} L_i^{rst} Q_r Q_s Q_t + \quad , \tag{3}$$

where the elements of the L-tensor, $L_i^r, L_i^{rs}, L_i^{rst}$, , have to be interpreted as first-, second-, and third order derivatives of the internal coordinate R_i with respect to normal coordinates

The formulas for the transformation of the force constants from internal-, to normal coordinates (including only L-tensors up to the third order) may be readily obtained by substituting (3) in (1), and comparing the result with (2)

$$\lambda_r = \sum_{i,j} F_{ij} L_i^r L_j^r$$

$$\phi^{rst} = \sum_{i,j,k} F_{ijk} L_i^r L_j^s L_k^t + \sum_{i,j} F_{ij} \left(L_i^{rs} L_j^t + L_i^{rt} L_j^s + L_i^{st} L_j^r \right)$$

$$\begin{aligned} \phi^{rstu} = & \sum_{i,j,k,l} F_{ijkl} L_i^r L_j^s L_k^t L_l^u \\ & + \sum_{i,j,k} F_{ijk} \left(L_i^{rs} L_j^t L_k^u + L_i^{rt} L_j^s L_k^u + L_i^{ru} L_j^s L_k^t \right. \\ & \qquad \left. + L_i^{st} L_j^r L_k^u + L_i^{su} L_j^r L_k^t + L_i^{tu} L_j^r L_k^s \right) \\ & + \sum_{i,j} F_{ij} \left(L_i^{rs} L_j^{tu} + L_i^{rt} L_j^{su} + L_i^{ru} L_j^{st} \right. \\ & \qquad \left. + L_i^{rstu} L_j^u + L_i^{rsu} L_j^t + L_i^{rtu} L_j^s + L_i^{stu} L_j^r \right) \end{aligned}$$

As stated above, it is only the case of torsional coordinates we are dealing with in what follows The torsion coordinate involves four atoms If the atoms *a*, *b*, *c*, and *d* are linked by the bond vectors $r_i = ab$, $r_j = bc$ and $r_k = cd$, the torsion coordinate τ is defined as the dihedral angle between the planes abc and bcd The torsion "*displacement*" coordinate R_{ijk}, which is actually used as a normal coordinate, may then be defined as the difference

between the torsion coordinate and the corresponding equilibrium value τ_e

$$R_{ijk} = \tau - \tau_e = \arccos\left[\frac{(e_i \times e_j)\cdot(e_j \times e_k)}{\sin\phi_{ij}\sin\phi_{jk}}\right] - \tau_e, \tag{4}$$

where e_i, e_j, e_k are the unit vectors of the three bonds

The torsion L-tensor may be set up, as already pointed out, from the derivatives of the torsion displacement coordinate with respect to the normal coordinates The relations for the first four orders are

$$L_{ijk}^{r} = \frac{\partial R_{ijk}}{\partial Q_r}, L_{ijk}^{rs} = \frac{\partial^2 R_{ijk}}{\partial Q_r \partial Q_s}, L_{ijk}^{rst} = \frac{\partial^3 R_{ijk}}{\partial Q_r \partial Q_s \partial Q_t}, L_{ijk}^{rstu} = \frac{\partial^4 R_{ijk}}{\partial Q_r \partial Q_s \partial Q_t \partial Q_u} \tag{5}$$

In order to avoid the complications implied by repeatedly deriving the mixed vector product from the expression of the torsion displacement given by (4), we transform R_{ijk} making use of the well-known Lagrange identity

$$(a \times b)\cdot(c \times d) = (a\cdot c)(b\cdot d) - (b\cdot c)(a\cdot d)$$

Relating the obtained scalar products of the unit vectors to the angles defined by them

$$e_i \cdot e_j = -\cos\phi_{ij}, \quad e_j \cdot e_k = -\cos\phi_{jk}, \quad e_i \cdot e_k = \cos\phi_{ik},$$

the torsion displacement coordinate becomes

$$R_{ijk} = \arccos\left(\frac{\cos\phi_{ij}\cos\phi_{jk} - \cos\phi_{ik}}{\sin\phi_{ij}\sin\phi_{jk}}\right) - \tau_e \tag{6}$$

As one may notice, the angle ϕ_{ik} between the non-adjacent bonds i and k appears in the above relation, as well

In performing the operations required to derive the expressions of the torsion L

tensors, it is useful to keep in mind the definition of the first order angle bending L-tensor

$$L_{ij}^{r} = \frac{\partial \phi_{ij}}{\partial Q_r} \tag{7}$$

which, coming from the derivatives of the angles ϕ_{ij}, ϕ_{jk} and ϕ_{ik}, respectively, will enter in the expression of all torsion L-tensor

In order to simplify the expressions of the torsion L-tensors, we define the following auxiliary tensors

$$S_{ij}^{r} = L_{ij}^{r}/\sin\phi_{ij}, \tag{8}$$

$$T_{ijk}^{r} = S_{ij}^{r}\cos\phi_{ij} + S_{jk}^{r}\cos\phi_{jk}, \tag{9}$$

$$U_{ijk}^{rs} = S_{ij}^{r}S_{ij}^{s} + S_{jk}^{r}S_{jk}^{s}, \tag{10}$$

$$V_{ijk}^{rsl} = S_{ij}^{r}S_{ij}^{s}S_{ij}^{l}\cos\phi_{ij} + S_{jk}^{r}S_{jk}^{s}S_{jk}^{l}\cos\phi_{jk} \tag{11}$$

T_{ijk}^{r}, U_{ijk}^{rs} and V_{ijk}^{rsl} are obviously symmetric with respect to the index pairs "ij" and "jk"

The formulas for the torsion L-tensors yielded by *Mathematica* (according to the definitions (5)) are obtained employing a rather elaborate set of expression manipulation rules, which allow for massive simplification of the relations, use being made of the expressions of the already determined lower order tensors Here are the resulting formulas for the first order L-tensor

$$L_{ijk}^{r} = T_{ijk}^{r}\cot\tau_e + \csc\tau_e\left[L_{ij}^{r}\cot\phi_{jk} + L_{jk}^{r}\cot\phi_{ij} - \frac{L_{ik}^{r}\sin\phi_{ik}}{\sin\phi_{ij}\sin\phi_{jk}}\right], \tag{12}$$

the second order tensor

$$\begin{aligned} L_{ijk}^{rs} = {} & -L_{ijk}^{s}T_{ijk}^{r} - \cot\tau_e\left(L_{ijk}^{r}L_{ijk}^{s} + U_{ijk}^{rs}\right) \\ & - \csc\tau_e\left[\frac{L_{jk}^{r}S_{ij}^{s}}{\sin\phi_{ij}} + \frac{L_{ij}^{r}S_{jk}^{s}}{\sin\phi_{jk}} + \frac{L_{ik}^{r}}{\sin\phi_{ij}\sin\phi_{jk}}\left(L_{ik}^{s}\cos\phi_{ik} - T_{ijk}^{s}\sin\phi_{ik}\right)\right], \end{aligned} \tag{13}$$

the third order tensor

$$
\begin{aligned}
L_{ijk}^{rst} = {} & L_{ijk}^{r} L_{ijk}^{s} L_{ijk}^{t} + L_{ijk}^{s} U_{ijk}^{rt} + L_{ijk}^{t} U_{ijk}^{rs} - L_{ijk}^{st} T_{ijk}^{r} \\
& - \operatorname{cot}\gamma_e \left[L_{ijk}^{s} L_{ijk}^{t} T_{ijk}^{r} + L_{ijk}^{r} L_{ijk}^{st} + L_{ijk}^{s} L_{ijk}^{rt} + L_{ijk}^{t} L_{ijk}^{rs} - V_{ijk}^{rst} \right] \\
& + \operatorname{csc}\gamma_e \left\{ 2\cot\phi_{ij} L_{jk}^{r} S_{ij}^{s} S_{ij}^{t} + 2\cot\phi_{jk} L_{ij}^{r} S_{jk}^{s} S_{jk}^{t} + \frac{L_{ik}^{r}}{\sin\phi_{ij} \sin\phi_{jk}} \right. \\
& \left. \times \left[\cos\phi_{ik} \left(L_{ik}^{t} T_{ijk}^{s} + L_{ik}^{s} T_{ijk}^{t} \right) + \sin\phi_{ik} \left(L_{ik}^{s} L_{ik}^{t} - T_{ijk}^{s} T_{ijk}^{t} - U_{ijk}^{st} \right) \right] \right\},
\end{aligned}
\tag{14}
$$

and finally, the fourth order L-tensor

$$
\begin{aligned}
L_{ijk}^{rstu} = {} & L_{ijk}^{r} \left(L_{ijk}^{s} L_{ijk}^{tu} + L_{ijk}^{t} L_{ijk}^{su} + L_{ijk}^{u} L_{ijk}^{st} \right) + L_{ijk}^{s} \left(L_{ijk}^{t} L_{ijk}^{ru} + L_{ijk}^{u} L_{ijk}^{rt} \right) \\
& + L_{ijk}^{t} L_{ijk}^{u} L_{ijk}^{rs} + \left(L_{ijk}^{s} L_{ijk}^{t} L_{ijk}^{u} - L_{ijk}^{stu} \right) T_{ijk}^{r} + L_{ijk}^{st} U_{ijk}^{ru} + L_{ijk}^{su} U_{ijk}^{rt} + L_{ijk}^{tu} U_{ijk}^{rs} \\
& + \operatorname{cot}\gamma_e \left[L_{ijk}^{r} L_{ijk}^{s} L_{ijk}^{t} L_{ijk}^{u} - L_{ijk}^{rs} L_{ijk}^{tu} - L_{ijk}^{rt} L_{ijk}^{su} - L_{ijk}^{ru} L_{ijk}^{st} - L_{ijk}^{r} L_{ijk}^{stu} \right. \\
& \left. - L_{ijk}^{s} L_{ijk}^{rtu} - L_{ijk}^{t} L_{ijk}^{rsu} - L_{ijk}^{u} L_{ijk}^{rst} - \left(L_{ijk}^{s} L_{ijk}^{tu} + L_{ijk}^{t} L_{ijk}^{su} + L_{ijk}^{u} L_{ijk}^{st} \right) T_{ijk}^{r} \right. \\
& - 2\left(1 + 2\cos^2\phi_{ij}\right) S_{ij}^{r} S_{ij}^{s} S_{ij}^{t} S_{ij}^{u} - 2\left(1 + 2\cos^2\phi_{jk}\right) S_{jk}^{r} S_{jk}^{s} S_{jk}^{t} S_{jk}^{u} \\
& \left. + L_{ijk}^{s} L_{ijk}^{t} U_{ijk}^{ru} + L_{ijk}^{s} L_{ijk}^{u} U_{ijk}^{rt} + L_{ijk}^{t} L_{ijk}^{u} U_{ijk}^{rs} \right] - L_{ijk}^{s} V_{ijk}^{rtu} - L_{ijk}^{t} V_{ijk}^{rsu} - L_{ijk}^{u} - L_{ijk}^{u} V_{ijk}^{rst} \\
& + \operatorname{csc}\tau_e \left\{ -2(1 + 2\cos^2\phi_{ij}) \operatorname{csc}\phi_{ij} L_{jk}^{r} S_{ij}^{s} S_{ij}^{t} S_{ij}^{u} - 2(1 + 2\cos^2\phi_{jk}) \operatorname{csc}\phi_{jk} L_{ij}^{r} S_{jk}^{s} S_{jk}^{t} S_{jk}^{u} \right. \\
& + \frac{L_{ik}^{r}}{\sin\phi_{ij} \sin\phi_{jk}} \left[\cos\phi_{ik} \left(L_{ik}^{s} L_{ik}^{t} L_{ik}^{u} - L_{ik}^{u} T_{ijk}^{s} T_{ijk}^{t} - L_{ik}^{t} T_{ijk}^{s} T_{ijk}^{u} - L_{ik}^{s} T_{ijk}^{t} T_{ijk}^{u} \right. \right. \\
& \left. - L_{ik}^{u} U_{ijk}^{st} - L_{ik}^{t} U_{ijk}^{su} - L_{ik}^{s} U_{ijk}^{tu} \right) + \sin\phi_{ik} \left(- L_{ik}^{t} L_{ik}^{u} T_{ijk}^{s} - L_{ik}^{s} L_{ik}^{u} T_{ijk}^{t} - L_{ik}^{s} L_{ik}^{t} T_{ijk}^{u} \right. \\
& \left. \left. \left. + T_{ijk}^{s} T_{ijk}^{t} T_{ijk}^{u} + T_{ijk}^{u} U_{ijk}^{st} + T_{ijk}^{t} U_{ijk}^{su} + T_{ijk}^{s} U_{ijk}^{tu} + V_{ijk}^{stu} \right) \right] \right\}
\end{aligned}
\tag{15}
$$

As it is apparent from Eqs (12-15), all torsion L-tensor elements depend on the angle bending tensor elements L_{ij}^{r}, and on the torsion L-tensor elements of lower order It should

also be emphasized the explicit dependence of the torsion L-tensors on the equilibrium value of the torsion displacement coordinate τ_e only through the factors cot τ_e and cos τ_e

Another point worth discussing is the appearance of the "angle bending" L-tensor elements, L_{ik}^{r}, corresponding to the angle ϕ_{ik} defined by the non-adjacent bond vectors The significance of the mentioned elements may be regarded as purely mathematical, and for their computation the formulas for usual angle bending may be employed [1]

3. Sample calculations. We present in what follows fundamental frequency results for two sample cases involving torsional coordinates methanol and hydrazine In both cases there have been used only L-tensors up to the third order

The harmonic frequencies and normal coordinates have been calculated by the Wilson F-G method The anharmonicity correction is accomplished by employing the approach of Hoy, Mills and Strey [1] (briefly discussed in section 2) embedded in an original FORTRAN 77 computer code for general normal mode analysis, run both under the UNIX and DOS operating systems

The geometry and internal coordinates used to describe methanol are those of [4] The force constants are taken from the same reference, where all cubic force constants of the type F_{ijk}, with i, j and k all different, and all quartic force constants other than the diagonal stretching ones are neglected It should be noted that the calculations reported in [4] are performed strictly numerically, no use being made of analytical L-tensor formulas

Table 1 shows the computed fundamental frequencies of [4], the ones computed by means of our L-tensor formulas, along with the observed frequencies reported in [5] One may

notice the fair agreement between our frequency values and those of [4] Both sets of computed frequencies exhibit the same overestimating tendency as compared to the experimental values, however, the overall better agreement of our results (with a smaller maximum relative error of 6 7%) is obvious Exceptions are τ_2 (C-H bond stretching) and τ_9 (C-O-H angle bending), for which the errors are small anyway For the three torsion modes of methanol (τ_{10}, τ_{11} and τ_{12}) our relative errors are significantly smaller

Table I. Fundamental vibration frequencies of methanol ν^{obs} are the experimental values of [5], ν' are the calculated values of [4] and ν'' are the frequencies computed in this work (in cm^{-1}, the corresponding relative errors being expressed in %)

	ν^{obs}	ν'	$(\nu'-\nu^{obs})/\nu'$	ν''	$(\nu''-\nu^{obs})/\nu''$
A'					
ν_1	3682	3730	1 3	3728	1 2
ν_2	2999	3009	0 3	3011	0 4
ν_3	2844	2919	2 6	2865	0 7
ν_4	1478	1611	8 3	1583	6 6
ν_5	1455	1571	7 4	1559	6 7
ν_6	1334	1391	4 1	1364	2 2
ν_7	1075	1113	3 5	1080	0 5
ν_8	1034	1046	1 1	1 39	0 5
A"					
ν_9	2970	2988	0 6	3006	1 2
ν_{10}	1465	1583	7 5	1537	4 7
ν_{11}	1145	1234	7 2	1190	3 8
ν_{12}	271	262	3 4	263	3 0

FOURTH ORDER TORSION L-TENSOR FORMULAS

All relevant data for the hydrazine molecule (geometry, internal coordinates and force constants) are taken from [2]. Table II shows besides the calculated frequencies of [2] and of the present work, experimental data of [6] One should again notice the fair agreement between the two sets of computed frequencies The discrepancies between our frequencies and those of [2] (with maxima for the τ_7 N-N stretcing mode and τ_{12} antisymmetric NH_2 wagging mode) are probably due less accurate force constants listed in [2] and used in our calculations, than the ones actually used to produce the frequencies of [2]

Table II. Fundamental vibration frequencies of hydrazine. ν^{obs} are experimental data, ν' are computed values of [2], and ν'' are the frequencies computed in this work (in cm^{-1}, the corresponding relative errors being expressed in %)

	ν^{obs}	ν'	$(\nu'-\nu^{obs})/\nu'$	ν'	$(\nu'-\nu^{obs})/\nu''$
A					
ν_1	3390[a]	3413	0 7	3397	0 2
ν_2		3300		3297	
ν_3	1628[b]	1659	1 9	1671	2 6
ν_4	1324[c]	1344	1 5	1361	2 7
ν_5	1098[b]	1121	2 0	1119	1 9
ν_6	780[b]	840	7 1	843	7 5
ν_7	377[d]	398	5 3	350	-7 7
B					
ν_8	3398[a]	3402	0 1	3440	1 2
ν_9	3297[e]	3287	-0 3	3331	1 0
ν_{10}	1587[b]	1645	3.5	1655	4 1
ν_{11}	1283[e]	1320	2 8	1318	2 6
ν_{12}	937[f]	1045	10 3	1058	11 4

[a] [6], [b] [7], [c] [8], [e] [10], [f] [11]

4. Conclusions. New torsion *L*-tensor formulas up to the fourth order are presented, which, in contrast to some previous analytical results, are more compact, implying scalar operations with trigonometric functions instead of cumbersome vector operations The numerical results which have been subject to comparison, although affected by the employed set of force constants and the adopted numerical strategy, compare favourably with one another and with experimental data from the literature

Acknowledgements The autor is indebted to Prof U Buck for his kind hospitality and many helpful discussions during the two visits at the Max-Planck-Institut fur Stromungsforschung from Gottingen, where essential parts of the reported research have been accomplished The author would like to thank Dr B Schmidt for many suggestions of substance

REFERENCES

1 Hoy, A R , Mills, I M , Strey,G Mol Phys **24**, 1265 (1972)
2 Tanaka,N , Hamada,Y , Sugawara,Y , Tsuboi,M J Mol Spectrosc **99**, 245 (1983)
3 Beu, T A Z Phys D **27**, 263-266 (1993)
4 Schlegel, H B , Wolfe, S , Bernardi,F J Chem Phys, **67**, 4181 (1977)
5 Serrallach,A , Meyer, R , Gunthard, Hs H J Mol Spectrosc , **52**, 94 (1974)
6 Tipton, T , Stone, D A , KuBulat, K , Person, W J Phys Chem , **93**, 2917 (1989)
7 Giguére, P A , Liu, I D J Chem Phys **20**, 136 (1952)
8 Durig, J , Bash, S F , Mercer, E E J Chem Phys **44**, 4238 (1966)
9 Yamaguchi, A , Ichishima, I , Shimanouchi, T , Mizushima, S spectrochim Acta **16**, 1471 (1960)
10 Catalano, E , Sanborn, R H , Frazer, J W J Chem Phys **38**, 2265 (1963)
11 Hamada, Y , Hirakawa, A Y , Tamagake, K , Tsuboi, M J Mol Spectrosc **35**, 420 (1970)

STUDIA UNIV BABEŞ-BOLYAI, PHYSICA, XXXVIII, 2, 1993

EXCITATION OF A LOWER HYBRID WAVES IN A WARM PLASMA BY A WARM RELATIVISTIC ELECTRON BEAM

J. KARÁCSONY and Z. KISS*

Received 2 08 1993

ABSTRACT. - The linear theory of excitation of electrostatic lower hybrid waves into a warm magnetized plasma by a warm relativistic electron beam is presented It is found that electrostatic lower hybrid waves can be excited by Cherenkov resonance The frequencies and growth rates for excited waves are calculated

1. Introduction. Absorbtion of a lower hybrid waves seems to be a very efficient method for heating ions in a plasma [1,2] In recent years, considerable attention has been focused on theoretical and experimental studies of lower hybrid waves for plasma heating and current generation in tokamaks These waves have been succesfully employed to heat electrons and to drive plasma current in a number of tokamaks [3-8]

On the other hand, has been demonstrated that lower hybrid waves generated by auroral electrons can produce transversally accelerated ions in ionosferic plasmas [9, 10]

In the space physics context a great attention has been accorded to the lower hybrid drift instability generated by density and magnetic field inhomogenities [11, 12] The lower hybrid wave can be also excited by an electromagnetic pump wave [13] and by electron beams The linear theory of the lower hybrid waves excited by a nonrelativistic electron beam streaming through a cold plasma along the magnetic field has been discussed in detail by Papadopoulos and Palmadesso [14] The relativistic electron beam temperature effects on this

* *University of Cluj-Napoca, Faculty of Physics, 3400 Cluj-Napoca, Romania*

instability has been studied in [15] In the present paper we demonstrate that such waves can be generated by a warm relativistic electron beam into a warm magnetized plasma

In our model a warm relativistic electron beam with density n_{ob} and a velocity $\vec{v}_o$ streams through a plasma with warm electrons and cold ions along a magnetic field B_o The unperturbed plasma density is considered to be $n_{op} >> n_{ob}$ Because we are interested with lower hybrid waves excitation we will study the almost perpendicular propagation of plasma waves to the magnetic field

2. Dispersion equation. The general dispersion equation for longitudinal waves can be written as [19]

$$\varepsilon_{11} \sin^2\theta + \varepsilon_{33} \cos^2\theta + 2\varepsilon_{13} \cos\theta \sin\theta = 0 \qquad (1)$$

where ε_{ij} $(i,j = 1,3)$ are the dielectric tensor components of the system and θ represents the angle between the wave vector k and the direction of the external magnetic field B_o (One assumes that the wave vector k lies in the xOz-plane and Oz-axis is oriented parallel to the external magnetic field)

The dielectric tensor can be expressed by means of the conductivity tensor σ in the following way [19]

$$\varepsilon_{ij} = \delta_{ij} + \frac{4\pi i}{\omega}\sigma_{ij} \qquad (2)$$

We will use the expressions calculated in [17] for the conductivity tensor components of the warm relativistic electron beam and the expressions calculated in [16] for the conductivity tensor components of the warm plasma with temperature anizotropy Considering cold plasma ions and using relation (2) we can write the dielectric tensor components under

the form

$$\varepsilon_{xx} = 1 - \frac{\omega_{pi}^2}{\omega^2 - \omega_{ci}^2} - \frac{\omega_{pe}^2}{\omega^2}\left\{1 - \sum_n n^2 \frac{A_n(\lambda_e)}{\lambda_e}\left[\frac{n\omega_{ce}}{k_z^o \bar{v}_{\parallel e}} Z(s_{ne}) + \right.\right.$$
$$\left.\left. + \frac{T_{\perp e}}{T_{\parallel e}} Y(s_{ne})\right] + \sum_n n^2 \frac{A_n(\lambda_b)}{\lambda_b} P_n\right\} \tag{3}$$

$$\varepsilon_{xz} = \frac{\omega_{pe}^2}{\omega^2} tg\theta \left\{\sum_n n \frac{A_n(\lambda_e)}{\lambda_e} \frac{T_{\perp e}}{T_{\parallel e}}\left[\frac{\omega}{\omega_{ce}} + n\left(\frac{T_{\parallel e}}{T_{\perp e}} - 1\right)\right] Y(s_{ne}) + \right.$$
$$\left. + \frac{\eta}{\gamma_o} \sum_n n \frac{A_n(\lambda_b)}{\lambda_b} Q_n\right\} \tag{4}$$

$$\varepsilon_{zz} = 1 - \frac{\omega_{pi}^2}{\omega^2} + \frac{\omega_{pe}}{\omega^2} tg^2\theta \left\{\left(\frac{\omega}{\omega_{ce}} - n\right)\frac{T_{\perp e}}{T_{\parallel e}}\left[\frac{\omega}{\omega_{ce}} + n\left(\frac{T_{\parallel e}}{T_{\perp e}} - 1\right)\right]\right\} \times$$
$$\times Y(s_{ne}) + \frac{\eta}{\gamma_o} \sum_n \left(\frac{\omega\gamma_o}{\omega_{ce}} - n\right) \frac{A_n(\lambda_b)}{\lambda_b} Q_n\Bigg\} \tag{5}$$

where the following notations have been used.

$$P_n = 1 - \frac{n\omega_{ce}}{\gamma_o k_z v_{\parallel b}} Z(s_{nb}) - \frac{T_{\perp b}}{T_{\parallel b}} Y(s_{nb}) \tag{6}$$

$$Q_n = n\left[\frac{v_o}{v_{\parallel b}} Z(s_{nb}) + \left(1 - \frac{T_{\perp b}}{T_{\parallel b}}\right) Y(s_{nb})\right] + \frac{\omega\gamma_o}{\omega_{ce}} \frac{T_{\perp b}}{T_{\parallel b}} Y(s_{nb}) \tag{7}$$

and

$$A_n(\lambda) = e^{-\lambda} I_n(\lambda) \tag{8}$$

$I_n(\lambda)$ are the Bessel functions of the first kind of imaginary argument with

$$\lambda_e = \frac{k_x^{o\,2} \bar{v}_{\perp e}^2}{\omega_{ce}^2} \tag{9}$$

for the plasma and

$$\lambda_b = k_z^{o2} \frac{\overline{v}_{\perp b}^2 \gamma_o^2}{\omega_{ce}^2} \tag{10}$$

for the beam.

The quantity ω_{pe} represents the electron plasma frequency and ω_{pi} the ion plasma frequency, while ω_{ce} and ω_{ci} are the electron and ion cyclotron frequencies, respectively The perpendicular and parallel mean square velocity for beam electrons have been defined by the following relations [18]

$$T_{\perp b} = m_e \gamma_o^3 \overline{v}_{\perp}^2 b \tag{11}$$

$$T_{\parallel b} = m_e \gamma_o^3 \overline{v}_{\parallel}^2 b \tag{12}$$

where $T_{\perp b}$ and $T_{\parallel b}$ are the perpendicular and parallel beam temperature, respectively $\gamma_o = \left(1 - v_o^2/c^2\right)^{1/2}$ is the usual relativistic factor and $\eta = n_{ob}/n_{op} \ll 1$

In the expressions (3)-(7) we used the plasma dispers in functions [18]

$$Z(s_n) = (2\pi)^{-1/2} \int_{-\infty}^{\infty} \frac{\exp(-t^2/2)}{t - s_n} dt \tag{13}$$

and

$$Y(s_n) = (2\pi)^{-1/2} \int_{-\infty}^{\infty} \frac{t \exp(-t^2/2)}{t - s_n} dt \tag{14}$$

with

$$s_{ne} = \frac{\omega - n\omega_{ce}}{k_z^o \overline{v}_{\parallel e}} \tag{15}$$

for the plasma and

$$s_{nb} = \frac{\omega - \vec{K}\vec{v}_o - n\omega_{ce}/\gamma_o}{k_z \overline{v}_{\parallel b}} \tag{16}$$

for the beam

The perpendicular and parallel mean square velocity for the plasma electrons have been defined by the relations [16]

$$T_{\perp,\parallel e} = m_e \overline{v}_{\perp,\parallel,e}^2 \tag{17}$$

where $T_{\perp_e}$ and $T_{\parallel_e}$ are the perpendicular and parallel electron plasma temperature, respectively

Since we will be interested with almost perpendicular wave propagation with respect to plasma return current direction, in expressions (3)-(5) we neglected plasma return current effects

Substituting the expressions (30-(5) in (10 and taking into account that [18]

$$Y(s_n) = 1 + s_n Z(s_n) \tag{18}$$

the electrostatic dispersion relation becomes

$$D(\vec{K},\omega) = 1 - \frac{\omega_{pi}^2 \cos^2\theta}{\omega^2} - \frac{\omega_{pi}^2 \sin^2\theta}{\omega^2 - \omega_{ci}^2} + \frac{\omega_{pe}^2}{k^2 \bar{v}_{\parallel_e}^2}\left[1 + \sum_n A_n(\lambda_e) Z(s_{ne}) \times \right.$$

$$\left. \times \left(s_{ne} + \frac{n\omega_{ce}}{\vec{K}_z \bar{v}_{\parallel_e}} \frac{T_{\parallel_e}}{T_{\perp_e}} \right) \right] + \frac{\eta}{\gamma_o^3} \frac{\omega_{pe}^2}{k^2 \bar{v}_{\parallel b}^2}\left[1 + \sum_n A_n(\lambda_b) Z(s_{nb}) \times \right. \tag{19}$$

$$\left. \times \left(S_{nb} + \frac{n\omega_{ce}}{k_z \bar{v}_{\parallel b} \gamma_o} \frac{T_{\parallel b}}{T_{\perp b}} \right) \right] = 0$$

3. Excitation of lower hybrid waves. For electrostatic waves with $\omega_{ci} << \omega << \omega_{ce}$ and $\cos\theta \leq m_e/m_i$ some simplification of equation (19) is possible because $s_{ne} \gg 1$ Using the asymptotic values of $Z(s_{ne})$ [18]

$$Z(s_{ne}) \approx -\frac{1}{s_{ne}} - \frac{1}{s_{ne}^3} - \ldots + i\sqrt{\frac{\pi}{2}} e^{-\frac{S_{ne}^2}{2}} \tag{20}$$

and neglecting the higher order terms, the dispersion equation (19) reduces to

$$D(\vec{K},\omega) = 1 - \frac{\omega_{pi}^2}{\omega^2} - \frac{\omega_{pe}^2}{\omega^2} A_o(\lambda_e) \cos^2\theta - \frac{\omega_{pe}^2}{k^2 \bar{v}_{\parallel_e}^2} \sum_n A_n(\lambda_e) \frac{n\omega_{ce}}{\omega - n\omega_{ce}} \frac{I'_{\parallel_e}}{T_{\perp_e}} +$$

$$+ i\sqrt{\frac{\pi}{2}} \frac{\omega_{pe}^2 \omega}{k^2 k_z \bar{v}_{\parallel_e}^3} A_o(\lambda_e) e^{-\frac{\omega^2}{2k_z^2 \bar{v}_{\parallel_e}^2}} - \frac{\eta}{\gamma_o^3} \frac{\omega_{pe}^2}{k^2 \bar{v}_{\parallel b}^2}\left[1 + \sum_n A_n(\gamma_b) \times \right. \tag{21}$$

$$\times Z(s_{nb})\left(s_{nb}+\frac{n\omega_{ce}}{k_z v_{\|b}\gamma_o}\frac{T_{\|b}}{T_{\perp b}}\right)\Bigg] = 0$$

Now, taking into account that for lower hybrid waves we can use for $A_n(\lambda_e)$ the expression [19]

$$A_n(\lambda_e) \approx \frac{\lambda_e^{|n|}}{2^{|n|}|n|!} \tag{22}$$

and we finally have the dispersion relation in the form

$$D(\vec{k},\omega) = 1-\frac{\omega_{pi}^2}{\omega_2}-\frac{\omega_{pe}^2}{\omega^2}\cos^2\theta+\frac{\omega_{pe}^2}{\omega_{ce}^2}+i\sqrt{\frac{\pi}{2}}\frac{\omega_{pe}^2\omega}{k^2k_z\overline{v}_{\|e}^3}e^{-\frac{\omega^2}{2k_z^2\overline{v}_{\|e}^2}}- \\ -\frac{\eta}{\gamma_o^3}\frac{\omega_{pe}^2}{k^2\overline{v}_{\|b}^2}\left[1+\sum_n A_n(\lambda_b)Z(s_{nb})\left(s_{nb}+\frac{n\omega_{ce}}{k_z v_{\|b}\gamma_o}\frac{T_{\|b}}{T_{\perp b}}\right)\right]=0 \tag{23}$$

With the purpose to investigate this dispersion equation, we will follow the usually applied procedure in plasma physics [19] According to this, when Im ω << Re ω, the excited wave frequencies can be calculated from the equation

$$\mathrm{Re}\, D(\vec{k},\omega) = 0 \tag{24}$$

and the corresponding growth rates from the relation

$$\mathrm{Im}\,\omega = -\frac{\mathrm{Im}\, D(\vec{k},\omega_r)}{\partial\,\mathrm{Re}\, D(\vec{k},\omega_k)/\partial\omega_k} \tag{25}$$

where $\omega_k = \mathrm{Re}\,\omega(\vec{k})$

Writing the $Z(s_{nb})$ function under the form [18]

$$Z(s_{nb}) = -\exp\left(-\frac{S_{nb}}{2}\right)\left[\int_0^{s_{nb}}\exp\left(\frac{\xi^2}{2}\right)d\xi - i\left(\frac{\pi}{2}\right)^{1/2}\right] \tag{26}$$

and taking into account that in $\mathrm{Re}\, D(\vec{k},\omega)$ the contribution of the beam terms are of order η, we obtain for the excited wave frequencies the expression

$$\omega_k^2 = \frac{1}{1+\alpha^2}\left(\omega_{pi}^2 + \omega_{pe}^2\cos^2\theta\right) \tag{27}$$

where

$$\alpha^2 = \frac{\omega_{pe}^2}{\omega_{ce}^2} + \frac{\eta}{\gamma_o^3}\frac{\omega_{pe}^2}{k^2\bar{v}_{\parallel b}^2}\left[1 + \sum_n A_n(\lambda_b)\cdot\right.$$
$$\left.\cdot \operatorname{Re} Z(s_{nb})\left(s_{nb} + \frac{n\omega_{ce}}{k_z\bar{v}_{\parallel b}\gamma_o}\frac{T_{\parallel b}}{T_{\perp b}}\right)\right]_{\omega=\omega_{ko}} \tag{28}$$

with

$$\omega_{ko}^2 = \frac{\omega_{pi}^2 + \omega_{pe}^2\cos^2\theta}{1 + \omega_{pe}^2/\omega_{ce}^2} \tag{29}$$

The growth rate for the instability can be found from (24) using for $D(K,\omega)$ the expression (23)

Taking into account that Im $Z(s_{nb})$ with $n \neq 0$ are small compared with Im $Z(s_{nb})$, we obtain for Im ω the following expression

$$\operatorname{Im}\omega = -\frac{\sqrt{\pi}}{2^{3/2}}\frac{\omega_{pe}^2}{k^2}\frac{\omega_k}{1+\alpha^2}\left[\frac{\omega_k}{k_z\bar{v}_{\parallel e}^3}e^{-\frac{\omega_k^2}{2k_z^2\bar{v}_{\parallel b}^2}} + \right.$$
$$\left. + \eta\sqrt{\frac{\pi}{2}}A_o(\lambda_b)\frac{\omega_k - \vec{K}\vec{V}_o}{k_z\bar{v}_{\parallel b}^3\gamma_o^3}e^{-\frac{(\omega_k - \vec{K}\vec{V}_o)^2}{2k_z^2\bar{v}_{\parallel b}^2}}\right] \tag{30}$$

The fastest growing instability of the lower hybrid wave is then obtained when

$$\omega_k \approx \vec{K}\cdot\vec{V}_o \tag{31}$$

with the beam electron speed just a little faster than the phase velocity of the wave in the beam direction This is necessary to assure Im $\omega > 0$

The first factor in the bracket caracterizes the damping of excited waves due to plasma electrons

4. Conclusions. The above results show that a warm relativistic electron beam can excite lower hybrid waves in warm magnetized plasma These waves can be excited by Cherenkov resonance when $\omega_k \approx \vec{k} \cdot \vec{v}_o$ We calculated the frequencies and growth rate for excited waves The obtained growth rate expression contains also the damping effects due to the plasma electrons [first term in the bracket of expresion (30)] on the excited waves When the Chereakov resonance condition is satisfied the damping term becomes small compared with the term which is responsible for the qrowth of the wave amplitudes [the second term in the bracket of expression (30)] Thus it results an instability for the lower hybrid waves.

Another important conclusion can be also drawn for beam electron temperature effect The expression which was derived for the growth rate shows that parallel beam temperature has an stabilizing effect on the instability.

REFERENCES

1. Porkolab M , Nucl Fusion 12, 329 (1972).
2. Allen G R et al , Phys Rev Lett 41, 1045 (1978)
3 Fisch N J , Rev Mod Phys 59, 175 (1987)
4 Bell R E et al , Phys Rev: Lett 60, 1294 (1988)
5 Yamamoto T et al , Phys Rev. Lett 63, 1148 (1989)
6 Nemoto M et al , Phys Rev. Lett 67, 70 (1991)
7. Fisch N J , Rax J M , Phys Rev. Lett 69, 612 (1992)
8 Maekawa T et al , Phys Rev Lett 70, 2561 (1993)
9 Chang T , Coppi B , Geophys Rev Lett 8, 1253 (1981)
10 Kintner P.M et al , Phys Rev Lett 68, 2448 (1992)
11 Huba J D , Papadopoulos K , Phys Fluids 21, 121 (1978)
12 Huba J D , Gladd N.T , Papadopoulos K , J Geophys Res , 83, 5217 (1978)
13 Hasegawa A , Chen L , Phys Fluids 19, 1321 (1975)
14 Papadopoulos K , Palmadesso P , Phys Fluids 19, 605 (1976)
15. Karacsony J , Rev Roum Phys 29, 705 (1984)
16 Alexandrov A F , Bogdankevic L S , Ruhadze A a , Osnovy Electrodinamiki Plasmy, Moskva, 1978
17 Karacsony J , Selinger V , Bull. Math Soc Sci Math R S R , 24 363 (1980)
18 Bludman S A , Watson K M , Rosenbluth M N , Phys Fluids 3, 747 (1960)
19 Akhiezer A I , Stepanov K N , Akhiezer I A , Polovin R V , Sitenko A G , Elektrodinamika Plazmy, Nauka, Moskva, 1974

STUDIA UNIV BABEŞ-BOLYAI, PHYSICA, XXXVIII, 2, 1993

ANALYSIS OF THE PHYSICAL CHARACTERISTICS OF A DUSTY PLASMA I. THE GRAIN CHARGES AND THEIR EFFECTS

Speranţa COLDEA*

Received 5 09 1993

ABSTRACT. - The charge of a dust in a plasma is not a fixed one, depending on the characteristics of the plasma, on other phenomena as secondary and field emission, photoemission, etc By supposing the grains being at rest in a Maxwellian plasma, an analysis for the properties of grain charges in a dusty plasma is made The corresponding effects are shortly discussed In the second part of the paper other effects of the electrostatics of dusty plasmas will be analysed

1. Introduction. A dusty plasma can be defined as a plasma with a phase of solid objects (grains or dusty particles), that usually exist in laboratory plasmas, planetary and cosmic plasmas For the understanding of the ionosphere properties and of the consequences for earth atmospheric pollution, a modern knowledge of the dusty plasmas characteristics is needed Generally, the method of study such plasmas characteristics is based on the theory of the composite plasma dynamics (kinetic model or fluid model) Experimentally, the Ionospheric Radar Scatter Technique is used, based on the analysis of the statistical properties of radar returns from ionosphere Measurements of physical properties of dusty plasma in ionosphere or planetary ring (magnetosphere) are also made by satellites The conclusion of the experiments is that the present of dust may change the structure and properties of the plasma The present paper deals with the study of fundamental properties of a dusty plasma with impurities, that are electrically charged A short analysis of the grain charging and of the

* *"Babeş-Bolyai" University, Faculty of Physics, 3400 Cluj-Napoca, Romania*

corresponding effects in a dusty plasma is given, based on the fundamental equations of such a plasma and on some quantitative considerations

2. The basic equations. Firstly we shall present the equations that describe the charging of dust grains in a plasma, process driven by plasma currents, photoelectron and secondary emission currents [1]-[7] The basic equations for all thesse currents in the case of a number of grains in a plasma comparatively with those of a single grain in plasma or in vacuum will be presented

By considering that a grain is at rest in a Maxwellian plasma with electron and ion temperatures T_e and T_i ($T_e \sim T_i$) and by neglecting the other charging effects, the potential of the grain ϕ is obtained to be negative (if $Flow_i << Flow_e$) The currents to the surface of the grain are [1]-[3], [7].

$$I_e = -\frac{4\pi a^2 n_e e}{(2\pi\beta_e m_e)^{1/2}} \cdot \exp(e\beta_e\phi) \tag{1}$$

$$I_i = \frac{4\pi a^2 n_i Ze}{(2\pi\beta_i m_i)^{1/2}} \cdot (1-\beta_i Ze\phi) \tag{2}$$

where $\beta = 1/kT$ and a is the grain radius, m_e, m_i being the electron and ion mass and T_e, T_i the corresponding temperatures, ϕ is the grain surface potential

If $\phi > 0$ then $I_i \sim \exp(-eZ\beta_i\phi)$ and $I_e \sim (1-e\beta_e\phi)$ The equilibrium potential is found from the condition

$$I_i + I_e = 0 \tag{3}$$

and it is independent of plasma density

Because the charging time is nonzero and it is proportional to $1/a$, a specific

gyrophase drift motion of grain in plasma takes place

The secondary and photo-emissions determine a positive current to the grain Two cases could be discussed

(a) If $\phi < 0$, all the released electrons by secondary emission escape and the corresponding electron current is of the form

$$I_{sec} = 3.7\delta_m \cdot n_e \left(\frac{kT_e}{2\pi m_e}\right)^{1/2} \cdot F_5\left(\frac{E_m}{4kT_e}\right) \cdot e^{\frac{e\theta}{kTe}} \tag{4}$$

where

$$F_5\left(\frac{E_m}{4kT_e}\right) = \frac{E_m^2}{16k^2T_e^2} \cdot \int du \cdot u^5 \cdot \exp\left[-\left(\frac{E_m \cdot u^2}{4kT_e} + u\right)\right] \tag{5}$$

and δ_m is a material parameter of value $0.5 < \delta_m < 30$ and E_m is the value $E_m(\delta_m) \in (0.1-2)\,keV$

(b) If $\phi > 0$, several electrons are reabsorbed in the secondary emission process and then we have

$$I_{sec} = 3.7\delta_m n_e \left(\frac{kT_e}{2\pi m_e}\right)^{1/2} \cdot \left(1 + \frac{e\phi}{kT_i}\right) \cdot \exp\left[-\frac{e\phi}{k}\left(\frac{1}{T_i} - \frac{1}{T_e}\right)\right] \cdot F'(x) \tag{6}$$

where $x = \frac{B_m}{4kT_e}$, $T_i \sim 10^4 K$, $B = \left(\frac{e\theta}{E_m}\right)^{1/2}$ and

$$F_5' = x^2 \int du \cdot u^5 \cdot e^{(-xu^2+u)} \tag{7}$$

The photoelectrons flow is of the following form [9]

$$\begin{aligned} I_p &= \pi a^2 \cdot K && \text{if } \phi < 0 \\ I_p &= \pi a^2 \cdot K \cdot \exp\left(-\frac{2\phi}{2T_f}\right) && \text{if } \phi > 0 \end{aligned} \tag{8}$$

where T_f is the temperature of photoelectrons ($T_f \sim 1\,eV$) and $K = \eta \cdot x$ is the flow of photons (η being the photoefficiency of value $\in (0\ 1 - 1)$)

When a grain of $a = 1\mu$ m in a plasma of $T_f = 1\,eV$ is taken, and the plasma and secondary emission currents are considered, three steady states are possible (if $I_{total} = 0$), the midle one is unstable and the other two ones stable From some considerations that we don't introduce here it could be seen that this behaviour leads to a coagulation of dust grains effect [6], that will be discussed elsewhere

The case of a moving grain in plasma can be also assumed, the corresponding electron and ion currents being given by

$$I_e = -\frac{2\sqrt{2\pi}\, a^2 e n_e}{(\beta_2 \cdot m_e)^{1/2}} \cdot \exp(e\beta_e \phi) \tag{9}$$

and

$$I_i = \pi a^2 n_i Ze \left[\left(1 + \frac{T_{thi}}{2\mu^2} - \frac{2Ze\phi}{m_i \mu^2} \right) + \frac{\alpha}{\omega\sqrt{\pi}} \cdot \exp\left(-\frac{\omega^2}{T_{thi}^2} \right) \right. \tag{10}$$

where $T_{thi} = \left(\frac{2kT_i}{m_i} \right)$ is the ion thermal velocity and ω is the grain velocity Because $\omega \ll T_{thi}$, the grain may be considered at rest and I_e is the same as (1) From the equilibrium condition $I_e + I_i = 0$ the potential $\phi = \phi(\omega)$ could be obtained

At this point a qualitative discussion must be made the capacitance of a grain in vacuum $C_g = a$, if the grain is introduced in a plasma, the potential around it is $\phi = Q \cdot \frac{\exp[-k(r-a)]}{r(1+ka)}$ where $k = \frac{1}{\lambda_D}$, r is the distance between grains [3] The effect of this like a spherical capacitor grain sorrounded by positive sheats (outer conducting shells) is the following when $r \sim \lambda_D$, the positive shell is pushed closer to grain surface and its capacitance increases If grains are in a neutral plasma they become negatively charged and there are

excess ions in plasma; the condition $I_e = I_i$ at the grain surface is satisfied

3. The effects of grain charge in a dusty plasma. The relation for ion and electron densities $n_i(\vec{r})$ are given by the Boltzmann factor

$$n_i(\vec{r}) = C_i \cdot \exp[-q_i \beta_i \phi(\vec{r})] \tag{11}$$

where $C_i (i = e, i)$ is taken from the condition $\int n_i(\vec{r})\, d^3r = N_i$, N_i being the total number of "i" species, ϕ - the potential around the grain and q_i is the charge

The Poisson equation that will be used in this case is

$$\begin{aligned} \nabla^2\phi + 4\pi\rho_g(\vec{r}) &= -4\pi\sum_i n_i \cdot q_i = \\ &= -4\pi\sum_i \frac{N_i q_i \exp[-\beta_i q_i(\phi(\vec{r}) - \phi)]}{\int d^3r' \cdot \exp[-\beta_i q_i(\phi(\vec{r}') - \phi)]} \end{aligned} \tag{12}$$

with $\rho_g(\vec{r})$ being the charge density on the grain After using the method of expansion of electric potential in $\beta_i q_i(\phi - \bar{\phi})(\bar{\phi} \ll 1)$, we obtain to the lower order the relation

$$\begin{aligned} \nabla^2\phi - k^2\phi + 4\pi q_e(\vec{r}) &= -4\pi\sum_i \bar{n}_i \cdot q_i \\ &- \frac{k^2}{V}\int d^3r'(\phi - \bar{\phi}) - k^2\bar{\phi} \end{aligned} \tag{13}$$

where

$$k = 4\pi\sum_i \bar{n}_i q_i^2 \cdot \beta_i \tag{14}$$

and

$$\bar{n}_i = \frac{1}{V}\int d^3r \cdot n_i(\vec{r}) \tag{15}$$

with V - the volume of integration, $\bar{\phi}$ being the averaged value of ϕ over V

The final Poisson equation is gauge invariant

$$\nabla^2(\phi - \bar{\phi}) - k^2(\phi - \bar{\phi}) + 4\pi\rho_e(\vec{r}) = -4\pi\sum_i \bar{n}_i q_i \tag{16}$$

It can be observed that the currents on the grain are driven by the difference $(\phi - \bar{\phi})$, The solution of the last equation could be obtained under the following form if a neutral grains-plasma system $(Q(<0) - Q_p(>0)$, with N grains of same radius a and charge Q, is considered

$$\phi - \bar{\phi} = \phi(\vec{r}) + \frac{4\pi}{k^2}\sum_i \overline{n_i} \cdot q_i \tag{17}$$

where $\phi(\vec{r})$ is the solution of the boundary condition

$$\nabla^2\phi(\vec{r}) - k^2\phi(\vec{r}) + 4\pi\rho_e(\vec{r}) = 0 \tag{18}$$

that could be written as an integral equation using the Green's theorem

$$\phi(\vec{r}) = \frac{1}{4\pi}\sum_j \int dr_j' \left[\frac{\exp(-k|\vec{r}-\vec{r}'|)}{|\vec{r}-\vec{r}'|} \cdot \frac{\vec{r}_j - \vec{r}'}{|\vec{r}-\vec{r}'|} \cdot \nabla'\phi(\vec{r}') - \right. \\ \left. - \phi(\vec{r}) \frac{\vec{r}_j - \vec{r}'}{|\vec{r}_j - \vec{r}'|} \cdot \nabla' \frac{\exp(-k|\vec{r}-\vec{r}'|)}{|\vec{r}-\vec{r}'|} \right] \tag{19}$$

The center of i^{th}-grain is choosen as the origin of the system and only the i^{th} term $\phi_i(\vec{r})$ of the above sum $\sum_i$ is considered The grain surface potential is $\phi(a)$ and the electric field $-\nabla\phi(\vec{r}')$ is the same over the grain surface From Gauss' theorem it can be obtained

$$\frac{(\vec{r}_i - \vec{r}')}{|\vec{r}_i - \vec{r}'|} \cdot \nabla'\phi(\vec{r}') = \frac{Q_i}{a^2} \tag{20}$$

By integrating the equation (19) the following result is obtained

$$\phi(\vec{r}) = \frac{Q_i}{r}\exp(-kr)\frac{\exp(ka) - \exp(-ka)}{2ka} + \\ \frac{\phi(a)}{2kr}\exp(-kr)[\exp(-ka)(1+ka) - \exp(ka)(1-ka)] \tag{21}$$

Furter the other grains ($j \neq i$) are considered and the collective effects between grains may be taken into account and then the potential $\phi(r)$ is given after integration of eq (19), for any distribution function

$$\sum_{j\neq i} f(\vec{r}_i, \vec{r}_j) = N\int d^3 r_j \cdot f(\vec{r}_i, \vec{r}_j) \tag{22}$$

If f = 1, this condition is of the form $4\pi R^3/3 = N$, that defines a distance $R \sim \frac{r}{2}$ In this case the potential is

$$\phi(r) = \frac{Q}{r}\exp[-k(r-a)] \cdot \cdot \frac{1 + 2\pi N k^{-3}\exp(-kR)(1+kR)(\exp(2kr)-1)}{1 + ka - 2\pi N k^{-3}\exp(-kR)\cdot[(1+ka)-(1-ka)\exp(2ka)]} \tag{23}$$

and then

$$\phi(r) - \bar{\phi} = \phi(r) - \frac{4\pi NQ}{k^2\left(1 - \frac{4\pi a^3 N}{3}\right)} \tag{24}$$

For equilibrium the condition $I_e + I_i = 0$ is imposed, and in above equation the currents are given by the eq (1) - (2), with the $\bar{n}_e$, $\bar{n}_i$, $\phi(a) \to \bar{\phi}$ and $\bar{n}_e \neq \bar{n}_i$, $\bar{n}_i - \bar{n}_e = -\frac{Q}{e}\cdot\frac{N}{\left(1 - 4\pi a^3\frac{N}{3}\right)}$ The ion charge is taken as unity and $\beta_e = \beta_i$ Then the equilibrium grain charge is deduced from the equation

$$1 - e\beta[\phi(a) - \bar{\phi}] = \left(\frac{m_i}{m_e}\right)^{1/2}\frac{\bar{n}_e}{\bar{n}_i}\cdot\exp[e\beta(\phi(a) - \bar{\phi}] \tag{25}$$

A dimensionless parameter A(N) that contains the dependence of ϕ on grain and plasma parameters is introduced, defined by

$$A(N) = \frac{4\pi N\frac{Q(N)}{(\phi(a) - \bar{\phi})}}{k^2\left(1 - \frac{4\pi a^3 N}{3}\right)} \tag{26}$$

with the aim to write the equilibrium charge equation (23) as follows

$$1-e\beta\left[\phi(a)-\bar{\phi}\right]\left[1-e\beta\left(\phi(a)-\bar{\phi}\right)A(N)\right]=$$
$$=\left(\frac{m_i}{m_e}\right)^{1/2}\left[1+e\beta\left(\phi(a)-\bar{\phi}\right)\cdot A(N)\right]\cdot\exp\left[e\beta\left(\phi(a)-\bar{\phi}\right)\right] \qquad (27)$$

It can be seen that A(N) α N If the ratio $\frac{Q(N)}{Q(0)}$ of grain charges (for a number of $\frac{N}{V}$ grains in plasma) and the charge of a single grain in the considered plasma are introduced, this ratio is

$$\frac{Q(N)}{Q(0)}=\frac{\phi(a)-\bar{\phi}}{\left[\phi(a)-\bar{\phi}\right]_{N=0}}\cdot\frac{C(N)}{C(0)} \qquad (28)$$

where $\frac{\phi(a)-\bar{\phi}}{\left[\phi(a)-\bar{\phi}\right]_{N=0}} < 1$ but $\frac{C(N)}{C(0)} > 1$

As an example the F-ring of the Saturn, that contains a dusty plasma, may be considered The specific parameters are in this case a = 1μm, R = 0,2 cm, T = 10 μmeV, n = 100 cm^3 (O^+ ions) and λ_D = 166 cm The result for the value of capacitance ratio is

$\frac{C(N)}{C(0)}$ = 1 0009 and $\frac{\left[\phi(a)-\bar{\phi}\right]}{\left[\phi(a)-\bar{\phi}\right]_{N=0}}$ = 2 7 10^{-4}

From the presented analysis two conclusions could be deduced for the present state of the considered problem

a) The grain charge, under the given conditions, is not so large as we could expect if the plasma temperature T = 10 eV is taken Q(N) = 2 70243·10^{-4}·Q(0)

b) The corresponding electromagnetic forces are smaller in the considered example, for the evaluated smaller grain charge

The same discussion could be made for dense dusty plasmas [9] and also for high

dust-grain density by using the same kind of analysis

The other effects on a charged grain in a dusty plasma, as drag on a moving grain, the motion of such a dust and coagulation of grain in plasma will be discussed in the second part of the paper

REFERENCES

1 Hill J R and Mendis D A , Moon and Plan , 21, 3, (1979)
2 Hill J R and Mendis D A , Can J Phys , 59, 897, (1980)
3 Whipple E C , Rep Progr Phys , 44, 1197, (1981)
4 Mendis D A , Houpis H L F and Hill J R , J Geophys Res , 87, 3449, (1982)
5 Ikezi H , Phys Fluids, 29, 1764, (1986)
6 Northrop T G and Hill J R , J Geophys Res , 87, 661, 1982, 88, 1, 6102, 1989
7 de Angelis U , Physics of dusty plasmas, Spring College on Plasma Physics, ICTP, Trieste, Italy, (1991)
8 Goertz C K and Ip W H , a) Geophys Res Lett, 11, 349, 1984, b) Geophys Res Lett, 15, 84, 1988
9 Goertz C K , rev Geophys , 27, 271, (1990)

STUDIA UNIV BABEŞ-BOLYAI, PHYSICA, XXXVIII, 2, 1993

ANALYSYS OF THE PHYSICAL CHARACTERISTICS OF A DUSTY PLASMA II. THE COLLECTIVE EFFECTS FOR THE DRAG ON A MOVING DUST GRAIN

Speranţa COLDEA*

Received 5 09 1993

ABSTRACT. - The plasma collective effects are included to analyse the process of the plasma drag on a charged dust grain moving through a plasma, due to Coulomb collisions The conclusion of the analytical discussion is that the forces among the ions modify the grain influence on the ions trajectories, which is the source of the collective effects and that the drag on a grain is independent of the presence or absence of plasma particles moving faster than the dust

1. Introduction. The effects of a charged particle on the grains in a dusty plasma can be considered from two points of view·

(a) the effects of electric and magnetic forces on the dynamics of the grains in the plasma, and

(b) the effects of the grain charge on the properties of a plasma waves propagation, instabilities and new modes

In the case (a) the electromagnetic force should be added to the gravitational or radiation pressure forces and the orbits of the grains in plasma could be altered

The equation of motion of a grain is of the form [1]-[2]

$$m\cdot\nabla\vec{v} = eZ_g\left(E + \frac{1}{e}\cdot(\vec{v}XB)\right) + F_g - \pi a^2\cdot P \qquad (1)$$

where F_g is the gravitational force and P is the radiation pressure Such a theory is called gravito-electrodynamics [1]-[2] The plasma physics is modified by the presence of some

* *"Babeş-Bolyai" University, Faculty of Physics, 3400 Cluj-Napoca, Romania*

charged dusty particles

Depending on the considered particular phenomenon that is discussed two kinds of theories could be used

(i) the dust-grain can be taken as another plasma component (heavy ions) and then the known results of many-component plasma theory could be applied

(ii) the grains could be considered as external fixed impurities, acting as local and strong perturbations for plasma particles

Grains moving through the plasma could be also considered

For a dusty plasma, without the case when the grain radius $a(\mu) \leq 1$ and when it contains very low frequency oscillation modes, the grain dynamics can be neglected with respect to the plasma ion electron dynamics. The following simple physical model for a dusty plasma can be taken into account a nonneutral plasma $(n_e \neq n_i)$ in the presence of a distribution of fixed charged centers that determines a stationary potential distribution of the system, being the solution of the Poisson equation

$$\nabla^2\phi = -4\pi\left[\sum_\alpha q_\alpha \int f_{\alpha 0}(\vec{r},\vec{u})\, d^3u + \rho_g(\vec{r})\right] \tag{2}$$

where $f_{\alpha 0}(\vec{r},\vec{u})$ $\alpha = i,e,h$ are the distribution functions of the plasma components in the presence of grains and the charge density of the grain ρ_g is given as

$$\rho_g(\vec{r}) = e \cdot \sum_\beta Z_g^\beta \delta(\vec{r} - R_\beta) \tag{3}$$

$\rho_g(\vec{r})$ is a given function and does not change the plasma response in the presence of a wave or of any other perturbation

This is the simplest model for a dusty plasma, but other more complex physical models are used, such as the spherical capacitor model, where the spherical symmetry

assumption is made and for which the nearest neighbor approximation is not needed Other two models are those of impermeable grains and of permeable grains in a plasma, the last being artificial because it was considered that plasma permeates the grain and the system is overall neutral

The collective effects could be included or not in the theory of dusty plasmas In this second part of the paper [3] the collective effects in the plasma drag process on a charged grain are analysed We take into account only the effects of electric forces due to ion Coulomb collisions on the grains in the plasma

2. Collective effects on a dust grain in the case of drag process. A charged grain interacts with the other charged dusty plasma particles The collective effects occur because there are forces among the plasma particles that are altered by the presence of a grain charge The inclusion of collective effects requires the use of the Vlasov - Maxwell equations Usually a linearization is needed, giving an inexact solution

A more complex collective effect, the drag on a grain in a dusty plasma, when the grains move through the plasma, is analysed in the paper, the collective effects between the plasma ions exist due to their interaction and are considered here The interaction of the grains among themselves is not considered The charging curents could be calculated, the factor by which the grain charge and the electromagnetic force on such a particle are altered by the presence of the other grains in a dusty plasma may be also evaluated The plasma is considered as a perturbed reservoir (with $n_e \neq n_i$, because some charges are given to the grains) The velocity distribution of such a plasma is a Maxwellian one and the plasma has

an average potential $\bar{\phi}$, the difference $\phi(a) - \bar{\phi}$, where $\phi(a)$ is the grain surface potential determines the ion and electron currents to a grain [1]-[2], all the other charging processes are neglected here It is considered that $\beta_e = \beta_i$ An analysis could be made by considering a gauge-invariant Poisson equation

$$\nabla(\phi(a) - \bar{\phi}) - k^2(\phi(a) - \bar{\phi}) + 4\pi \cdot \rho_e(\vec{r}) = -4\pi \sum_{\alpha} n_\alpha \cdot q_\alpha \tag{4}$$

The solution of this equation can be given for the different earlier considered models The detailed theory of the motion of a charged grain in a plasma and of the collective effects on such a grain is not given here The analysis for the electrostatics of a dusty plasma, with the study only of the drag on a dust grain moving in the plasma is made

The drag force on a moving grain in a plasma is a phenomenon due to direct ions impact and to the grain-ion collisions and is defined as the product of the acceleration of grains (of velocity v_0) and of the grain mass m_g, e g $m_g \cdot \underline{u}(v_0)$ (we will adopt the Chandrasekhar approximation of finite m_g) The direct ion impact drag is given by an equation of the form [4], if the collective effects are neglected

$$F_{id} = -n_i \cdot \pi a^2 m_i \cdot \alpha^2 \left[\frac{\omega}{\sqrt{\pi}\ \alpha} \cdot (\exp - \omega_i^2) + \left(\frac{\omega}{\alpha} + \frac{1}{2} \right) \cdot f_{er}\left(\frac{\omega}{\alpha} \right) \right] \tag{5}$$

where $m_i\alpha^2 = 2kT_i$

There are two cases that may be taken into consideration

(i) if $\omega \leq \alpha$ the grain is moving slowly and in this case

$$F_{id} = -2\sqrt{\pi}\, n_i \cdot a^2 m_i \alpha\omega \tag{6}$$

and

(ii) if $\omega \geq \alpha$ the grain is moving faster and then

$$F_{id} = \pi n_i \cdot a^2 \cdot m_i \cdot \omega^2 \tag{7}$$

The assumption that the dusty grains do not interact is made The collective effects among the ions could be or not considered, the force among the ions modifies the grain influence on the ion trajectory It is necessary to linearize the ion distribution by assuming that $\delta f \leq f$, e g the force is slightly changed in the presence of a grain charge, that means to not consider the smallness of scattering angles This is the same as expanding the product of grain and ion charges in Qe, this product being proportional to the grain-ion coupling

The expressions for F_{id} in the case of no large scattering angles (for the limit of small product Qe) can be given under the following form

$$F_g = \frac{4\pi Q^2 e^2}{m_i} \cdot \ln\frac{\lambda_D}{a} \cdot \int d^3v \cdot \frac{f(v)\vec{v}}{v^3} \tag{8}$$

that is the expression given by eq (5) if f(v) is taken as a Maxwellian distribution and for the case of large scattering angles is given by the relation [5]

$$F_g = \frac{2\pi Q^2 e^2}{m_i} \int d^3v \cdot \frac{f(v)\cdot\vec{v}}{v^3} \cdot \ln \frac{1 + \dfrac{m_i v^4}{Q^2 e^2}\lambda_D^2}{1 + \dfrac{m_i v^4}{Q^2 e^2} b^2} \tag{9}$$

where the impact parameters are $b_{max} = \lambda_D$ and $b_{min} = b$

With the aim to include all effects discussed above, the equations given for the drag force in the considered approximations are coupled and it is possible to give a more realistic result The difference between the eqs (8) and (9) is a measure of the errors that appear due to linearization of the Vlasov-Maxwell equations, if the impact parameters satisfy the condition $a \leq b \leq \lambda_D$ This correction is used together with the drag force obtained with the inclusion of collective effects in the set of Vlasov-Maxwell equations (for $a \leq b \leq \infty$)

$$F_g = -\frac{Q^2}{2\pi^2} \int d^3k \, \frac{i\vec{K}}{k^2} \cdot \frac{1 - K(\vec{K},\omega)}{K(\vec{K},\omega)} \tag{10}$$

where $K(R,\omega)$ is the plasma dispersion function [6] Only for the condition $b > \lambda_D$ (the scattering angles are small) a correction is not needed Then for $a \leq b \leq \lambda_D$ the collective effects are not so important and only the grain charge imposes the ion trajectory and not the other ions

A possibility to find the radial motion velocity of dust in a magnetospheric (planetary) plasma (the migration motion), that is due to the drag effect, appears as the result of the earlier made analysis The rotating plasma gives then to a grain a large circular orbit added to its angular momentum motion Inside of syncrotronous radius a dust grain overtakes the plasma and falls towards any considered planet Usually the ions are not influenced by the other neighbours (ions) are describe hyperbolic orbits The forces among ions modify the grain influence on the ion trajectories, this fact being the source of the collective effects.

The conclusion of this short analysis is that we can choose some particular data for a given plasma, as the density n_i of ions, the temperature T_i, the Landau wavelength λ_D, the charge Q of the grain and the grain velocity ω, then the force F_{id} could be evaluated for a specific case, this fact giving the possibility to see the correct comportament of the dusty grains in a planetary plasma Some numerical evaluations of the drag force in a particular case will be done elsewhere

REFERENCES

1 Mendis D A , Houpis H L F , Hill J R , J Geophys Res , 87, 3449, (1982)
2 de Angelis U , Physica Scripta 45, 465 (1992)
3 Coldea S , Studia Univ Babeş-Bolyai, ser, Physica, 38 nr 2, (1993)
4 Chandrasekhar S , Ap J , 97, 255 (1943)
5 Morfill G E , Goerts C K , Planet Space Sci, 28, 1087, (1980), Icarus, 55, 111 (1983)
6 Krall N A and Trivelpiece A W , Principles of Plasma Physics, McGrow-Hill ed , New York (1973)

STUDIA UNIV BABEŞ-BOLYAI, PHYSICA, XXXVIII, 2, 1993

VIBRATIONAL AND ROTATIONAL RELAXATION IN PYRROLE PURE LIQUID AND SOLUTIONS STUDIED BY RAMAN SPECTROSCOPY

T. ILIESCU, A. SIKE*

Received 5 06 93

ABSTRACT. - Rotational and vibrational relaxation of pure liquid pyrrole al temperatures 283, 293, 303, 313, 333 K and in CS_2 solution at 283 K have been studied by Raman bande shape analysis The activation energy for molecular reorientation of pyrrole molecule was determined The experimental vibrational correlation functions were compared with the Kubo-Rothschild and Oxtoby relations

1. Introduction. Different spectroscopic techniques (IR, depolarised Rayleigh, Raman, NMR) are used for the study of molecular dynamics in condensed phases [1,2]

Rotational relaxation was studied first for the molecules in which vibrational relaxation appeared as an additional and often very weak phenomenom

Therefore in order to test the different theories of vibrational relaxation, heavy molecules in which vibrational relaxation has an important contribution, should be preferred

Recently Navarro and al [3] were obtained the IR relaxations from the molecules of biological interest

Among the different spectroscopic techniques, Raman Spectroscopy has the advantage to separate the contributions of rotational and vibrational relaxation, in the line hope

From the experimental spectra I_{VV} and I_{VH} (the indexes refer to the polarisations of incident and scattering light, respectively) we can obtain the isotropic line profil (I_{iso}) which

* *"Babeş-Bolyai" University, Faculty of Physics, 3400 Cluj-Napoca, Romania*

offers information only on the vibrational relaxation and anisotropic one (I_{aniso}) from which we obtain information about rotational relaxation [4]

$$I_{iso}(\omega) = I_{VV}(\omega) - \frac{4}{3} I_{VH}(\omega) \tag{1}$$

$$I_{aniso}(\omega) = I_{VH}(\omega) \tag{2}$$

By eliminating the contribution of the slit width of the spectrometer and by assuming a lorentzian shape line, we can obtain the real vibrational widths of the line (full widths at half maximum, fwhm)

$$\Gamma_{iso} = \Gamma_V \tag{3}$$

$$\Gamma_{aniso} = \Gamma_{iso} + \Gamma_{2R} \tag{4}$$

(Γ_{2R}) being the line width of the rotational contribution

Vibrational (τ_V) and rotational (τ_{2R}) correlation times are obtained by using

$$\tau_{V,2R} = 1/\pi\Gamma_{V,2R} \tag{5}$$

The vibrational ($G_V(t)$) and rotational ($G_{2R}(t)$) correlation functions, offer another possibility to estimate the different relaxation mechanisms

$$G_V(t) = \int I_{iso}(\omega) exp(i\omega t)\, d\omega \tag{6}$$

$$G_{2R}(t) = \int I_{aniso}(\omega) exp(i\omega t)\, d\omega / G_V(t) \tag{7}$$

The main purpose of the present work is the Raman study of vibrational and rotational relaxations for ring breathing vibration (1144 cm^{-1}, A_1, $\rho \approx 0.05$) of liquid pyrrole and carbon disulfide solutions and to compare the experimental correlation function with theoretical Kubo-Rothschild and Oxtoby equations

2. Experimental. Raman spectrum was excited with 488 nm line (0.3-0.4 w) of a Ar

laser type ILA 120-1 the radiation being passed beforehand through a Glann-Thomson prism The scattered light collected at 90° was analysed with a double monochromator GDM 1000 and I_{VV} and I_{VH} components were obtained by a 90° rotation of the polaroid situated in the gathering optics

One of the Raman spectra in liquid pyrrole is shown in figure 1

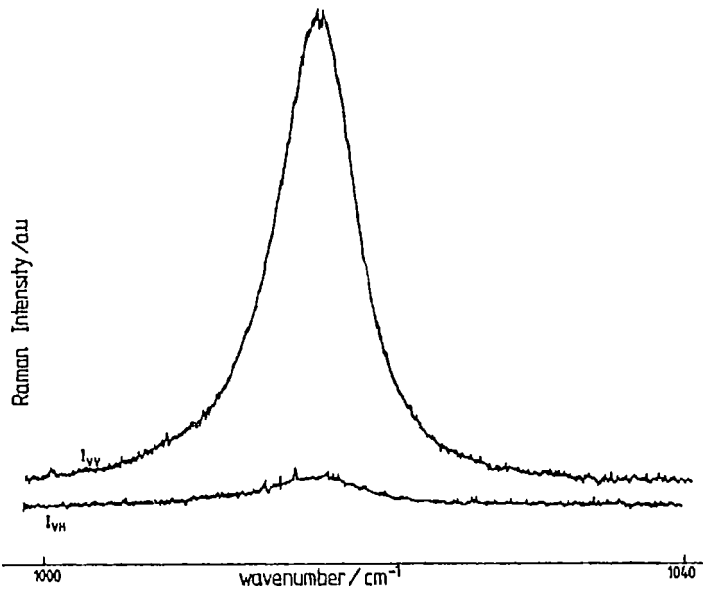

Figure 1. I_{VV} and I_{VH} Raman spectra for $\nu_{ring}(A_1)$ mode of liquid pyrrole at 283K, slit width of 0 6 cm^{-1} The intensity are expressed in arbitrary units

The monochromator slit width was set at 0 6-0 8 cm^{-1} (fwhm) for both scattering components The ratio between the slit width and apparent band width of I_{VV} component was 0 1, so that the finite slit width effect on the determinated Γ_{iso} and Γ_{aniso} values could be neglected In order to avoid a weak asymmetry of the band, I_{VI} and I_{HI} spectra were measured at every 0,4 cm^{-1} on the high wave number side of the band A distance of 5 5 half-

widths from the peak center was used in order to insure a flat base line

Fourier transforms of I_{iso} and I_{amiso} spectra were deconvoluted with the triangle slit function (obtained with Ar^+ plasma laser lines) The experimental vibrational second moment M_2^V was obtained by using the formula [5]

$$M_2^V = \int I_{iso}(\omega)(\omega - \omega_0)^2 d\omega - \int S(\omega)(\omega - \omega_0)^2 d\omega \qquad (8)$$

where $I_{iso}(\omega)$ and $S(\omega)$ are the normalised isotropic Raman spectra and experimental triangle slit function respectively

The pyrrole was purified by distilation and used immediately Solvent of "Merk" uvasol type was used without purification Only CS_2 was utilised because in other solvents (like CCl_4, C_2H_5OH, CH_5CN) the modification of the colour solution during the inllumination with the laser light was noticed

During the measurements the temperature was constant within ± 0 5 K

3. Results and disscution. The Raman band parameters obtained for ν_{ring} mode of pure liquid pyrrole using the relations (1-5) and neglecting the influence of slit width, are summarized for different temperatures in table 1

In the limit of the experimental errors ± 0 5 cm^{-1} there is a coincidence of both scattering components

The τ_V values calculated from the slope of ln $G_V(t)$ are very close to values obtained from Γ_V without slit correction The computation of τ_{2R} from the slope of ln $G_{2R}(t)$ is very difficult because $G_{2R}(t)$ oscillate after 1 5 ps

Fig 2 presents vibrational and rotational correlation functions on logarithmic scale at

303 K for pure liquid pyrrole

From τ_{2R} values (see table 1) is evident that the reorientational contribution to the band shape increases with temperature, as expected On the other hand, in the limit of experimental errors the vibrational correlation times τ_V are temperature independent

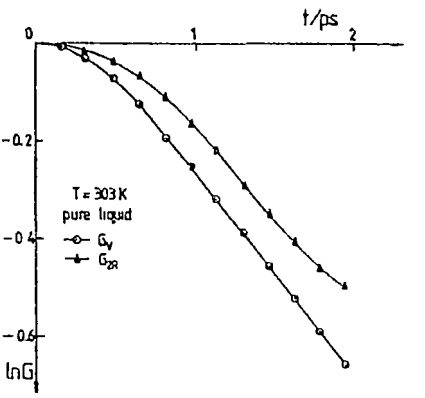

Fig 2 Vibrational, reorientational correlation functions of $\nu_{ring}(A_1)$ mode for pure liquid pyrrole for T = 283 K

Table 1 Raman line parameters for ν_{ring} mode pure liquid pyrrole at several temperatures (line width (fwhm) correlation time τ

T/K	Scattering component	Γ/cm^{-1}	τ_V ps	τ_{2R}/ps
	I_{iso}	5 7		
283			1 8	8 1
	I_{aniso}	7 0		
	I_{iso}	5 6		
293			1 9	5 9
	I_{aniso}	7 4		
	I_{iso}	5 7		
303			1 8	5 3
	I_{aniso}	7 7		
	I_{iso}	5 6		
313			1 9	4 4
	I_{aniso}	8 0		
	I_{iso}	5 7		
333			1 8	3 9
	I_{aniso}	8 4		

Assuming an Arrhenius type relationship for temperature dependence of the rotational correlation time [6]

$$\tau_{2R} = A \exp(E_a/RT) \quad A = const \tag{9}$$

The activation energy E_a for the reorientation of pyrrole molecule is estimated to be

9 5 KJ/mol (fig 3)

We will use the τ_{2R} values in order to conclude about the relativ importance of different relaxation mechanism For all the temperatures studied the vibrational relaxation is the most important mechanism in forming the bande shape

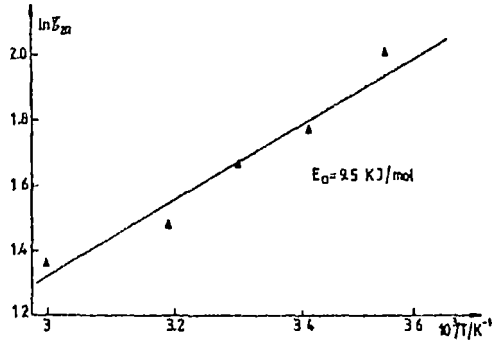

Fig 3 The logarithm of the reorientational correlation times (τ_{2R}) for $\nu_{ring}(A_1)$ mode vs 1/T

In order to understand the evolution of relaxation times and the interactions between pyrrole molecules and solvents, the experimental vibrational (G_V) and rotational (G_{2R}) correlation functions were determined for different concentrations of pyrrole in the carbon disulfide solutions Fig 4 presents the rotational and vibrational correlations functions for pyrrole in CS_2 at concentrations (molar fractions m.f) 0 72, 0 46, 0 22

In solution at short times G_V decays faster than G_{2R}, and therefore the vibrational relaxation is the main mechanism, responsable for the band shape broadening A parabolic character of the vibrational correlations functions (Fig 2 and 4) is noticed at short times and the function becomes almost linear in logarithmic scale at long time This character corresponds respectively to lorentzian function in the central section of the line and to a gaussian in the wings In this situation we can apply the relation (4) even the profile is not a pure lorentzian shape

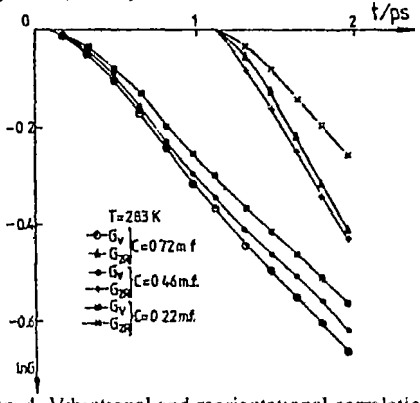

Fig 4 Vibrational and reorientational correlation functions of ν_{ring} mode of pyrrole CS_2 solution

The application of the vibrational dephasing theory developed by Kubo and Rothschild [7] suplies some additional informations concerning the vibrational relaxation processes of the ν_{ring} mode in pyrrole According to this theory the vibrational correlations functions is expressed by

$$G_t(t) = exp\left[-<\omega^2(0)>\left\{\tau_C^2[exp(-t/\tau_C) - 1] + \tau_C t\right\}\right] \tag{10}$$

This vibrational correlation function is essentially determined by a measurement of vibrational second moment M_2^V (in cm^{-2}), which gives the mean-square frequency displacement of the instantaneous vibrational frequency $\omega_0 + \omega(t)$

$$<\omega^2(0)> = 4\pi^2 c^2 M_2^V \quad [ps^{-2}] \tag{11}$$

and the modulation time τ_C, which characterizes the correlation decay of the stochastic perturbation of $\omega(t)$

$$<\omega(t)\omega(0)>/<\omega^2(0)> = exp(-t/\tau_C) \tag{12}$$

Two typical situations are distinguished, depending on whether,

$$<\omega^2(0)>^{1/2}\tau_C < 1 \; or > 1 \tag{13}$$

the processes which modulate $\omega(t)$ are either "fast" or "slow"

Equation (10) describes the vibrational dephasing process and the two limiting cases can be examinated For extremely low modulation ($\tau_C \to \infty$) or for short times ($t \ll \tau_C$) eq (10) leads to a gaussian vibrational function

$$G_V(t) = exp\left[-<\omega^2(0)>t^2/2\right] \tag{14}$$

The half width corresponding to a gaussian spectrum being

$$\Gamma_V^G = (2\ln 2)^{1/2} <\omega^2(0)>^{1/2}/\pi c \tag{15}$$

For a very fast modulation ($\tau_C \to 0$) or for long times ($t > \tau_C$), eq (10) becomes a simple

exponential relaxation function

$$G_v(t) = exp\left[-<\omega^2(0)>\tau_c t\right] \tag{16}$$

The half width for a lorentzian spectrum being

$$\Gamma_v^L = <\omega^2(0)>\tau_c/\pi \tag{17}$$

Another expression for relation (12) has been proposed by Oxtoby [8]

$$<\omega(t)\omega(0)>/<\omega^2(0)> = sech^2(t/\tau_c) \tag{18}$$

which gives the correlation function

$$G_v(t) = exp\left[-<\omega^2(0)>\tau_c^2 \ln cosh(t/\tau_c)\right] \tag{19}$$

Theoretical equationas (10) and (19) were applied to our experimental correlations functions The experimental second moments M_2^v, obtained from isotropic Raman spectra (eq 8) were used to calculate $<\omega^2(0)>$ (eq 11)

The theoretical vibrational correlations functions were computed according to eq (10,19) by inserting experimental $<\omega^2(0)>$ and adjusting τ_C for the best agreement between the theoretical and experimental correlation functions

Table 2 present the application of Kubo-Rothschild's and Oxtoby's equations to ν_{ring} mode of pyrrole pure liquid at different temperatures and for solutions at 283K

Table 2 Application of Kubo-Rotschild's and Oxtoby's equations to ν_{ring} mode pyrolle pure liquid and solutions

System	T (K)	Oxtoby					Kubo-Rotschild			Γ_v (cm^{-1}) exp
		$<\omega^2(0)>$ (ps^{-2}) exp	τ_c (ps) Ox	$<\omega^2(0)>^{1/2}*\tau_C$ Ox	$\Gamma_t^G = \Gamma_v^G$ (cm^{-1}) Ox	Γ_v^G (cm^{-1}) Ox	τ_C ps KR	$<\omega^2(0)>^{1/2}*\tau_C$ KR	Γ_v^G (cm^{-1}) KR	
pure pyrolle	285	1 14	0 41	0 43	13 3	4 9	0 44	0 46	5 3	5 6
	293	0 97	0 48	0 47	12 3	4 9	0 52	0 51	5 3	5 9
	303	0 65	0 71	0 57	10 0	4 8	0 80	0 64	5 5	5 7
	313	0 90	0 70	0 66	11 8	6 6	0 84	0 79	8 02	5 6

Solution m f										
0 72	283	0 94	0 46	0 44	12 1	4 5	0 50	0 48	4 9	5 0
0 46	283	0 92	0 41	0 39	11 9	4 0	0 43	0 41	4 2	4 8
0 22	283	0 72	0 52	0 44	8 9	3 7	0 56	0 47	4 2	4 4

With experimental vibrational second moment $<\omega^2(0)>_{exp}$, Γ_V^G (eq 15) and Γ_V^L (eq 17) were calculated These values were compared with the experimental $\Gamma_V^{exp} = \Gamma_{iso}$

Inspection of table 2 shows that Γ_V^L values are very close to Γ_V^{exp} which implies an important contribution of lorentzian part in the band shape

The τ_C values for pure liquid pyrrole are 0 4-0 8 ps and increase as the temperature is raised Thus the correlation decay of stochastic perturbation is slow at high temperatures At high temperatures a polymerization of pyrrole molecules take probably place In general, for solution, τ_C values decrease with dilution due to the decrease of the velocity of fluctuation

The vibrational second moment $<\omega^2(0)>$ decrease with increasing dilution It is known that an increase in the $<\omega^2(0)>$ appears in the systems where the oscillators interact strongly with the neighboring molecules This means that in our case the interaction between pyrrole molecule and surrounding molecules is larger in concentrated solution than in diluted one, as expected, CS_2 molecule being nonpolar molecule

In condensed phase at low concentration the main mechanism of vibrational relaxation is the phase relaxation (vibrational dephasing) [9] In addition to the above mentioned mechanism, in concentrated solution, two other mechanisms may contribute to the broadening of the isotropic Raman spectra resonance energy exchange [10] and concentration fluctuation [11]

These theories predict a concentration dependence of the line widths of the $\Gamma_{1/2}$

type From table 2 we noticed a decrease of Γ_V(exp) values with dilution Fig 5 present, this linear dependence By extrapolating $C^{1/2} \to 0$, the line width due to pure dephasing for CS_2 solution to be 3 2 cm^{-1}

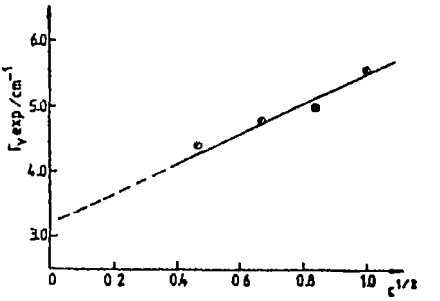

Fig 5 The experimental isotropic Raman line widths (fwhm) vs square root of mole fraction carbon disulfide solution.

From relation (13) and inspection of table 2 we observe that Kubo product $<\omega^2(0)>^{1/2} \tau_c$ is approximately similar for both equation (10,19) and its value for different temperatures in pure liquid pyrrole 0 43 - 0 7 indicate an intermediate modulation regime for vibrational dephasing τ_{nng} mode of pyrrole The fact that the Kubo product values are ~ 0 4 in dilution is an indication that there is a faster modulation regime than in pure liquid

In fig. 6 the experimental vibrational correlation function is compared with the theoretical Kubo-Rothschild's and Oxtoby's correlation functions for pure liquid pyrrole and dilutied in CS_2

Particulary for short times, the Oxtoby equation fits better than Kubo-Rothschild equation the experimental data

4. Conclusions. The results obtained indicate that for the entire time scale studied, the vibrational relaxation is the most important mechanism for ν_{nng} vibrational mode of pure pyrrole and in CS_2 solution From Arrhenius type dependence of τ_{2R} vs 1/T, an activation energy of 9 5KJ/mol for pyrrole molecule was determined

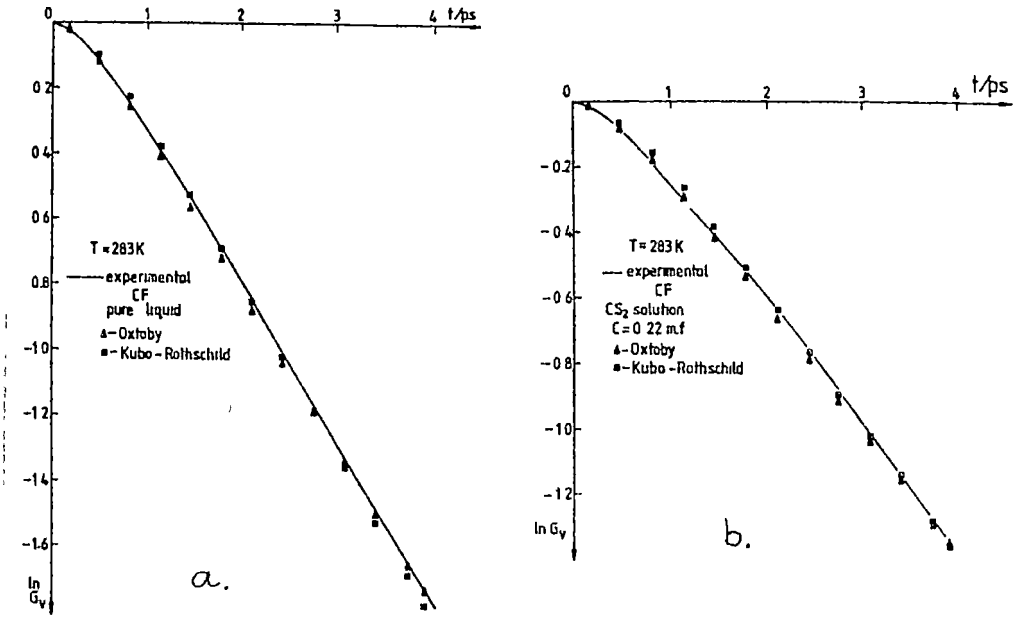

Fig 6 Experimental vibrational correlation functions fitted with Kubo and Oxtoby equations
a-purre liquid
b-carbon disulfide solutions
To simplify the figure only one temperature for pure and CS_2 solution are presented To simplify the figure only one temperature for pure and CS_2 solution are presented

A pure dephasing line width of 3 2 cm^{-1} was obtained from the linear dependence $\Gamma_V(exp)$ vs $C^{1/2}$

A better fit with the experimental date is obtained using the Oxtoby equaion instead of Kubo-Rothschid equation The Kubo product corresponds to an intermediate modulation regime In diluted solutions this regime is faster than in pure liquid pyrrole

To simplify the figure only one temperature for pure and CS_2 solution are presented

REFERENCES

1 W G Rothchild, "Dynamics of Molecular Liquids", John Wiley New York 1984
2 S.Bratos, R M Pick (Eds) "Vibrational Spectrosopy of Molecular Liquids, Plenum Press, New York, 1980
3 R Navarro, I Bratu, A Hernanz, J Phys Chem 97 9081(1993)
4 F J Bartoli, T.A Litovitz, J Chem Phys 56 404(1972)
5. T Kato, T Takemaka, Chem Phys Lett 62(1978)
6 T Kato, T Takemaka J Chem Phys 84 3405(1986)
7 W G Rothschild, J Chem Phys 65 455(1976)
8 D W Oxtoby, J Chem Phys 74 1503(1981)
9 I Bratu, K Klosterman, T Iliescu, S Astilean, J Molec Liquids 45 57(1990)
10 M Kakimoto, T.Fujiyama, Bull Chm Soc Japan 47 1983(1974)
11 A F Bondarev, Opt i spectr 35 350(1977)

STUDIA UNIV BABEŞ-BOLYAI, PHYSICA, XXXVIII, 2, 1993

TOTAL CROSS SECTION DETERMINATION BY FAST NEUTRONS SPECTROMETRY ON AN ISOTOPICALLY ENRICHED ^{15}N TARGET USING AN ^{241}Am-^{9}Be NEUTRON SOURCE

L. DĂRĂBAN*, T. FIAT*, E. VARI-NAGY*

Received 10 07 1993

ABSTRACT. - We have build a method, for measuring the excitation function, based on the analysis of the transmitted spectrum of the fast neutrons generated by ^{241}Am-^{9}Be isotopic source and using a spectrometer with recoil protons and pulse - shape discrimination We have demonstrated that, in case of ^{15}N nucleus as target, acceptable values of the total cross sections can be obtained by means of this method

1 **Introduction.** In the field of nuclear reactions induced by fast neutrons, a lot of interest is concentrated on the problems which refer to the mechanism of the fast neutrons interaction with the nucleus, and on the information that can be inferred about the nuclear structure from these interactions

Analysing the experimental data from a statistic point of view, we may observ that the nucleus of the stable isotopes with little natural abundance are of a special interest These nucleus been less research subject, but, because of the more unstable nuclear structure, they have a spectacular behaviour during the nuclear processes

2. Experimental. The experimental methodology for measuring total cross sections is presented Lately, there have been used "white" neutron sources, based on cyclotrons, linear accelerators or tandem generators, to measure excitation functions $\sigma_t(E)$ We used for the first time the ^{241}Am-^{9}Be source spectrum It should be mentioned that these kind of measurements can be realised only with a fast neutrons spectrometer and the use of the Am-Be source needs a good n-γ discrimination

The probability of interaction between the fast neutrons and the nucleus is

* *"Babeş-Bolyai" University, Faculty of Physics, 3100 Cluj-Napoca, Romania*

characterized by the cross section σ_T and is defined in the following way [1]

$$\sigma_T = \frac{dN}{Nnd}$$

where dN is the number of interactions between the neutrons and the target nucleus, N is the neutrons number that fall on 1 cm^2 of target area, n is the nucleus concentration per target volume unit of pure element and d is the target thichness In the case of a molecular target the relation (1) became much complex like in relation (16)

When using a thick target, the density of the flux changes with thickness "x" In order to find out the number of the neutrons penetrating the target, one should give the differential equation of the layer fullfilling the following requirement for a given thin layer haveing a thickness dx at a depth X in the sample the following equation is valid

$$dN = -N(x)n\ \sigma_T\ dx$$

The solution of the equation (2) has this form

$$N(x) = N_0 \exp(-n\ \sigma_T\ x)$$

where N_0 is the initial neutron flux This means that, for finding out the cross section of the neutrons interaction with the nucleus is sufficient to measure in one experiment the decrease of the neutrons flux $N(d)/N_0$, during the penetration of the target

$$\sigma_T = \frac{\ln\frac{N_0}{N(d)}}{nd}$$

This formula can be turned into another one containing more accesible experimental parameters In this way

$$n = \frac{N'}{V}, \qquad V = Sd \quad \Lambda \quad N' = \frac{m}{A}N_A c$$

It results the next formula

$$\sigma_T = \frac{A \ln\frac{N_0}{N(d)}}{N_A\ c\ \frac{m}{S}}$$

where N(d) is the number of the neutrons which are left after the penetration of the target, A is the atomic mass of the target isotope, N_A is the Avogadro's number, c is the isotopical concentration, m is the mass of the pure element and S is the transversal section of the target The relation $N/N_0=T$ is called transmission factor

TOTAL CROSS SECTION DETERMINATION

If we have the possibility to verify the energy of the neutrons with a neutron spectrometer, then we can measure the total cross sections corresponding to already known values of the neutrons energy

Measurements are done through the transmission method, by mans of the so-called "good geometry arrangement" We place the sample in the way of a collimated bundle of monoenergetic neutrons We measure N_0 and N in order to be able to calculate T [2]

If we want to extract an excitation function having the following form $\sigma_t=f(E_n)$, then we register the spectrum of neutrons, measuring both with and without sample, on the whole energy field, and we calculate, by means of the formula (6), σ_T for every value of the energy of the spectrum

Our purpose was to determine the excitation function for ^{15}N For that purpose we used a sample of $^{15}NH_4{}^{15}NO_3$ (double marked), enriched by isotopes up to the concentration of 98,5% in ^{15}N

In order to measure the cross sections, we use an ^{241}Am-^{9}Be source of neutrons of 1Ci, generating 10^6n/s, enclosed in a collimator of borate parafine, a fast neutron spectrometer with stilbene crystals and a pulse-shape discrimination circuit (fig 1), studied in [3-8]

To extract the latelly scattered neutrons, we used a beam stopper The common methods is to put a long metal bar (of Fe, Cu, or Pb) in the place of the sample, through which the neutrons cannot enter Then, the transmission factor corrected by the background is.

$$T = \frac{N - N_b}{N_0 - N_b}$$

where N_b is the laterally scattered neutrons intensity, which arrives in the detector

We have performed preliminary studies on the ^{12}C nucleu using the spectrum of the Am-Be source, for improving the measurement method of the total cross section at fast neutrons and we obtained the excitation function of ^{12}C nucleus This shows broader and thicker resonances The purpose of these measurements was to see if we could collect nuclear data in a 10^6 n/s total pencil (the Am-Be source gives 10^6 n/s in 4π) Another purpose was to estimate the neutrons spectrometer resolution depending on resonances separation

We collimated the neutrons source with a borated paraffine collimator and we placed

a neutron detector to 0,5 m distance of the collimator A grafit sample with m/s=3,78 g/cm^2 was placed in the middle, between the detector and the collimator We registered the incident neutron spectra $N_0(E_n)$ and the transmitted spectra $N(E_n)$ in 2 hours each other, to have a good statistic We made the calibration of the multichannel analyser's channels in protons energies and operated the neutron spectrometer with stilbene in the same conditions, but with the gate in anticoincidance, this means opposite to the neutron signal of the pulse-shape discrimination circuit (fig 1). Using the method of calibration in electronic energies with

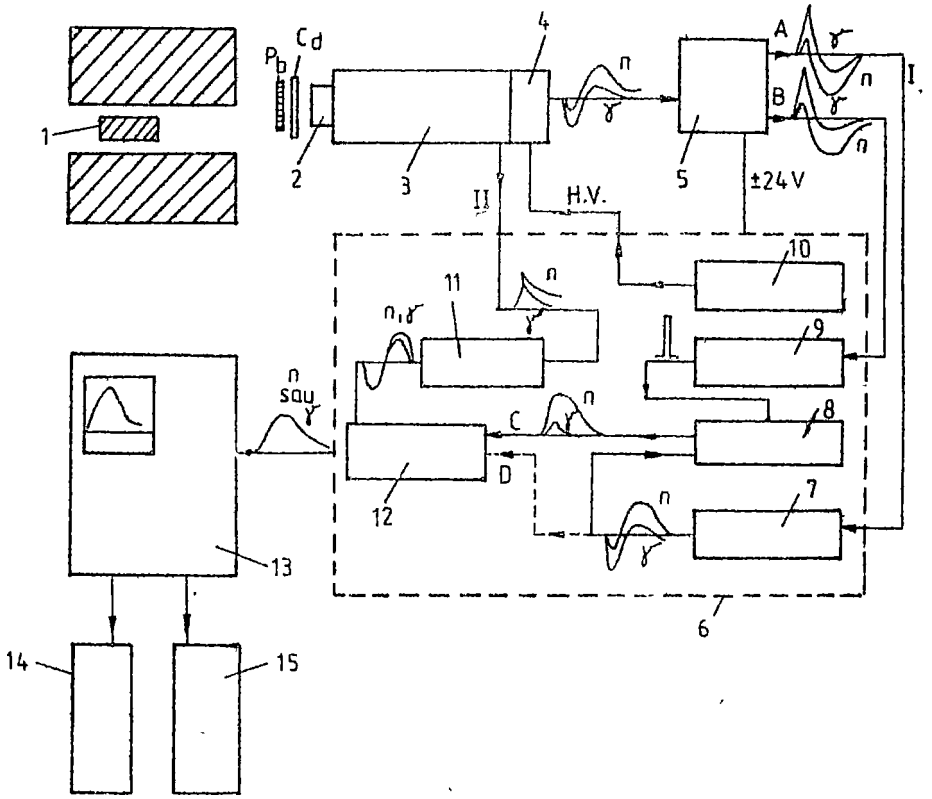

Fig 1. The scheme of neutron spectrometer with n-γ discrimination I-The P S D input, II. Spectrometric input, A,B identical output, C -double discrimination, D - simple discrimination

1 The Am-Be source in borated parafine collimator; 2 Stilbene scintilation crystal 20x30 mm, 3 Fotomultiplicator φ γ 19, 4 The PSD circuit, 5 The charge preamplifier type 1141 FAN, 6 Power source with cadre for NIM modules type ST 614, 7 Mixer reversor type NE 4618, 8 Linear gate (I) type 1183 FAN, 9 Energy analyser type NE 4664, 10 High voltage power supply type 1135, 11 Spectrometric amplifier type NE 4698, 12 Linear gate (II) type 1183 FAN, 13 Multichannel analyser ICA-70, 14 Printer 15 Potentiometric recorder

γ sources, these have been turned in proton energies with a luminosity function having the next form $L(E_p)=C_1E_p^{C2}$

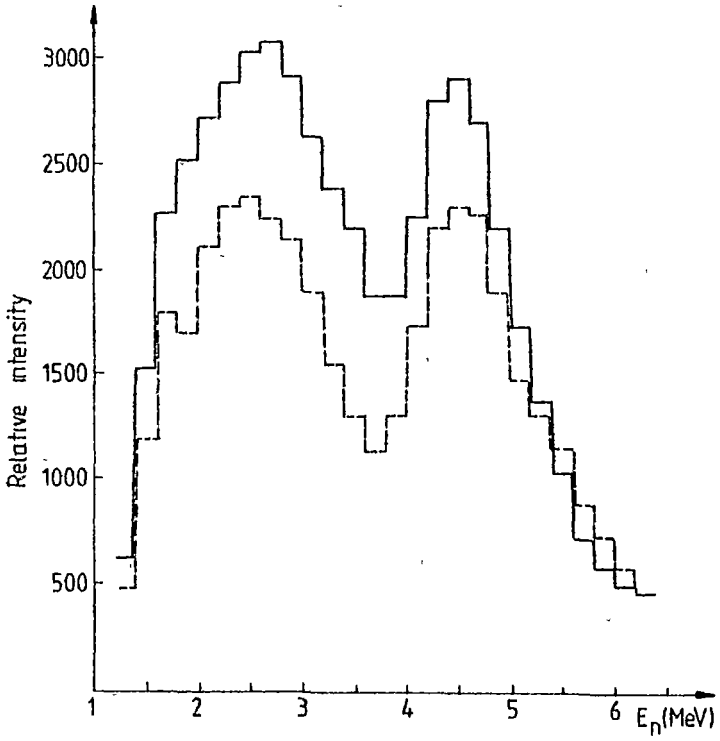

Fig 2 The transmission neutrons of the ^{241}Am-^{9}Be source neutrons through carbon

The data-were transferred in one computer CORAL 4021 that was working in tandem with a multichannel analyser ICA-70 Using a program named SPEC-N, we obtained the incident neutron spectrum $N_0(E_n)$, and in a carbon sample transmitted neutrons spectrum $N(E_n)$ (fig 2)

Using the relation (6), we calculated point by point, the values of the function $\sigma_1(E)$ and in order to find the transmission factor T, we divided the two spectras Fig 3 shows the results, in comparation with the results obtained in [9] In conclusion, we have·

a After the calibration of the Am-Be source spectrum with gamma sources, (without controll by the monoenergetics neutrons), there are appearing deviation from the real energy of the neutrons until 0,5MeV This is illustrated by the position of the carbon's resonances

b The absolute values of the cross section are not in accordance with the data given in literature [9], these have the tendency to be systematically less in the two neutron peaks region and systematically greater where we have less neutrons

The "good geometry" condition requite that the value of the transmission factor to be cc 0,5 for each energetics group So, in order to determine the excitation function, we can't use the continuous spectrum the way it's shaped in fig 3, so only by measuring the transmission factor in the energy region

Also, introducing a set of changed values set (Ei,Ei) in the SPEC-N program, we

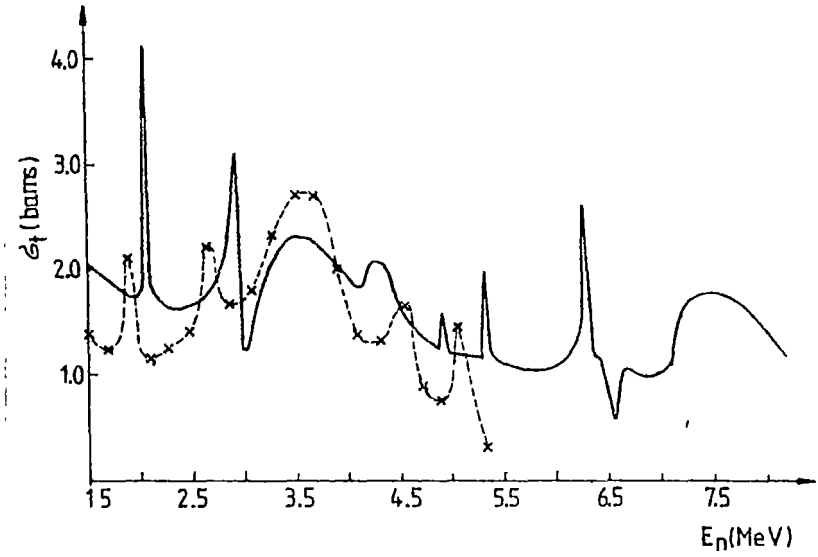

Fig 3. The continous line - the results indicated by [10] The broken line - the measurements effectued on the Am-Be source.

adjusted the luminosity function $L(E_p)$ depending on the shift established comparatively with the carbon's resonances In that way, we used the carbon resonances for the recalibration of the neutron spectrometer, we obtained for a stilbene crystal with 3 cm diameter and 2 cm thickness

$$L(E_p) = 0{,}184\ E_p^{1{,}4044}$$

With this measurement technique, perfected on the ^{12}C nucleus, we obtained the [illegible]

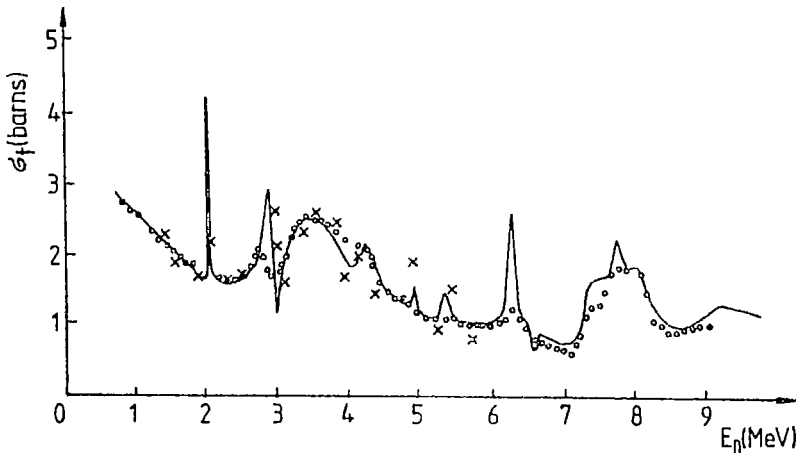

correct values of the excitation function (using an Am-Be source) (fig 4)

By using fig 4, we can study the resolution of our neutron spectrometer with the stilbene crystal By the way this spectrometer solves the carbon resonances at 2,08 MeV or 2,45 MeV, you can see that the equipment (built and perfected in our laboratory) has a resolution of 0,2 MeV, we can estimate the equipment measurement error,by using the results from the fig 4, too 10%

3 **Total cross section determination of ^{15}N** In order to calculate the total cross section of ^{15}N, we measured the initial neutronic spectrum of the ^{241}Am-^{9}Be source and the spectrum transmitted through the sample double marked with ^{15}N (enriched at 98,5% in ^{15}N)

In order to verify the contribution of the oxygen and hydrogen of the NH_4NO_3 sample, we also registered the spectrum transmitted through the natural sample, having the same mass and containing ^{14}N, as well as the spectrum of the laterally scattered neutrons (fig 5)

It is true that the curves of fig 5 are close, but, as a result of our experience with the program SPEC-N, we found that the difference was stell therte, because the sample marked with ^{15}N absorbs more intensive the neutrons than the natural sample

Knowing these curves, the excitation function of ^{14}N, as well as the major isotopical concentration C_{15N}, C_{14N} and respectively, the minor isotopical concentration C_{15N}, C_{14N} of the ^{15}N and ^{14}N from the sample, we are able to calculate the microscopic cross section of ^{15}N for the maximal values of the spectrum in fig 5, where we had a better statistics

The macroscopic cross section of the chemical compound NH_4NO_3, can be defined in accord with [3], in the following way

$$\Sigma_t(E_n) = n_{15N}\,\sigma_{15N}(E_n) + n_H\,\sigma_H\,(E_n) + n_O\,\sigma_O\,(E_n) + n'_{14N}\,\sigma_{14N}\,(E_n)$$

where n_i is the concentration of the i nucleus in 1 cm^3, n_i' is the concentration of the minor isotope, and $\sigma_i(E_n)$ is the cross section according to the value E_n of the neutrons

From the relations (3) and (9), we can obtain the next relation

$$\Sigma_t(E_n) = \frac{1}{d}\ln\frac{N_0(E_n)}{N(E_n)}$$

We can extract the neutron background, which is exactely the spectrum measured with the beam stopper, using the relation (7)

$$\Sigma_t(E_n) = \frac{1}{d}\ln\frac{N_0(E_n) - N_0(E_n)}{N(E_n) - N_0(E_n)}$$

If we couple the relations (9) and (11), then we will obtain a relation for the microscopic

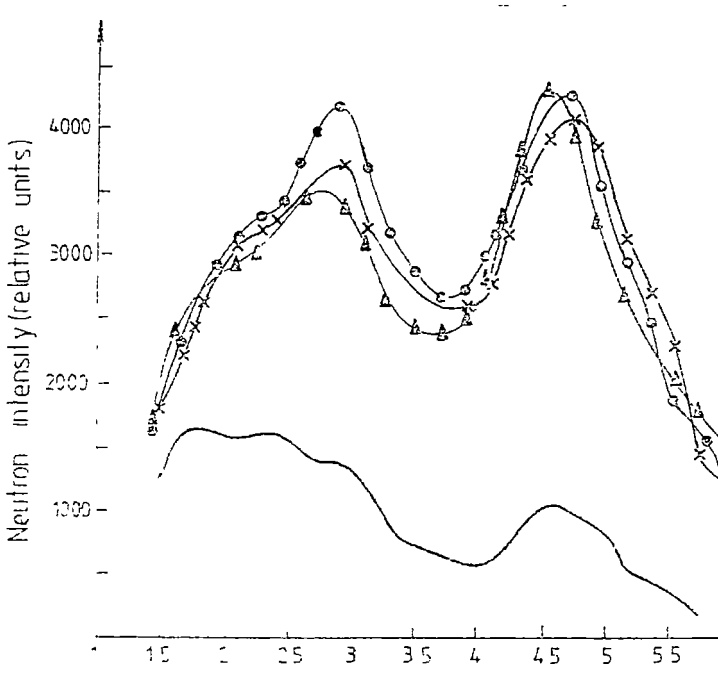

Fig 5 Neutron spectra used in cross section determination.

cross section of ^{15}N

$$\sigma_{15N}(E_n) = \frac{1}{N_{15N}} \left\{ \frac{1}{d} \ln \frac{N_0(E_n) - N_0(E_n)}{N(E_n) - N_0(E_n)} - \left[n_H \sigma_H(E_n) + n_0 \sigma_0(E_n) + n'_{14N} \sigma_{14N}(E_n) \right] \right\}$$

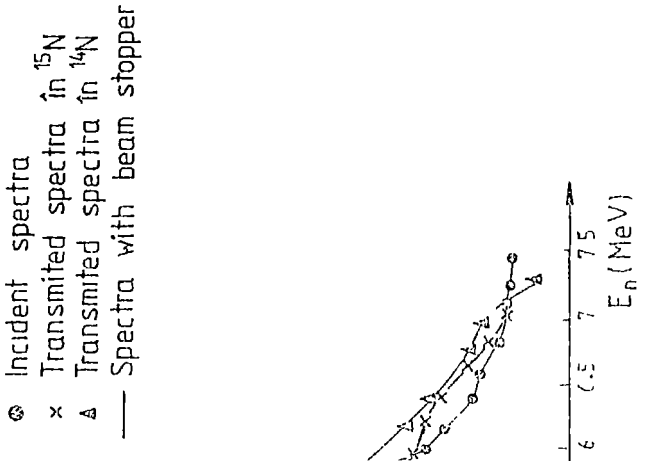

We need to know the excitation functions of the oxygen, hydrogen and nitrogen - 14 (minor in this sample on this energetic domain) and the nucleus numbers in one volume unit n_H, n_0 and n'_{14N}

But the utilisation of relation (12) is not the most comfortable way to measure the cross section of the ^{15}N with minimum error Therefore, we made a measurement in the same conditions on one natural sample NH_4NO_3, having the same mass and geometrical form (the natural isotopical concentration of ^{15}N is 0,37%). We wrote for this sample a similar relation to (12) After that, we made the differences of the two relations

$$\sigma_{15N}(E_n) = \sigma_{14N}(E_n) + \frac{1}{d\, n_{15N}} \ln\frac{N_0(E_n) - N_b(E_n)}{N_{15N}(E_n) - N_b(E_n)} -$$

$$- \frac{1}{d\, n_{14N}} \ln\frac{N_0(E_n) - N_b(E_n)}{N_{14}N(E_n) - N_b(E_n)} + \left(\frac{n_H^{14}}{n_{14N}} - \frac{n_H^{15}}{n_{15N}}\right) \sigma_H(E_n) +$$

$$+ \left(\frac{n_0^{14}}{n_{14N}} - \frac{n_0^{15}}{n_{15N}}\right) + \frac{n'_{15N}}{n_{14N}} \sigma_{15N}(E_n) \frac{n'_{14}}{n_{15}N} \sigma_{14N}(E_n)$$

Because we worked with samples having the same mass, we can prove that

$$\left(\frac{n_H^{14}}{n_{14N}} - \frac{n_H^{15}}{n_{15N}}\right) \sigma_H(E_n) = 0{,}03\ \sigma_H(E_n)$$

(it will be neglected)

$$\left(\frac{n_0^{14}}{n_{14N}} - \frac{n_0^{15}}{n_{15N}}\right) \sigma_0(E_n) = 0{,}06\ \sigma_0(E_n)$$

Relation (13) becomes

$$\left(1 - \frac{C'_{15N}}{C_{14N}}\right) \sigma_{15N}(E_n) = \left(1 - \frac{C'_{14N}}{C_{15N}}\right) \sigma_{14N}(E_n) +$$

$$+ \frac{1}{d\, n_{15N}} \ln\frac{N_0(E_n) - N_b(E_n)}{N_{15N} - N_b(E_n)} - \frac{1}{d\, n_{14N}} \ln\frac{N_0(E_n) - N_b(E_n)}{N_{14N}(E_n) - N_b(E_n)}$$

In that way, knowing the microscopic cross section of ^{14}N, we can find the microscopic cross section of ^{15}N. If we consider that the thicknesses of the sample are the same, using formula (2) we can turn relation (15) into another one, more useful

$$\left(1 - \frac{C'_{15N}}{C_{14N}}\right)\sigma_{15N}(E_n) = \left(1 - \frac{C'_{14N}}{C_{15N}}\right)\sigma_{14N}(E_n) +$$

$$+ \frac{1}{N_A \frac{m_N^{enriched}}{S}} \frac{A_{15N}}{C_{15N}} \ln\frac{N_0(E_n) - N_b(E_n)}{N_{15N}(E_n - N_b(E_n)} -$$

$$- \frac{1}{N_A \frac{m_n^{natural}}{S}} \frac{A_{15N}}{C_{15N}} \ln\frac{N_1(E_n) - N_b(E_n)}{N_{14N}(E_n) - N_b(E_n)}$$

where $N_b(E_n)$ represented the spectrum measured by means of the beam stopper, $N_{14N}(E_n)$ is the spectrum transmitted through the natural sample, and A_{15N} and A_{14N} are the respective isotopical masses.

We have made the calculation with relation (16), using the spectras from fig. 5. We found out that the only sure values are those from the region of the two intense groups of the neutrons. This value is fulfiels the "good geometry" condition for the transmission factor.

The values obtained by, using formula (16) were placed over the excitation function given by [11, 12], our points being marked by *. Regarding the order of magnitude the results proved to be in accordance with the results given by [11, 12] (fig. 6).

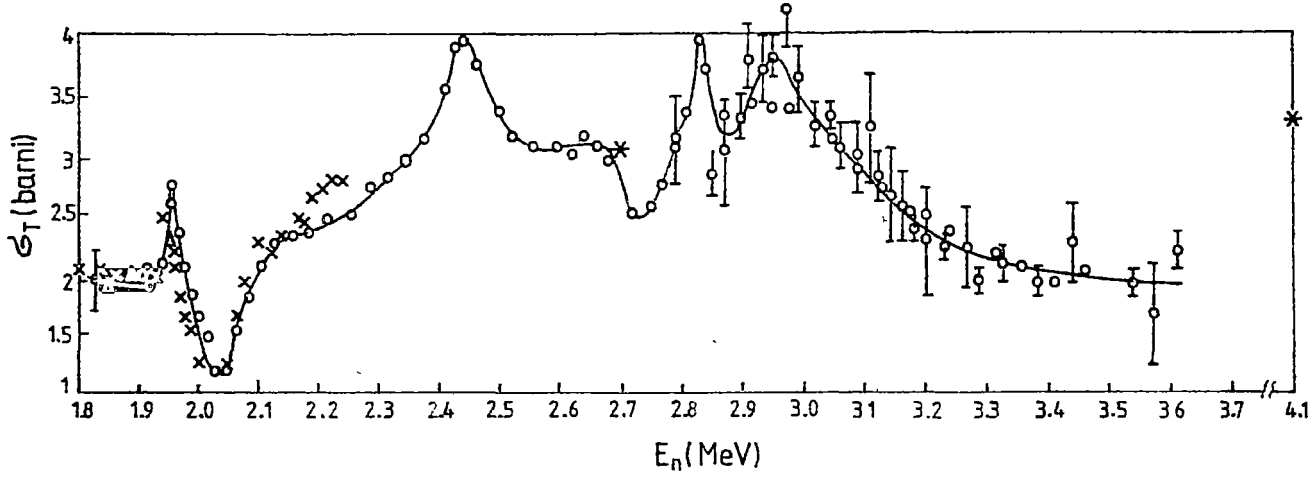

Fig. 6 The excitation function of ^{15}N given by /11/, /12/ and our measurements are marked by *

REFERENCES

1 K N Muhin, Fizică nucleară experimentală, vol I, Ed Tehnică, Bucureşti, 1981
2 L Bratenahl et al , Phys Rev ,**110**,927 (1958)
3 Yu A Egorov, Scintilationni metod spectrometrii gama izlucenii i bistrih neutronov, Gostatomizdat, Moskva, 1963
4 M Bormann et al , Nucl Instr Meth., **92**, 61 (1971)
5 G Dietze, H Klein, Nucl Instr Meth , **193**, 549 (1981)
6 H W Broek, C E Anderson, Rev Sci Instr , **31**, 1063 (1960)
7 M Sirbu, St Cerc Fiz., **38**, 714 (1986)
8 N M N.Wasson, The use of stilbene with decay time discrimination, as a fast neutron spectrometer, reprint AERE-R, 4169, U K , G B Harwele, Berkshire, 1963
9 V I Kuhtevich et al , At energhia, **23**, 191 (1967)
10 J B Marion, J L Fowler, Fizica bistrih neitronov, 231, Gostatomizdat, Moskva, 1963
11 A Ajzenberg-Selove, Nucl.Phys , **A152**,6,43 (1970)
12 B N L 325, Neutron cross sections, supl 1, no 2, vol 1, z=1 to 20 (1964)

STUDIA UNIV BABEŞ-BOLYAI, PHYSICA, XXXVIII, 2, 1993

SPECTROSCOPIC INVESTIGATION OF THE INFLUENCE OF MELTING TEMPERATURE ON THE REDOX EQUILIBRIUM OF URANIUM IONS IN $0.95Na_2B_4O_7$-0 $05Al_2O_3$-0 $02UO_3$ GLASS

E. CULEA and I. MILEA*

Received 15 06 1993

ABSTRACT. - The influence of the melting temperature on the redox equilibrium of uranium ions in the 0 $93Na_2B_4O_7$-0 $05Al_2O_3$-0 $02UO_3$ glass was studied using optical spectroscopy The obtained optical data prove that increasing melting temperature determine the reduction of the U^{6+} ions to U^{4+} ions in the studied glass

1. Introduction. Since glass is used to immobilization of nuclear waste [1,2] the study of glasses containing radionuclides becomes important Uranium is one of the important radionuclides that appears in nuclear wastes As was previously reported[3,4] uranium ions appear in oxide glasses in different valence state, such as U^{+6}, U^{+5} and U^{+4} The study of redox equilibrium between these valence states is of considerable interest

This paper presents the results of a spectroscopic investigation of the influence of the melting temperature on the redox equilibrium of uranium ions in the 0 $93Na_2B_4O_7$-0 $05Al_2O_3$-0 $02UO_3$ glass

2. Experimental Method. Samples were prepared using reagent grade borax $Na_2B_4O_7\ 10H_2O$, Al_2O_3 ("Reactivul" Romania) and uranyl nitrate $UO_2(NO_3)_2\,6H_2O$ ("Chemapol" Czechoslovakia) First a borax glass was obtained by melting borax at 1000°C for 30 minutes UO_3 was obtained by thermal decomposition of the uranyl nitrate Then, adequate amounts of $Na_2B_4O_7$(powdered glass), UO_3 and Al_2O_3 were melted to obtain the

* *Technical University of Cluj-Napoca, 3400 Cluj-Napoca, Romania*

0 93$Na_2B_4O_7$-0 05Al_2O_3-0 02UO_3 glass The samples were prepared using five different melting temperatures, namely 800, 900, 1000, 1100 and 1200°C The melts were equilibrated at these temperatures for 2 hours Glass samples were obtained as slabs (20x8x3 mm) by pouring the melts in a stainless steel piece having an appropriate grove

Optical absorption spectra for the visible and UV region(10,000-30,000cm^{-1}) were recorded using a Specord UV-VIS(Germany) spectrometer To obtain the optical spectra the glass slabs were polished on two opposite sides

3. Results and Discussion. All the samples containing UO_3 were yellow This suggests the presence of uranium ions mainly as U^{6+}, probably in UO_2^{2+} (uranyl) form

The 0 02UO_3 content of the studied samples permits to obtain optical absorption spectra with well resolved spectral features A representative absorption spectrum of the 0 93$Na_2B_4O_7$-0 05Al_2O_3-0 02UO_3 glass for the UV and visible region is presented in figure 1 (spectrum 1)

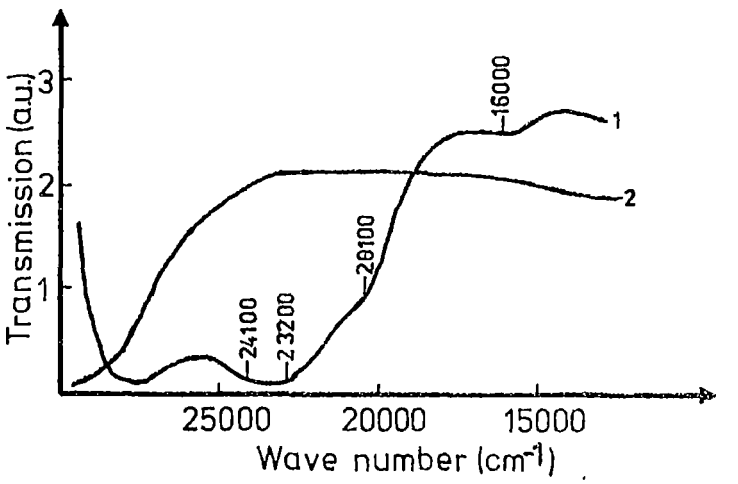

Fig 1 Optical spectra of 0 93$Na_2B_4O_7$-0 05Al_2O_3-0 02UO_3 (curve 1) and 0 93$Na_2B_4O_7$-0 05Al_2O_3 (curve 2) glasses

Spectrum 2 in this figure corresponds to the basic $0\,93Na_2B_4O_7$-$0\,05Al_2O_3$ glass The comparison of the two spectra proves that the spectral features exhibit by spectrum 2 belong to the uranium ions The spectroscopic features evidentiated by this spectrum are characteristic for oxide glasses containing uranium ions[3,4]

The most important features of the $0\,93Na_2B_4O_7$-$0\,05Al_2O_3$-$0\,02UO_3$ glass appear at about 16,000cm^{-1}(assigned to U^{4+} ions), 20,700cm^{-1}(assigned mainly to U^{6+} ions), 23,200cm^{-1}(assigned mainly to U^{4+} ions), and from 24,100cm^{-1}(assigned to U^{6+} ions) The assignements were made according to some previously reported data concerning some borosilicate and borate glasses[3,4] We note that the positions of the absorption bands belonging to the U^{4+} and U^{6+} ions observed for the $0\,93Na_2B_4O_7$-$0\,05Al_2O_3$-$0\,02UO_3$ glass are close to those reported for other borate and borosilicate glasses This suggests the fact that the coordination sites of uranium valence states seem to be independent of glass composition

The variation of the melting temperature generates some changes of the spectral features These changes are shown in figure 2

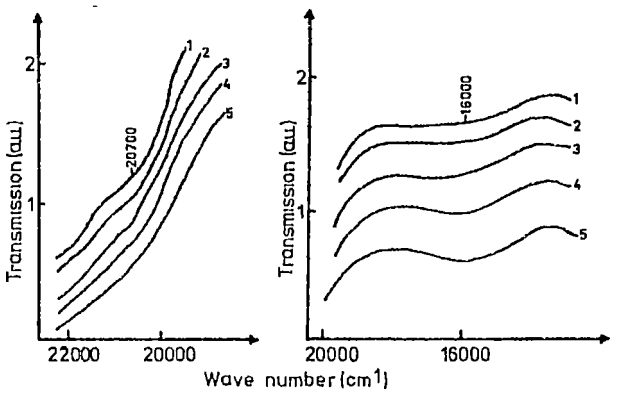

Fig 2 Changes produced in the optical spectra of the $0\,93Na_2B_4O_7$-$0\,05Al_2O_3$-$0\,02UO_3$ glass by increasing the melting temperature (1 for 800°C, 2 for 900°C, 3 for 1000°C, 4 for 1100°C and 5 for 1200°C)

Thus increasing melting temperature generates the increase of the bands from 16,000 and 23,200cm^{-1} and the decrease of the shoulder from 20,700cm^{-1} These changes indicate an increase of the amount of U^{+4} ions in the samples with increasing the melting temperature The increase of the melting temperature of the samples seem to determine the reduction of the uranium ions according to the equation

$$4U^{6+}(melt) + 4O^{2-}(melt) = 4U^{+4} + 2O_2(gas) \quad (1)$$

It is possible that this process implies not only U^{+6} and U^{+4} ions but also U^{5+} ions and follows a two step process, according to the equations

$$4U^{6+}(melt) + 2O^{2-}(melt) = 4U^{+5}(melt) + O_2(gas) \quad (2)$$

$$4U^{+5}(melt) + 2O^{2-}(melt) = 4U^{+4}(melt) + O_2(gas) \quad (3)$$

Our spectroscopic data did not permit to evidentiate the presence of U^{5+} ions However we do not exclude the possibility of appearence of U^{5+} ions, but we estimate that the 5+ valence state is probably less stable in the studied glass than 6+ and 4+ ones

4. Conclusions. An optical spectroscopic investigation was made on the $0.93Na_2B_4O_7$-$0.05Al_2O_3$-$0.02UO_3$ glass in order to study the influence of the melting temperature on the redox equilibrium of the uranium ions The obtained data indicate that the increasing melting temperatures determine the reduction of the U^{6+} ions to U^{4+} ions

REFERENCES

1 J L Crandall, Scient Basis Nucl Waste Mgmt, 2(1980) 39
2 M J Plodinec, Scient Basis Nucl Waste Mgmt, 1, (1979) 31
3 H D Schreiber and G B Balasz, Phys Chem Glasses 23, 5(1982) 139 and H D Schreiber G B Balasz, P L Jamison and A P Shaffer, Phys Chem Glasses 23, 5(1982) 147
4 E Culea, I Milea and I Bratu, J Molec Struct 291 (1993) 271

In cel de al XXXVIII-lea an (1993) *Studia Universitatis Babeş-Bolyai* apare în următoarele serii:

matematică (trimestrial)
fizică (semestrial)
chimie (semestrial)
geologie (semestrial)
geografie (semestrial)
biologie (semestrial)
filosofie (semestrial)
sociologie-politologie (semestrial)
psihologie-pedagogie (semestrial)
ştiinţe economice (semestrial)
ştiinţe juridice (semestrial)
istorie (semestrial)
filologie (trimestrial)
teologie ortodoxă (semestrial)
educaţie fizică (semestrial)

In the XXXVIII-th year of its publication (1993) *Studia Universitatis Babeş-Bolyai* is issued in the following series:

mathematics (quarterly)
physics (semesterily)
chemistry (semesterily)
geology (semesterily)
geography (semesterily)
biology (semesterily)
philosophy (semesterily)
sociology-politology (semesterily)
psychology-pedagogy (semesterily)
economic sciences (semesterily)
juridical sciences (semesterily)
history (semesterily)
philology (quarterly)
orthodox theology (semesterily)
physical training (semesterily)

Dans sa XXXVIII-e annee (1993) *Studia Universitatis Babeş-Bolyai* paraît dans les series suivantes:

mathematiques (trimestriellement)
physique (semestriellement)
chimie (semestriellement)
geologie (semestriellement)
geographie (semestriellement)
biologie (semestriellement)
philosophie (semestriellement)
sociologie-politologie (semestriellement)
psyhologie-pedagogie (semestriellement)
sciences économiques (semestriellement)
sciences juridiques (semestriellement)
histoire (semestriellement)
philologie (trimestriellement)
theologie orthodoxe (semestriellement)
éducation physique (semestriellement)

CONTENTS

Theoretical Physics

Plasma Physics

Optics, Spectrometry and Nuclear Physics

Lei 60